AD-A020 275

TEST EVALUATION AND MODIFICATION OF PROTOTYPE ROTATING GRAVITY GRADIOMETER

Charles B. Ames, et al

Hughes Research Laboratories

Prepared for:

Air Force Cambridge Research Laboratories

July 1975

Best
Available
Copy

042062

AFCRL-TR-75-0419

TEST EVALUATION AND MODIFICATION OF PROTOTYPE ROTATING GRAVITY GRADIOMETER

CHARLES B. AMES, ROBERT L. FORWARD,
PHILIP M. LA HUE, AND DAVID W. ROUSE

HUGHES RESEARCH LABORATORIES
3011 MALIBU CANYON ROAD
MALIBU, CALIFORNIA 90265

ADA020275

JULY 1975

FINAL REPORT
FOR PERIOD 1 MAY 1975 THROUGH 30 JUNE 1975

SUPPORTED IN PART BY DEFENSE MAPPING AGENCY
DMA PE 63701B/3201/03, MC & G INVESTIGATIONS

AIR FORCE CAMBRIDGE RESEARCH LABORATORIES
AIR FORCE SYSTEMS COMMAND
UNITED STATES AIR FORCE
HANSCOM AIR FORCE BASE, MA 01731

UNCLASSIFIED

SECURITY CLASSIFICATION OF THIS PAGE (When Data Entered)

REPORT DOCUMENTATION PAGE

READ INSTRUCTIONS BEFORE COMPLETING FORM

1. REPORT NUMBER: AFCRL-TR-75-0419	2. GOVT ACCESSION NO. / 3. RECIPIENT'S CATALOG NUMBER
4. TITLE (and Subtitle): TEST EVALUATION AND MODIFICATION OF PROTOTYPE ROTATING GRAVITY GRADIOMETER	5. TYPE OF REPORT & PERIOD COVERED: 1 May 1975 - 30 June 1975 FINAL REPORT
	6. PERFORMING ORG. REPORT NUMBER
7. AUTHOR(s): Charles B. Ames, Robert L. Forward, Philip M. LaHue, and David W. Rouse	8. CONTRACT OR GRANT NUMBER(s): F19628-75-C-0201
9. PERFORMING ORGANIZATION NAME AND ADDRESS: Hughes Aircraft Company, Research Laboratories Division, Malibu, CA 90265	10. PROGRAM ELEMENT, PROJECT, TASK AREA & WORK UNIT NUMBERS: 8607-02-01, 62101F
11. CONTROLLING OFFICE NAME AND ADDRESS: Air Force Cambridge Research Lab, Hanscom AFB, Massachusetts 01731, Contract Monitor: Jack A. Cook, Lt. Col./LWG	12. REPORT DATE: July 1975
	13. NUMBER OF PAGES: 128
14. MONITORING AGENCY NAME & ADDRESS (if different from Controlling Office)	15. SECURITY CLASS. (of this report): UNCLASSIFIED
	15a. DECLASSIFICATION DOWNGRADING SCHEDULE

16. DISTRIBUTION STATEMENT (of this Report)

Approved for public release; distribution unlimited

DDC
RECEIVED
FEB 9 1976
D

17. DISTRIBUTION STATEMENT (of the abstract entered in Block 20, if different from Report)

18. SUPPLEMENTARY NOTES

This research was sponsored by the Defense Mapping Agency.

19. KEY WORDS (Continue on reverse side if necessary and identify by block number)

Gravity Gradiometer
Gravitational Mass Sensor
Gravitational Gradient Sensor
Gravity Mapping
Mass Detection
Airborne Gradiometer
Vertical Deflection
Motion Isolation and Stabilization
Inertial Guidance
Navigation

20. ABSTRACT (Continue on reverse side if necessary and identify by block number)

This effort was a contiguous follow-on to the original 39-month contract, F19628-72C-0222, to develop a prototype Rotating Gravity Gradiometer (RGG). The two major objectives of this two-month contract were directed at identifying and correcting spin bearing problems and continuing the RGG test and evaluation program in the laboratory.

DD FORM 1 JAN 73 1473 EDITION OF 1 NOV 65 IS OBSOLETE

UNCLASSIFIED

SECURITY CLASSIFICATION OF THIS PAGE (When Data Entered)

Spin bearing activities included are analysis of prior bearing failures and a subsequent redesign, followed by fabrication of replacement bearings. The bearing work was accomplished in conjunction with Shaker Research Inc., the subcontractor originally selected to design and fabricate the first set of bearings.

The laboratory test program was directed at developing and improving a better understanding of RGG performance characteristics. It was highly successful. The RGG sensor noise output was reduced by a factor of ten (10) and the bias level by a factor of three-to-five (3-5) over the best performance obtained during the last weeks of the prior contract. For the first time, meaningful demonstrations of gravity gradient sensitivity could be performed with the prototype RGG.

TABLE OF CONTENTS

LIST OF ILLUSTRATIONS

I. INTRODUCTION

This report documents the work performed on the prototype Rotating Gravity Gradiometer (RGG) during May and June 1975. This two month contract was contiguous with contract F19628-72-C-0222 a 39 month effort during which one prototype RGG sensor was designed, fabricated, assembled, analyzed, adjusted and system tested.

The purpose of this contract was to provide continuity of effort at a particularly critical time during the development program, and to investigate the bearing failures and provide solutions. It also continued the laboratory test and evaluation of the RGG sensor system which had only just begun during the last weeks of the prior contract.

The status of the development program at the outset of this contract was that the RGG sensor operation had been demonstrated in both the horizontal and vertical spin axis orientations. The noise level was approximately 300 Eötvös Units (EU) at ten seconds integration time. This high level of noise prevented demonstrations of gravity gradient sensitivity with present laboratory equipment. Because of two bearing failures, the original spin bearings were not used for the April 1975 demonstrations. Instead, they were replaced with commercial ball bearings because their ready-availability made them the most expedient substitute for the original, high precision journal bearings. This report will show that the April 1975 system performance, which was far short of the performance objectives, can be substantially attributed to the use of the interim ball bearings.

II. SPIN BEARING ACTIVITY

One of the first tasks in this contract was directed at establishing the cause of the RGG spin bearing failures and to study alternative designs. A subcontract was let to Shaker Research Inc. for engineering services, for preliminary studies, for detailed design, and for fabrication and test of a new hydrodynamic journal oil bearing. The new bearing is specifically designed to operate in a vacuum (~1 μm Hg).

These steps and certain alternatives are discussed in this Section.

A. Bearing Failure Analysis

After study of the failed bearings, available test data, and discussions with Shaker Research personnel, the following conclusions were reached:

1. Both bearings failed due to lack of lubricant. In one case the oil was lost when a vacuum was applied to the bearing. In the other case, insufficient oil was provided for proper operation due to an inadvertent underfill.

2. The bearing filling procedures initially used were not the best for vacuum operation of these bearings. Tests made during this program show that the bearing and pintle must be assembled and filled in a vacuum or the assembly will froth and bubble and lose oil at the pintle-seal plate joint.

3. Nyebar — an oleophobic coating material — does not repel oil or resist wetting by oil with sufficient force to provide a practical seal in a vacuum environment. Relatively extensive tests, discussed in Section III-B, demonstrated that only under the most optimum condition could the capillary seal concept be made to operate as an effective seal.

4. The spin bearings had been designed for exposure to ambient air pressure. They were manufactured several months before the January 1974 RGG configuration final selection, a decision which would cause the bearings to be exposed to the sensor vacuum environment.

Preceding page blank

Unfortunately, it was not until May 1975 that the negative impact of this decision was fully appreciated: careful examination revealed the need to vent several voids and to reduce the maximum static head of the lubricant. Thus, a major redesign was required.

5. As nearly as could be determined, the bearings did meet their break-away torque, stiffness, and load carrying capability when operating in air.

6. The surface tension of the oil that we are using is the same in air or vacuum. A simple capillary height rise test gave the same surface tension in air as vacuum.

Based on the above failure analysis items, it was decided that a new bearing could probably be designed that would meet all of the RGG specifications, including the vacuum requirement.

B. New Bearing Procurement

Except for a significant weakness in oil retention, the spin bearings originally designed by Shaker Research appeared to have met all design objectives. Since Shaker Research was intimately familiar with all of the RGG problems, it was decided to hold a design conference on a new bearing design at Shaker Research. There were two objectives of this conference: first, to determine if a "medium performance — quick and dirty" bearing could be built that would allow Hughes to perform some tests on the rotating sensor with only a few weeks delay. Second, to explore a design concept to reasonable depth that would provide the required RGG spin bearing performance in a vacuum environment.

The first part of the conference was conducted on a wide-open concept basis; i.e., we had a specific bearing problem and the question addressed the potential solutions. It quickly became evident that our RGG requirements ruled out quick-and-dirty designs. The spin bearings must operate in the hydrodynamic (thick-film) mode to maintain the torque noise at an acceptable level.

After the first bearing failure in March 1975, we designed, manufactured, installed and tested bearings using Oilite as the bearing material. These bearings operate in the thin film (boundary layer) mode. The necessity for the thick-film mode became conclusively evident when the resulting noise and bias levels of the RGG became worse than when operating on a pair of ball bearings. The weak points of the original Shaker bearing design seemed to involve marginal seal (oil retention) capability and an inadequate oil reservoir. Thus, attention was turned to these areas at the start of the conference. Preliminary calculations demonstrated that the drag and torque noise of an "O" ring or lip seal would be within the RGG bearing specification requirements. Such a seal, although not leak-proof, would provide a rugged positive seal with an acceptable life. This type of seal was accepted as a base line.

The oil reservoir problem became a combined problem of vacuum filling, oil feed, and loss of very small amounts of oil from a small reservoir. The best solution necessitated the use of a rather large reservoir, with wick feed, and a vent to the outside of the bearing. This concept too, was accepted as the second base line.

These two base lines were broadly formulated into a very preliminary bearing concept. Shaker was then authorized to complete the preliminary design.

After the preliminary design and test programs at Shaker, a subcontract was let to Shaker to complete the design, fabricate and test one pair of prototype bearings. This bearing pair will be the same as a final bearing except that pintle and bearing total indicated roundness (TIR) will be limited to 20 μin (0.5 μm). Five microinches (0.13 μm) TIR will be required for the final bearing. The 20 μin (0.5 μm) TIR specification speeds delivery and reduces the cost of the prototype bearing. The performance will be the same as the final bearing in every respect except the torque noise. The prototype bearing set will be tested at atmospheric pressure and in a vacuum to evaluate all pertinent characteristics.

C. New Bearing Characteristics

The assembly and parts detail of the newly designed Shaker Research Corp. spin bearing for the Hughes RGG are shown in Fig. 1 through 5. The pintle size, land, and groove configuration are identical to those of the original bearing.

In this bearing design, the pintle (Item No. 1) is attached to the rotor of the RGG. Since the pumping lands and grooves are on the pintle, which will now become the rotating part, this bearing will be very slightly noisier than the original reversed configuration. However, the noise will be within the specification limits. The rotating pintle configuration has the advantage of being easier to seal and to provide with an adequate oil reservoir.

The oil reservoir is in the bearing housing (Item No. 4). The reservoir has a total volume of about 2 cubic centimeters, about half of which will be filled with oil. Thus, with the RGG in any attitude, about half of the pintle bearing surface will be submerged in oil. Oil is distributed to the bearing and pintle surfaces not already submerged in oil by means of wicks (Items No. 9 and No. 10). The oil reservoir is vented to the pintle atmosphere environment by a vent hole (visible in the reservoir structure, Item No. 3).

This vent hole restricts the angular orientation of the sensor when the spin axis is horizontal to $\pm 75^{\circ}$ about the vent hole up position. This is not considered to be a significant restriction. A lip oil seal (Item No. 13) is visible in the assembly drawing.

The overall length of the new design has been increased by 0.406 cm (0.160 in.) to accommodate the oil reservoir and other features. The increased bearing length can be accommodated by shims under the bearing seats and by relieving the stator end cover.

The new bearing design has been reviewed in detail by several engineers, and appears to meet all of the RGG requirements.

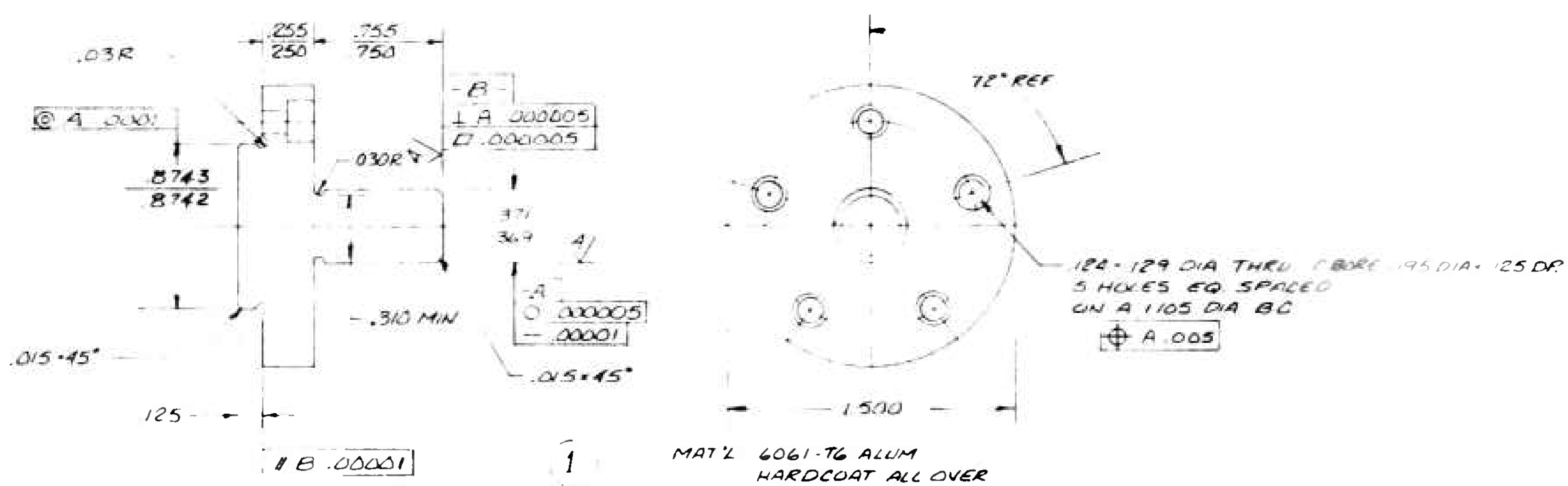
.03R
.255
250
.755
750
-B-
⊥ A .000005
▱ .000005
.030R
.8743
.8742
.371
.369
4
-A-
○ .000005
— .00001
-.310 MIN
.015×45°
.015×45°
125
∥ B .00001
1
72° REF
.124-.129 DIA THRU
5 HOLES EQ SPACED
ON A 1.105 DIA BC
⌖ A .005
1.500
MAT'L 6061-T6 ALUM
HARDCOAT ALL OVER

Fig. 1. Pintle

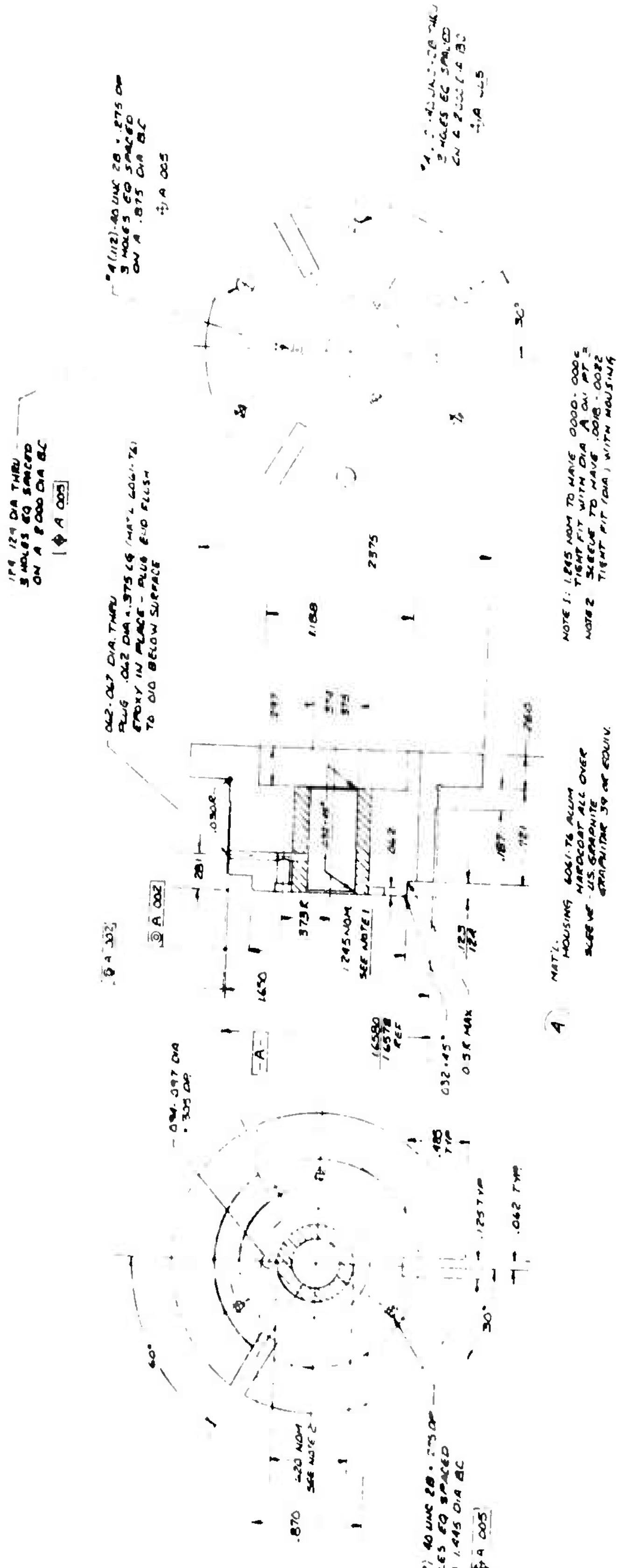

Fig. 2. Bearing Housing

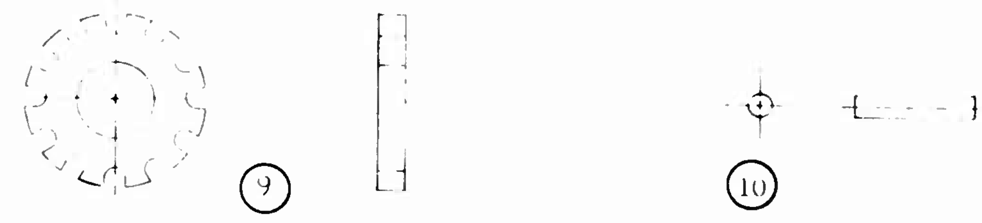

Fig. 3 Oil Wicks

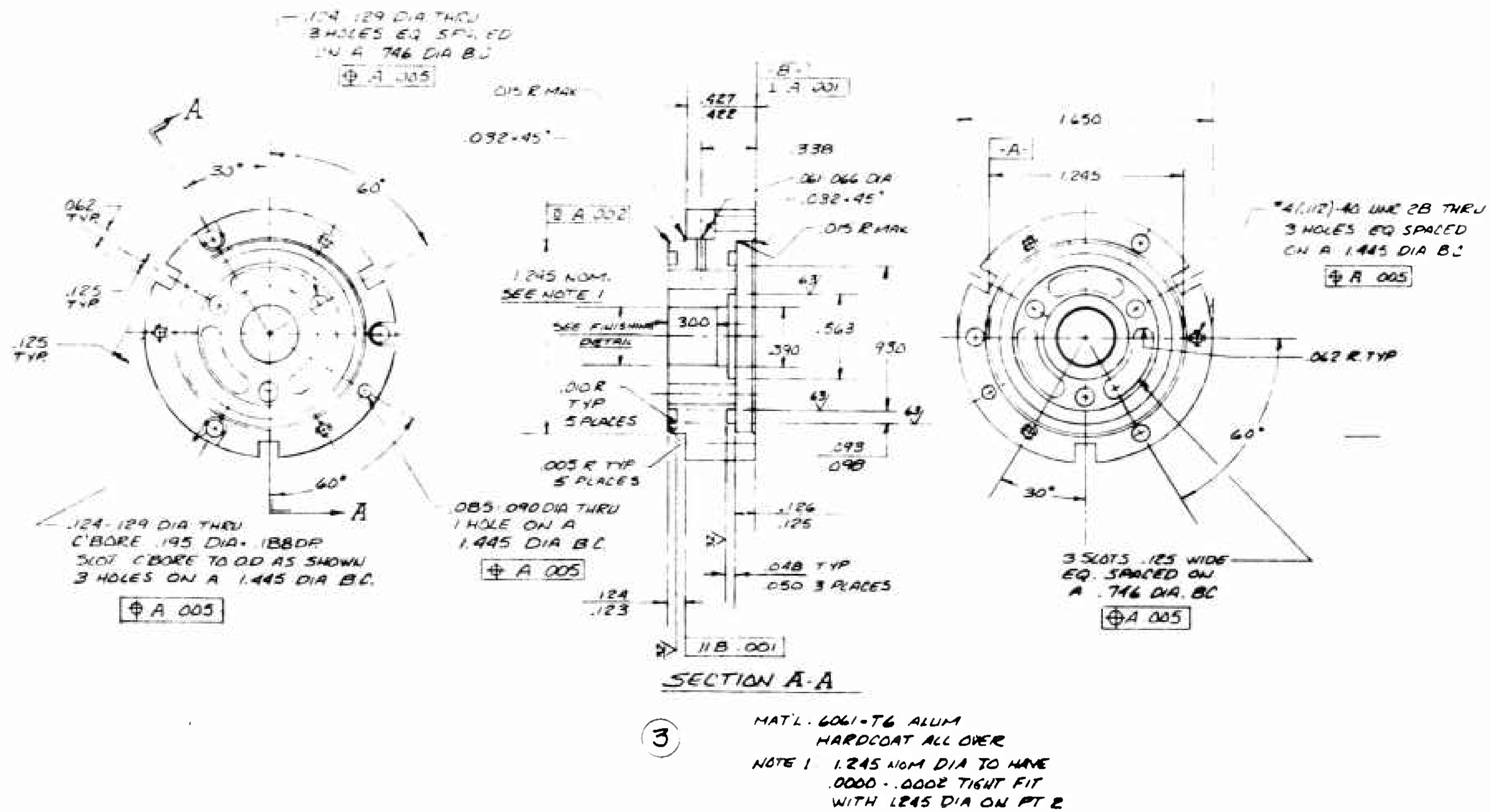

Fig. 4. Oil Reservoir

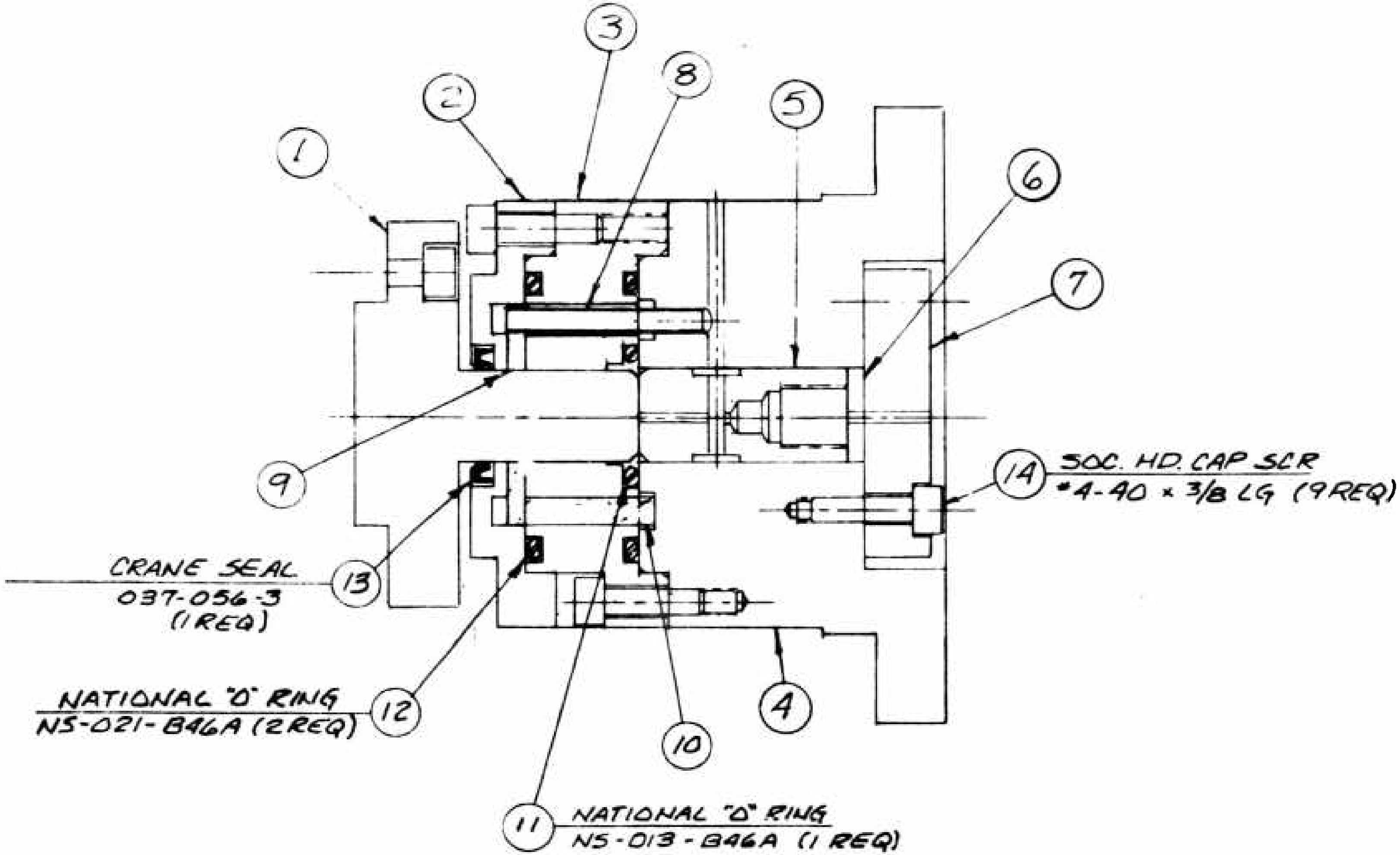

ASSEMBLY

Fig. 5. Assembly Drawing

D. Bearing Component Tests

Two components of the new bearing design required specific tests since design data were meager. These new features are: the use of a wick (which raises the question of the wick's ability to supply the required flow of lubricant), and the use of lip seal (which raises questions of torque drag and torque variations).

The wick feed rate was tested and found to provide a feed rate of three to five times that required by the bearing. Preliminary tests of the lip seal torque and torque variations were inconclusive. The average torque at low speeds, the only test speed available at the time, was considered to be satisfactory. However, at the slow speeds, the seal exhibited a stick-slip friction characteristic that is considered to be undesirable. Additional tests will be made, using the new bearing as soon as possible, to further evaluate lip seal torque variability.

E. Bearing Alternatives

Although the new spin bearing has been carefully thought out, two areas of uncertainty exist.

The first concerns the possibility of excessive torque noise caused by the lip seal. If this becomes a problem, four or more alternatives exist. They include: (1) use of an annular mercury seal; (2) use of an "O" ring instead of the lip seal; (3) use of a magnetic fluid seal. and (4) oleophobic surface coatings. The substitution of an "O" ring or the use of an oleophobic coating would be simple and straightforward, if they can be made to work. The annular mercury seal or the magnetic fluid seal would require rather extensive test programs and significant bearing modification.

The second area of uncertainty is that the bearing, as designed, may not operate in a hydrodynamic mode in a vacuum due to the lack of sufficient pressure head to force oil into the depleted regions. Two theories exist. The first postulates that a conventional hydrodynamic oil journal bearing may not operate properly in a vacuum. Without atmospheric pressure, there may be insufficient pressure to feed oil into the depletion regions. The second theory postulates that with an adequate oil supply, the cohesive forces (surface tension) within the oil will provide sufficient pressure to feed oil into the bearing.

Alternatives exist if the latter theory does not prove valid. These include:

> Seal and evacuate the rotor and operate the bearings at atmospheric pressure. This alternative would require extensive modification of the outer rotor structure.
>
> Make a small viscous pump an integral part of the bearing; designing a pump into the bearing would require more design effort, relatively extensive testing and very complex bearing manufacturing.
>
> Design and install a small piezoelectric or magnetostriction pump within the bearing. Piezoelectric or magnetostriction pumps are novel devices and are poorly understood. Again extensive design and experimental effort would be required.
>
> Operate the sensor as a whole at some reduced pressure where the bearings can still operate properly. The rotor would be crudely sealed but not evacuated. Operating the sensor at a reduced pressure, but not a hard vacuum, would require considerable testing and some rotor modification. However, this alternative is the least complex of all if it can be made to work.

In summary, there are two areas of uncertainty and we have given them due consideration. However, they are only considered possibilities, and not probabilities at this time. The necessity to further consider alternatives is not required until the next bearing test program has been completed.

III. RGG LABORATORY TEST PROGRAM

The second major part of this two-month program has concerned the evaluation of the RGG Sensor in the rotating mode. The more significant tests and findings are described in the following paragraphs.

A. Spin Bearing Alternatives – Near Term

As described in the Final Report under Contract F19628-72-C-0222, the original hydrodynamic oil bearing had been damaged by operation with insufficient lubricant. As an expedient, the RGG sensor was then successfully demonstrated using commercially available, Class No. 7 ball bearings.

At the outset of this contract, the near-term spin bearing alternatives were reviewed. It was determined that new, better quality ball bearings could not be purchased without undesirable time delays needed for a special procurement. Further, it was calculated that better ball bearings would offer noise improvements of no better than a factor of 3.

Interim journal bearings were considered. Because of the urgent need for bearings, the time span to design, manufacture and test was insufficient to produce the quality bearing required. Compromises would have resulted in producing bearings of marginal performance and a possibility that the bearings would be noisier than ball bearings.

Use of the existing, damaged bearings was then considered. Minor modifications, rework and filling tests were considered. After deliberation, we concluded there was an excellent chance that the original hydrodynamic journal oil bearings could be made to operate sufficiently well for reasonable periods of time.

In view of these alternatives, the latter course was chosen. First, the burrs on the pintles, caused by the seizure, were polished. Next, the oil reservoir hole in the pintle of bearing No. 1 was plugged. The bearing and RGG rotor were then vented at all points of possible air entrapment.

Fill tests were then conducted as described below. The end result of these efforts is also described below. It will be shown that within seven weeks from the start of this contract, the Prototype RGG Sensor was successfully demonstrated as a mass detector.

B. Spin Bearing Fill Tests

The damaged spin bearings were utilized in a series of tests to determine if the bearing could be filled with degassed lubricant without creating voids or air pockets. It was determined that due to dimensional tolerances, the correct volume of oil could only be determined experimentally.

The fill tests consisted of filling the bearing repeatedly, using increasing amounts of oil, until an overflow condition was created when the pintle and bearing were assembled. For serial No. 1, the amount of oil required to just fill the bearing is 30 microliters.

Although the fill seems to be correct, bearing No. 1 lost a significant amount of lubricant when operated in a vacuum in the vertical spin axis orientation and located at the top end of the sensor. In the above condition, the bearing acts as a cup with no gravitational or capillary forces tending to empty it. The fact that lubricant is lost under the foregoing conditions implies the existence of an entrapped air bubble, in spite of the apparent good fill, or that the Nyebar-capillary seal cannot accomplish the sealing function.

The design of the new bearing, described in Section II of this report, recognizes these problems with the original hydrodynamic journal bearing design. Specifically, the new bearing is directly vented to the pintle atmosphere through a liquid trap to prevent loss of fluid caused by bubbles formed during the evacuation process. Also, the new design will not utilize the capillary seal-Nyebar combination, instead a lip seal will be used. The attention given to these recent design changes is expected to solve the major shortcomings of the original design.

C. Hybrid Bearing Program

An effort was made to salvage the less damaged hydrodynamic spin bearing (serial No. 1) and evaluate its performance in the RGG. To accomplish this, we decided to install the hydrodynamic oil journal bearing (serial No. 1) at the top end of the vertically oriented RGG sensor. At the bottom end we installed one of the commercial ball bearings. This specific arrangement allowed the noncritical ball bearing to carry the axial load of the RGG rotor and the oil bearing was located in the least demanding attitude.

The RGG sensor was spun up and immediately tested for output bias and noise. Compared with the prior results obtained with ball bearings at each end of the spin axis, the results were dramatically improved. The bias was reduced by a factor of 3 to 5 and the noise was reduced by a factor of 10. For the first time, meaningful demonstrations of gravity gradient sensitivity could be performed with the Prototype RGG.

The factor of improvement was most welcome and quite reasonable. It is well known that with an opposed pair of ball bearings, as they were being used during the April 1975 demonstrations, the bearing torque noise is dependent upon: (1) the ball size match, (2) the contact angle, and (3) the contact angle match. Since our ball bearings were standard commercial items, good matching would not be expected. Thus, when one ball bearing was removed from the spin axis, the mismatch condition no longer existed. Only the inherent no[illegible]one ball bearing remained.

D. RGG Performance Results

The first operation of the RGG under rotation conditions occurred toward the end of our previous contract effort. Because of damage to the oil journal bearings originally designed for the sensor, it was necessary to operate the RGG on a temporary substitute set of ball bearings. Although the ball bearings were of highest quality (Class 7), they were obviously going to be much noisier than the oil journal bearings because of the ball and race design. The initial performance of the RGG on the ball bearings, shown below, was relatively good despite the high (audible) bearing noise, indicating that the sensor balance was good enough to reject most of this noise.

Horizontal Orientation	Per Channel
Bias	200,000 EU
Trend	(Not measured, but high)
Noise at 10 sec	300 EU

Vertical Orientation	
Bias	20,000 EU
Trend	(Not measured, but high)
Noise at 10 sec	300 EU

Our first few weeks of effort on this contract were spent becoming familiar with the effects of variations in the sensor parameters on sensor performance, and adjustments to the bearings themselves. The initial set of ball bearings became significantly more noisy in a short time, indicating that some damage had been done during assembly. A new ball bearing set was installed, with care taken not to introduce excessive loads on the balls during press fit procedures. The bearing preload was varied and its effect on bias and noise determined. Adjustment was made to the speed control servo gain and damping to reduce torque noise. After this procedure, the sensor performance figures improved somewhat.

Toward the end of May, the following performance characteristics were obtained:

Horizontal Orientation	Per Channel
Bias	150,000 EU
Trend	1,000 EU/hour
Noise at 10 sec	300 EU

Vertical Orientation	Per Channel
Bias	3,000 EU
Trend	200 EU/hour
Noise at 10 sec	300 EU

The effort to optimize the RGG on ball bearings is seen to have reduced the bias and trend levels significantly, but it essentially had no effect on the short-term noise level. The trend was due to both thermal effects and the slow deterioration of the ball bearings with time. Although the trend was not so large as to prevent fairly long (4 hours) data runs, it was large enough to make it very difficult to carry out the time consuming shake tests required to further balance the sensor.

Efforts to reduce the trend and short-term noise continued. Many variations of bearing position, orientation and preload were tried on the ball bearings. A number of new bearing sets were installed in an attempt to select a quiet pair. Variations in the orientation of the sensor in the horizontal position were made by rotating different sides of the stator to the "down" direction. All these variations produced only small variations in the RGG output. The horizontal bias could be varied about 20%, but no significant change in noise level could be obtained. The long-term trends still were large enough to make any further attempt at fine balancing of the sensor unfeasible.

As discussed in the previous section, one of the damaged oil journal bearings was then cleaned up and used to replace one of the ball bearings. The damaged oil bearing would not work in the horizontal orientation, but did work well in the vertical spin axis orientation. The short-term noise level of the sensor dropped significantly. This is demonstrated in Fig. 6 which shows the response of the RGG sensor to a 35 kg test mass placed nearby. The resultant 400 EU signal is easily seen above the 50 EU short-term noise level.

4288-7

- ROUGH BALANCED
- BALL BEARING PLUS REWORKED OIL BEARING

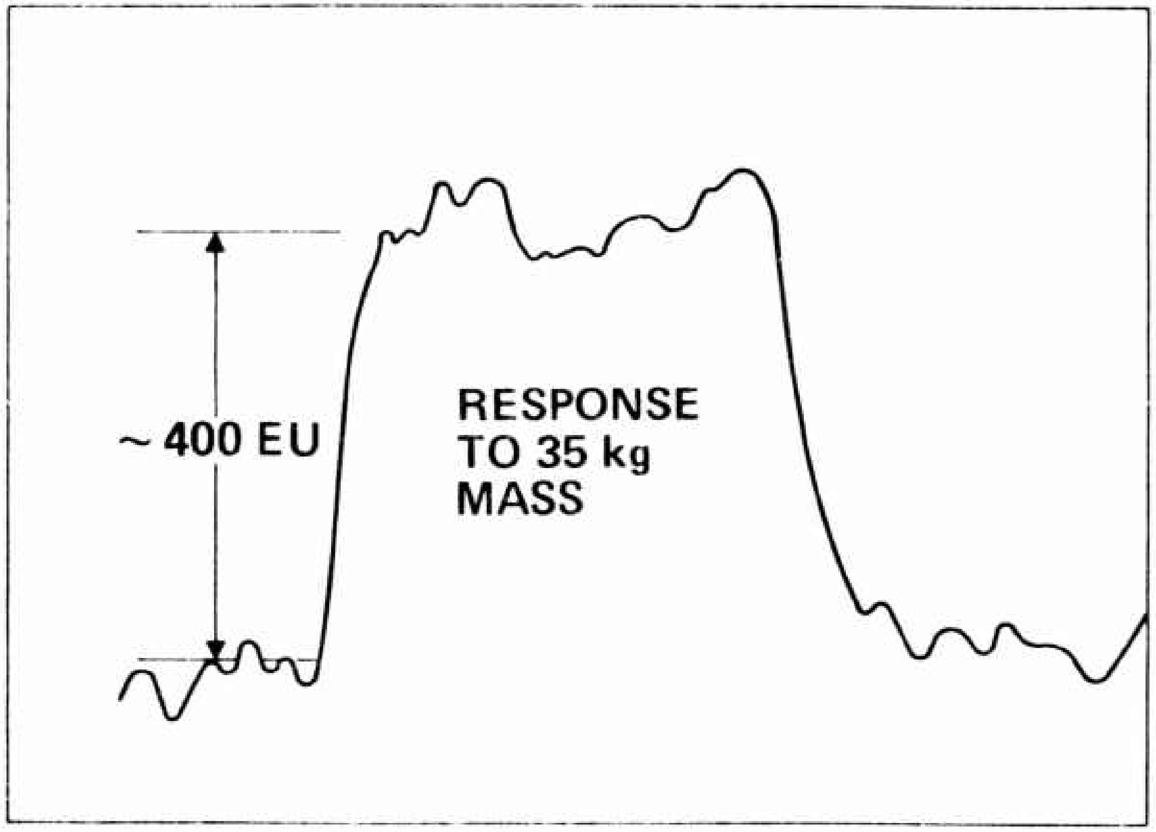

7500 EU BIAS
50 EU AT 10 sec NOISE

Fig. 6 RGG Noise Performance.

The present performance of the sensor on the hybrid bearing pair (in the vertical orientation) is:

Bias: 4,500 EU

Trend: 100 EU/hour

Noise at 10 sec: 50 EU

The trend has improved somewhat but is still large enough to cause some problems with balancing tests. A 90 min trace of the sensor output showing the small trend is shown in Fig. 7. The trend variations are seen to be of the same magnitude as the short-term noise. Since the hybrid bearing does not work well in the horizontal position, the shake tests and further balancing of the sensor will have to be postponed until the new oil journal bearings are available.

The short-term noise of 50 EU is the variation in the output of an individual channel. If this output were combined with the outputs of other sensors in a system, this 50 EU level of sensor noise would contribute only 25 EU error to the calculation of the components in the gravity gradient tensor.

Because of the large drop in the noise level when one of the ball bearings was replaced, and because of the excellent results of the non-rotating noise tests, we feel that the present source of noise is generated by the remaining ball bearing (coupling through the residual unbalance errors in the sensor). This 25 EU system noise contribution measurement gives us a confident measure of the upper bound to all the remaining error sources. Replacement of the present bearings with the new oil journal bearings, presently under fabrication, should eliminate this last major error source and will result in RGG sensor performance approaching our 1 EU goal.

E. RGG Partial Disassembly

In order to make some of the changes mentioned in paragraph A above, it was necessary to partially dismantle the RGG sensor. While the electronics were exposed, the "Cap-Driver" circuits were tested

4288-8

- ROUGH BALANCE
- BALL BEARING PLUS REWORKED OIL BEARING
- NO THERMAL BLANKET

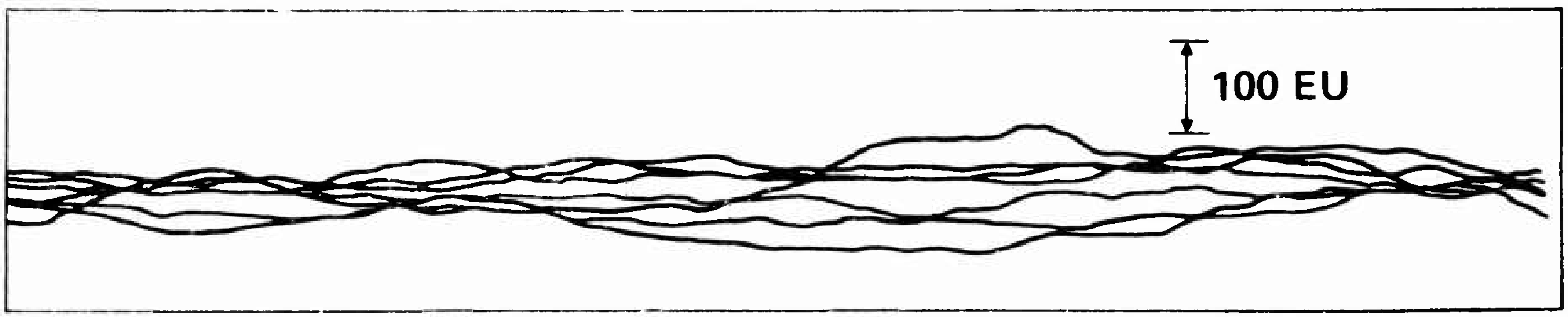

DRIFT OVER 90 min

Fig. 7. RGG Drift Performance

and modified. Due to pick-up and interference, this circuit had been operating erratically. Minor filtering and by-pass capacitors were added to the circuit. With these changes the circuit operated perfectly on the bench.

When the sensor was reassembled and tested as a unit, it was found that there are conditions that occasionally cause erratic operation; however, the system is considered usable at this time. The next time the sensor is dismantled, additional shielding will be provided to achieve the desired degree of perfection.

Also, while the sensor was dismantled, it became possible to examine the leads to the electrolytic balance tubes. The two sets of balance tubes on Arm No. 2 were tested for continuity – each set has eight tubes in series – and it was found that both sets were open. We do not know the cause of this failure, although it may have been caused by the rapid deceleration of the rotor when the bearing seizure occurred. Since the individual tubes are located in a relatively inaccessible position on the sensor, it was impossible to diagnose the condition of the individual tubes. It would have required a considerable amount of extra time to dismantle and reassemble the sensor just to properly inspect the tubes. Such action was not believed to be expedient at this time.

In the next phase of the program when the sensor is completely dismantled for anisoelastic trimming, the condition of the balance tubes will be fully evaluated.

F. Speed Control Servo and Bearing Torque Tests

Use of the hybrid bearing combination, described in paragraph III-C, has allowed us to make further evaluations of the RGG Sensor speed control servo. Every measurement that we have been able to make continues to indicate that the speed control is meeting all of its performance requirements. This performance is demonstrated in Fig. 8 which is explained in the following paragraphs.

```
HEA

 6, 4,75   17:37   TNO  1 BIAS 3600.0000      0.0       0.0      0.0000
MI-M8= 137. 120. 126.  87. 174. 181. 220. 163.
ARM1 0.5029 0.7368   ARM2 0.5133 0.5050    TU-FAC     14400.
LAST BAL   3, 6,75    10:28.  SPEED  563000.00 0.01   2W =   35.5240
SERVO  0.010   1.000  GAIN     11.34615    FAC     0.0937300

COND        COS          SIN         MAG        PHA    FM-CAR       OCT.PEP

OCT CLK   4836   4852   4836   4821   4841   4843   4847   4835

OCT CLK AVE

OCT CLK   4837   4853   4836   4820   4842   4842   4848   4834
OCT CLK   4836   4852   4836   4820   4841   4842   4849   4834
OCT CLK   4838   4853   4836   4821   4841   4842   4849   4834
OCT CLK   4836   4852   4837   4821   4840   4843   4849   4834
OCT CLK   4836   4852   4836   4822   4840   4843   4849   4834
OCT CLK   4836   4852   4836   4822   4841   4842   4849   4834
OCT CLK   4836   4852   4836   4820   4842   4843   4849   4834
OCT CLK   4836   4852   4836   4821   4842   4842   4849   4835
OCT CLK   4836   4852   4836   4821   4840   4843   4848   4835
OCT CLK   4836   4852   4837   4821   4841   4842   4849   4834
OCT CLK   4837   4853   4837   4821   4842   4842   4849   4834
OCT CLK   4836   4852   4836   4821   4841   4843   4849   4834
OCT CLK   4836   4852   4837   4820   4841   4844   4849   4835

O.C.ERRS      976=N       2.6 -13.1    2.9   17.9   -1.9   -3.9   -9.5    4.8
EA SD=      0.81
M1........,M8              7.    -6.    -3.    15.    13.     9.    -0.     5.
```

Fig. 8. Speed Control Performance

This computer print-out is part of the computer program that calculates the encoder disc slot corrections. The computer first reads the speed command in the heading (SPEED 563000. 00). This number represents the number of 10 MHz reference counts desired during one rotor revolution. The computer divides this by 8 to find the desired number of counts per eighth revolution (octant). Then, once every 35 revolutions, it prints out the actual octant count read in each of eight sequential octants during one revolution. Since computer printing speed and space are limited, the octant count has a count of 2^{16} substracted before the residual is printed. In this example, the ideal print-out would be 4839. The important thing for servo analysis is not whether the printed value is 4852 or 4836, but the variation in the last digit in each column. The off-sets merely indicate that the slot corrections had not been inserted exactly before the test was started. The last digit variation indicates the measured octant count variation in 1.1×10^{-5} rad increments, on a sampled basis. The largest variation in any column is ±1 count, which is within our instantaneous position error specification.

Bearing torques have been measured both by measuring servo motor voltages and by measuring rotor run-down times. No actual measurements have been made of the servo motor characteristics or the polar moment of inertia of the RGG rotor. However, using nominal values for these, the two methods correlate quite well and provide torque information in the range expected. In the future, both of these will be calibrated more accurately.

G. 3ω and 4ω Test Signal Implementation

Precision sine wave test signals, phase-locked to the sensor rotation phase, are required at three and four times the sensor rotation frequency to enable us to measure and separate the gradiometer error coefficients. One and two omega test signals were provided as a part of the original system design. These latter signals are generated by means of a flip-flop counter chain activated by, and synchronized with, the gradiometer slot corrected photocell output pulses. The phase of the square waves thus generated is accurate to $\pm 1.1 \times 10^{-5}$ rad.

A 4 Ω square wave was also generated as a part of the above-mentioned counter chain. This signal was then filtered, passed through a buffer amplifier and brought out to external terminals. A 3 Ω signal cannot be generated directly from an 8-slot encoder disc, but the 1 Ω square wave has a relatively large 3 Ω component and this component is inherently phase-locked to the 1 Ω. The 1 Ω signal was passed through a double section filter, amplified and brought out to external terminals.

These new signals, along with the original ones now provide 1, 2, 3 and 4 omega square and sine waves all available at 1.0 or 0.01 V levels. These signals have proven to be very useful during test and calibration of the gradiometer.

H. Thermistor-Temperature Computation

It was mentioned in paragraph III-B above that, by use of an external signal and the sensor logic, we could monitor the internal temperature of the RGG sensor. This is accomplished by applying a two omega square wave to the RGG sensor "Cap-Driver" terminals. This square wave triggers an internal high speed bi-stable multivibration in exact synchronism with the applied input wave. The output of the internal multivibrator applies the regulated sensor voltage to two resistance voltage dividers. One of these dividers is a pure resistance and the other is a resistance plus two Fenwall Type FA41J1 thermistors in series. The two thermistors at 25°C have a resistance of 20,000 Ω.

By means of the RGG sensor logic, the output of either of these voltage dividers can be printed on the computer. Thus, we can monitor either the internal regulated voltage or the internal temperature.

Since thermistors have good stability and repeatability but poor tolerances on their initial resistance and temperature coefficient of resistance, it has been necessary to calibrate the thermistors in the sensor. This was done by letting the sensor stabilize at two different precisely known temperatures, activating the sensor and alternately measuring the indicated temperature and regulated voltage. The regulated voltage varies slightly during warm-up transient. These data were plotted on a time scale and the curves extrapolated back to the indicated initial values. These curves are repeatable to about $0.2^{\circ}F$.

The nominal equation for thermistor resistance versus temperature is shown below. It is recognized that when using this equation, a slight error is introduced because the thermistor is part of resistor-thermistor voltage divider. However, this error is negligible at the small temperature differentials (10 to $20^{\circ}F$, $5.5^{\circ}C$ to $11^{\circ}C$) associated with the RGG temperature rise

$$\Delta T = \frac{\ln R_o - \ln R_x}{K}$$

where

R_o = resistance at the reference temperature

R_x = resistance at existing temperature

K = temperature coefficient of the thermistor

ΔT = temperature rise above the reference temperature.

Since R_o is known for two different temperatures, the equation can be solved for the temperature coefficient K. The final form of the practical equation is

$$\Delta T = \frac{\ln \left(\frac{964}{1172}\right) - \ln (R_x)}{0.02318} \; {}^{\circ}F$$

where

ΔT = temperature rise above $90^{\circ}F$ ($32.2^{\circ}C$)

$$R_x = \frac{\text{Temperature monitor print-out value}}{\text{Voltage monitor print-out value}}$$

The first factor is obviously "R_x" for 90°F. This is the most compact form of the R_o term for the accuracy needed. Although the above equations provide the most accurate indication of the internal sensor temperature, Table 1 provides a convenient approximation. It is based on the assumption that the stabilized voltage monitor output is 1160 units.

Table 1. Internal RGG Sensor Temperature versus Temperature Monitor Reading

Temperature °F	Temperature °C	Temperature Monitor
90	32.22	954
91	32.77	932
92	33.33	911
93	33.88	890
94	34.44	870
95	34.99	850
96	35.55	830
97	36.11	811
98	36.66	793
99	37.22	774
100	37.77	757

During future experiments, the calibration and tabulation will be extended to include all of the possible operating points. Also, we will be able to determine the nominal operating speed (sensor resonant frequency) from the same chart.

I. Sensor and Electronics Noise Tests

The RGG Sensor System speed and signal processing control concept is based on utilization of the pulses of light generated by the photocell-encoder disc, to control the sensor speed and provide a signal demodulation reference. The photocell output pulses occur at a rate of approximately 140 per second. Every eighth pulse is wider than the others to provide a phase reference. If the system receives a continuous string of pulses that meets the system requirements from any source whatever, the computer and servo system operate normally.

It is a simple matter to generate a simulated string of electronic pulses by use of a precision voltage-controlled oscillator acting as an electronic servo. W th such a simulated servo method, it is possible to measure the sensor output even though the RGG is not rotating. When this is done, we obtain a system noise test that includes the following noise sources:

- RGG Sensor thermal noise
- Transducer
- Electronic amplifier
- Electronic analog to digital conversion
- Data Processing
- Linear and angular vibration environment at two omega
- Simulated servo

These noise tests exclude the following important noise sources of an operating sensor: bearings, sensor servo, data processing of large signals, linear and angular vibration at 1, 3 and 4 omega, and resonant frequency shift. The noise due to these remaining sources can be tested as soon as precision spin bearings become available.

The results of two non rotating noise tests are shown in Figs. 9 and 10. In the first test, the spin axis of the sensor was vertical; in the second the spin axis was tilted 45° off vertical. The averages of both the cosine and sine terms are 0.1 EU or less, and the standard deviation of this short term noise is approximately 0.6 EU per channel in both tests.

In an operational system, consisting of three RGG sensors, this 0.6 EU noise level would contribute only a little more than 0.3 EU error to the calculations of the components in the gravity gradient tensor. This 0.3 EU measurement is in close agreement with the calculations for the contribution of thermal noise errors to the determination of the gravity gradient components, indicating that during these nonrotation tests, our system had reached the thermal noise limit. Thus, these results are considered to be entirely satisfactory and well within the design goals of the system.

HEA

```
 6,30,75  10:20  TWO  1 BIAS  360.0000     0.0      0.0      0.0000
 M1-MS=   0.   0.   0.   0.   0.   0.   0.   0.
 ARM1 0.5029 0.7368   ARM2 0.5208 0.5088   TU-FAC   14400.
 LAST BAL  3, 6,75   10:28.  SPEED  561000.00 0.01  2W =  35.6506
 SERVO  0.010  1.000  GAIN   11.34614   FAC   0.0937300

 COND     COS      SIN      MAG     PHA    FM-CAR     OCT.PER

 =
 S.L. CLEAR
 COEF=    0.0749838

ON ELECTRONIC SLOTS, MOTOR NOT RUNNING.  TABLE ON AIR, VAC LESS
THAN 1 MICRON, PUMP NOT RUNNING.  RF 5.0 VOLTS RMS.

SPEED OK FOR OVERNIGHT 90 DEG SOAK.   WILL TEST SYSTEM NOISE.

 2V AVE
```

2V245	-1.1	-1.1	1.6	-136.7	264692.3	4577
2V245	0.1	-1.6	1.6	-86.1	264680.4	4590
2V245	0.6	-0.5	0.8	-39.3	264674.1	4582
2V245	0.2	-0.1	0.3	-31.8	264659.9	4571
2V245	0.4	-0.3	0.5	-41.5	264656.6	4582
2V245	0.2	0.2	0.3	47.7	264659.4	4586
2V245	-0.1	0.1	0.2	135.0	264667.8	4586
2V245	-0.3	0.0	0.3	175.6	264677.9	4594
2V245	0.2	0.1	0.2	40.9	264635.1	4585
2V245	-0.3	0.2	0.4	144.5	264689.9	4584
2V245	-0.7	0.2	0.7	160.5	264696.1	4595
2V245	0.0	0.5	0.5	90.0	264698.7	4601
2V245	-1.0	0.4	1.1	157.6	264686.2	4582
2V245	-0.8	0.9	1.2	133.6	264672.3	4605
2V245	-1.2	0.1	1.2	176.8	264665.8	4595
2V245	-0.2	0.4	0.5	117.1	264650.5	4597
2V245	0.6	-0.0	0.6	-3.8	264641.4	4589
2V245	0.5	-0.0	0.5	-3.7	264640.1	4585
2V245	0.8	0.4	0.9	23.7	264638.3	4591
2V245	0.3	0.9	1.0	72.4	264630.1	4575
2V245	0.7	1.7	1.8	68.8	264622.2	4591
2V245	-0.7	1.2	1.4	118.4	264615.7	4597
2V245	1.1	-0.4	1.1	-22.5	264609.1	4575
2V245	0.3	0.1	0.3	24.1	264604.8	4575
2V245	0.1	-1.0	1.0	-83.1	264602.9	4573
2V245	0.4	-0.2	0.4	-21.0	264601.9	4573
2V245	0.3	-0.1	0.3	-18.4	264596.9	4591
2V245	0.1	0.8	0.8	84.7	264597.7	4574
2V245	0.3	1.2	1.3	76.4	264598.8	4570
2V245	-0.7	1.6	1.8	113.7	264596.7	4601
2V245	-0.4	0.3	0.5	141.7	264591.9	4585
2V245	0.7	-0.5	0.8	-34.7	264587.6	4601
2V245	0.5	-0.1	0.6	-12.2	264579.4	4580
2V245	0.7	-0.2	0.7	-14.5	264578.4	4576
2V245	-0.7	-0.1	0.7	-168.3	264575.3	4590
2V245	-0.1	-0.4	0.4	-100.7	264573.2	4603
2V245	-0.3	0.2	0.4	145.5	264558.4	4596

```
 2V AVE  37=N      0.0=C     0.1=S      0.57=SC     0.67=SS
                   0.1=MAG  0.88=SMAG            85.3071=PHA
```

Fig. 9. System Noise Test (Vertical)

HEA

6,30,75 10:49 TNO 2 BIAS 360.0000 0.0 0.0 0.0000
M1-M8= 0. 0. 0. 0. 0. 0. 0. 0.
ARM1 0.5029 0.7368 ARM2 0.5208 0.5088 TU-FAC 14400.
LAST BAL 3, 6,75 10:28. SPEED 561000.00 0.01 2W = 35.6506
SERVO 0.010 1.000 GAIN 11.34614 FAC 0.0937300

=

SAME AS TNO 1 EXCEPT THAT SENSOR IS NOW TILTED 45 DEG OFF VERTICAL.
TNO 1 +K WAS DOWN. NOW +K -135 DEG ABOUT +J. REVLED EAST.

2W AVE

COND	COS	SIN	MAG	PHA	FM-CAR	OCT.PER
2W245	-0.7	0.2	0.3	155.6	264271.8	4602
2W245	0.4	0.4	0.6	45.0	264273.7	4560
2W245	0.6	1.7	1.9	69.0	264269.9	4572
2W245	0.3	0.3	0.4	50.9	264262.4	4611
2W245	-1.6	-0.1	1.6	-175.3	264263.4	4533
2W245	-1.1	-0.4	1.1	-161.9	264263.0	4534
2W245	0.3	-1.4	1.4	-79.5	264263.1	4534
2W245	1.0	0.7	1.2	35.4	264265.7	4585
2W245	-0.7	-0.2	0.8	-164.1	264262.0	4568
2W245	0.2	0.1	0.3	12.3	264259.9	4599
2W245	0.2	-0.3	0.3	-60.9	264254.2	4563
2W245	-0.1	-0.9	0.9	-97.1	264255.4	4611
2W245	0.1	0.0	0.1	8.1	264252.7	4589
2W245	0.5	-0.2	0.6	-19.3	264247.2	4584
2W245	0.4	0.5	0.7	43.9	264249.6	4586
2W245	-0.1	0.3	0.3	114.1	264249.9	4590
2W245	-0.5	0.7	0.8	124.7	264245.5	4573
2W245	-0.2	0.3	0.3	105.0	264236.1	4568
2W245	-0.2	-0.4	0.5	-120.1	264231.9	4593
2W245	0.4	-0.2	0.4	-31.0	264227.3	4613
2W245	0.9	0.5	1.1	29.6	264227.4	4594
2W245	-0.2	0.1	0.2	133.3	264231.2	4603
2W245	0.6	-0.1	0.6	-11.3	264230.1	4580
2W245	-0.2	0.4	0.4	119.9	264230.9	4605
2W245	-0.4	0.1	0.4	167.0	264236.6	4594
2W245	0.3	-0.2	0.3	-29.7	264239.6	4592
2W245	0.0	-0.2	0.2	-84.8	264243.1	4586
2W245	-0.0	-0.0	0.0	-135.0	264251.9	4607
2W245	-0.1	0.2	0.2	131.2	264255.3	4584
2W245	-0.6	0.4	0.7	143.8	264261.8	4591
2W245	-0.4	-0.7	0.8	-120.7	264264.8	4599
2W245	0.8	-0.1	0.8	-6.7	264265.3	4603
2W245	-0.1	-0.8	0.8	-97.9	264265.4	4598
2W245	1.8	-0.9	2.0	-25.2	264259.6	4615
2W245	0.2	-0.2	0.3	-45.0	264260.1	4614
2W245	0.4	-0.0	0.5	-2.7	264250.1	4604
2W245	1.0	0.1	1.0	3.1	264246.1	4580
2W245	0.3	0.1	0.3	11.3	264242.4	4585

2W AVE 38=N 0.1=C 0.0=S 0.62=SC 0.54=SS
0.1=MAG 0.82=SMAG 6.3026=PHA

Fig. 10. System Noise Test (45° Tilt)

IV. CONCLUSIONS AND RECOMMENDATIONS

The objectives of this contract were met. First, the engineering services and full cooperation of Shaker Research Inc. were promptly directed toward the bearing problems. This expedited action resulted in a new design and second-tier subcontracts for the manufacture of the newly designed bearings. Further, the funds have been fully committed in an FFP contract to Shaker Research for test and analysis of the first pair of bearings and subsequent manufacture of the second pair.

Second, the work on improving the RGG sensor performance, and studying the error sources resulted in rapid improvement of noise performance. Further, the nonrotating noise test confirmed that the only significant noise source in the signal processing chain was the mechanical thermal noise of the RGG structure.

The rotating sensor tests strongly indicate that the remaining major error noise source is introduced by the substitute ball bearings. The 25 EU system performance demonstration puts a strong upper bound on all other rotation-dependent noise sources.

The evidence produced by this two month follow-on effort is sufficient to warrant acceleration of the development program in FY 76 and beyond. Many tasks remain before the RGG will have demonstrated the rotating performance objectives in the laboratory environment. First among these tasks is the need to verify the operation of the new bearing configuration. Once this requirement is satisfied, rotating tests will then be continued. Effort can then be directed toward evaluation and reduction of the anticipated, remaining smaller sources of noise.

Other near-term tasks should include the fabrication of a second RGG sensor, additional error analyses, and preliminary investigations of several aspects of moving vehicle requirements, including inertial platform technology.

APPENDIX

DESIGN/CONSTRUCTION/TESTING OF HUGHES RESEARCH LABORATORY GRAVITY GRADIOMETER BEARINGS

FINAL REPORT

MAY 1974

Prepared For:

Hughes Research Laboratory
3011 Malibu Canyon Road
Malibu, California 90265

SHAKER RESEARCH CORPORATION
Northway 10 Executive Park
Ballston Lake, New York 12019

DESIGN/CONSTRUCTION/TESTING OF HUGHES RESEARCH LABORATORY GRAVITY GRADIOMETER BEARINGS

FINAL REPORT

By

R. L. Smith
W. D. Waldron
C. H. T. Pan

Shaker Research Corporation

Technical Report

74TR4

May 1974

Prepared Under

Hughes Subcontract Number 01-188134-7

For

Hughes Research Laboratories
3011 Malibu Canyon Road
Malibu, California 90265

Preceding page blank

TABLE OF CONTENTS

APPENDIX I — Bonding Tests

APPENDIX II — Bearing Stiffness and Mean Square Error Analysis

APPENDIX III — Journal Film Thickness as a Function of Rotational Frequency

LIST OF ILLUSTRATIONS

LIST OF TABLES

1.0 INTRODUCTION

This report describes the work accomplished by Shaker Research Corporation on the detail design, manufacture, and testing of the bearings for the Hughes Research Laboratories moving base gravity gradiometer.

The work on the subject contract (work covered in this report) began with the production of the bearing detail manufacturing drawings. The actual bearing design analytical work had been accomplished prior to the subject contract. The starting point, or foundation, for the work described in this report is contained in Hughes Research Laboratoris "Bearing Specification" DS-1-473, Rev. 0 dated April 1973.

The objectives of the program (which are detailed in Section 2.0) were met in that the bearings met the performance objectives and that the methods required to retain the lubricant within the bearing for long periods of time (several months) were determined.

However, should it be necessary to operate the bearings in a vacuum environment (not an original program requirement), some unanswered questions with regard to air entrapment remain. Although investigation of the vacuum question was beyond the scope of the subject work, it is our conclusion that suitable modifications to the filling procedures described in this report will make vacuum operation possible.

The conclusions drawn from the program and recommendations with regard to procedures and application of the bearings to the gradiometer are contained in Section 3.0. Detail bearing and test equipment descriptions are contained in Sections 4.0 and 5.0. Test results are described in Section 6.0.

2.0 PROGRAM OBJECTIVES

The primary objectives of this program were to:

1. Prepare a detailed set of manufacturing drawings for the prototype gravity gradiometer bearings.
2. Fabricate and assemble the bearings in a "simulated" rotor gradiometer test rig.
3. Determine the following specific bearing characteristics:
   a. Break away torque,
   b. Running torque,
   c. Stiffness, and
   d. Temperature rise.
4. Perform lubricant tests to establish:
   a. Required seal clearance,
   b. Effectiveness of barrier films,
   c. Filling procedure,
   d. Flow patterns within the bearing, and
   e. Potential problem areas.

3.0 CONCLUSIONS AND RECOMMENDATIONS

The conclusions drawn and recommendations made based upon the results of the work conducted on this program are outlined in the following paragraphs. These are divided into the categories:

Detail Design and Manufacture

2. Bearing Performance

3. Lubricant Retention and Filling.

Detail Design and Manufacture

1. Critical bearing and mounting surface geometries (roundness, flatness, squareness, concentricity) met the general print requirements of 5 μ inches TIR max. However, because of available (stare-of-the-art) metrology equipment limitations, no conclusion as to how much better than 5 μ inches the finished parts actually were can be made with confidence. This is especially true in trying to discern the magnitudes of the second and third harmonic run-outs.

2. Finished spiral groove depths did not, in all cases, meet the print tolerances and depth variations were greater than had been anticipated. These deviations, however, did not produce a significant effect on the bearing system performance with respect to torque and stiffness.

   Two factors with respect to the effect of groove depth on bearing performance should be mentioned here. First, the groove depth specified on the drawings was near the theoretical optimum, that is the depth that would result in the maximum stiffness. Deviations from the optimum depth would be expected to result in a reduction in stiffness; with increasing groove depths producing a smaller reduction in stiffness as compared to corresponding deviations from optimum on the small side. Since the actual groove depths were all larger than the optimum (print specification), only small reductions in stiffness were anticipated, and as is indicated in Paragraph 6.1.2.2, the measured stiffness did exceed the specification minimum. Additionally, deep grooves lead to reduced torque, which is in the desired direction.

The second factor has to do with bearing induced vibration and torque noise. To minimize these, it was necessary to maximize stiffness, and to minimize the geometrical irregularities of the bearing (rotating) member. As was indicated above, the groove depth deviation did not cause a reduction in stiffness to below the specification minimum. Furthermore, since the grooves are on the stationary member, variations in their depth will not cause variations in force or torque as a function of bearing angular position, thus will not induce vibration or torque noise.

3. The technique of using an adhesive to bond the thrust bearing components to the journal bearing proved to be effective and certainly eased manufacture. However, a problem did persist in maintaining a long lasting bond between the aluminum thrust bearing and the experimental glass journal bearing because of thermal stress problems which might cast some doubt on the ultimate reliability of an aluminum to aluminum bond. For peace-of-mind, a preloaded spring, or an epoxy encapsulate between the thrust support plate and rotor could serve as a back-up support in the unlikely event of an aluminum to aluminum bond failure in the actual gradiometer bearing system.

4. In any redesign, elmination of the current button thrust runner should be considered to further ease manufacture. This could be accomplished by shortening the bearing and using the current support plate as the thrust runner.

5. The magnitude of bearing and seal mounting screw torques appeared to have only a second order effect on bearing distortion. The controlling factor was the relative flatnesses and cleanliness of the mating surfaces.

6 The manner in which the bearing test rig was constructed along with the various assembly procedures employed made assembly and disassembly operations relatively straightforward. The gradiometer designer is encouraged to review those sections of this report pertaining to rig design, inspection, and assembly operations.

Bearing Performance

1. The bearings met the specification torque and stiffness requirements at design speed (1050 RPM) over the load range of $\pm$ 1g.

2. Design operating specification performance can be met using a lubricant having a viscosity between 12.5 and 20.7 cs.

3. If prolonged operation at 3 g loads are anticipated, the higher viscosity oils should be used to provide more margin to the thrust bearing.

4. Thrust bearing total axial clearance could be increased from the current 200 ± 50 μ inches to 526 μ inches max. and still meet the "average" stiffness requirement of 57,000 lb/in. From a gradiometer standpoint, this would ease assembly and minimize differential thermal expansion problems.

Lubricant Retention and Filling

1. A non-wetting barrier film such as Nyebar should be employed in the seal area immediately adjacent to the bearing to discourage lubricant creepage from the bearing.

2. When treated with Nyebar, radial seal clearances of up to 4 mils appears acceptable. However, smaller clearances (1 mil) are recommended to give a greater margin of safety.

3. A bearing filling procedure was developed (and is discussed in detail later in this report) which should be adequate for the actual gradiometer application -- provided the rotor is NOT to be operated in a vacuum environment.

4. Tests with the glass bearing revealed that air could become entrapped in the unloaded region of the journal bearing clearance. The entrapped air did not detrimentally affect the bearing performance. From the experiments that were performed, no conclusions could be drawn as to whether the entrapped air came from desolved gas in the lubricant or from the ambient adjacent to the seal. However, it is clear that further experimentation would be appropriate if it is intended to operate the rotor in a vacuum environment.

5. As it is possible to inadvertantly overfill the bearing (causing a drop or two of oil to be expelled from the seal), some method of soaking up this excess oil should be employed. Inserting a cotton swab through the seal plate attachment screw access hole until it contacts the seal plate is one method of cleaning up any excess oil. In this case the rotor should be horizontal with the access hole in the "vertical down" position.

4.0 BEARINGS

This section identifies the reference documents describing the basis for the bearing design and describes the inspection and preassembly procedures that were employed prior to the mounting of the bearing into the test rig for performance testing.

4.1 Design

The final bearing design was based upon the procurement requirements generated by Hughes Research Laboratory. The bearing operational requirements of speed, load, stiffness and torque require maintaining several basic bearing physical characteristics over the intended operating temperature for proper operation. A full review of the bearing application, design criteria and typical analytical characteristics is contained in the following list of documents.

A. Hughes Prototype Rotating Gravity Gradiometer Procurement Specification Rev. A. No. AR-772, August 1, 1972.
B. Mechanical Technology Inc., Technical Report 72TR59, October 27, 1972.
C. Hughes Report, "Prototype Moving Base Gravity Gradiometer", January, 1973.
D. Shaker Research Corporation Technical Proposal EO-A-4-73.
E. Hughes Specification "Bearing Spec. DS-1-473", Rev. 0, April, 1973.

The detail design of the cylindrical pintle bearings for the gravity gradiometer are contained in Shaker Research Corporation drawing series 101 (see Appendix I).

4.2 Metrology

The production of the bearing parts and final test rig machining operations were accomplished by Athbro Precision Engineering Corporation in Sturbridge, Massachusetts. The inspection of the test rig and the bearing parts for alignment, roundness and squareness, as well as dimensional conformance was also carried out at Athbro. Applicable drawings and specifications were produced by Shaker Research. Critical measurements, such as the bearing roundness, squareness, mounting hole alignment and critical mating surface flatness were witnessed by Shaker personnel. A complete set of measurements of bearing components are included in Appendicies II and III.

It should be noted that the roundness charts shown in Appendix III have been copied on a Xerox copier and that there is a 15 percent distortion along one axis in the paper plane. Thus, the copied roundness charts of Appendix III should not be used for analysis or final checking of the bearing components. Only the originals or 1:1 copies can provide such data.

A critical examination of the original Indi-ron recordings reveal the bearing components to have roundness, squareness, and flatnesses within the specification tolerances (generally 5microinches) of the production drawings. These inspections (along with spiral groove depths) were made on the Indi-ron and Moore inspection machines. The major bearing components, as well as the two primary inspection machines, are shown in Figures 4.2.1 through 4.2.6. Figures 4.2.1 and 4.2.2 show close-up views of the main bearing components. Figures 4.2.3 and 4.2.4 are photos of the components being inspected on the Indi-ron and Moore machines respectively.

A pintle thrust surface flatness check which can be made quickly is illustrated by the photograph in Figures 4.2.5. Here, an optical flat is shown placed on top of the pintle thrust face and viewed under monochromatic light. Parallel interference bands appear at the glass interface. Since each band represents a gap change of 10 micro-inches, their parallelism and/or straightness can be used to determine flatness within 2.5 micro-inches. Although the light-to-dark band definition is not as well defined in the photo of Figure 4.2.5 as it is when viewed with the eye it is apparent that the pintle surface shown is flat well within 5μ in.

To determine the actual roundness, flatness, squareness, and concentricity from the indi-ron charts of Appendix III, it is necessary to overlay a transparent sheet having inscribed concentric circles of the same diameter as the indi-ron chart divisional markings over the actual indi-ron charts.

By moving the inscribed overlay in such a manner that two of its concentric circles envelope the measured "circle" on the actual indi-ron chart, the roundness or flatness of the subject feature can be determined. In addition, the location of the center of the subject feature relative to any other measured feature (on the same chart of appropriately referenced chart) can also be determined.

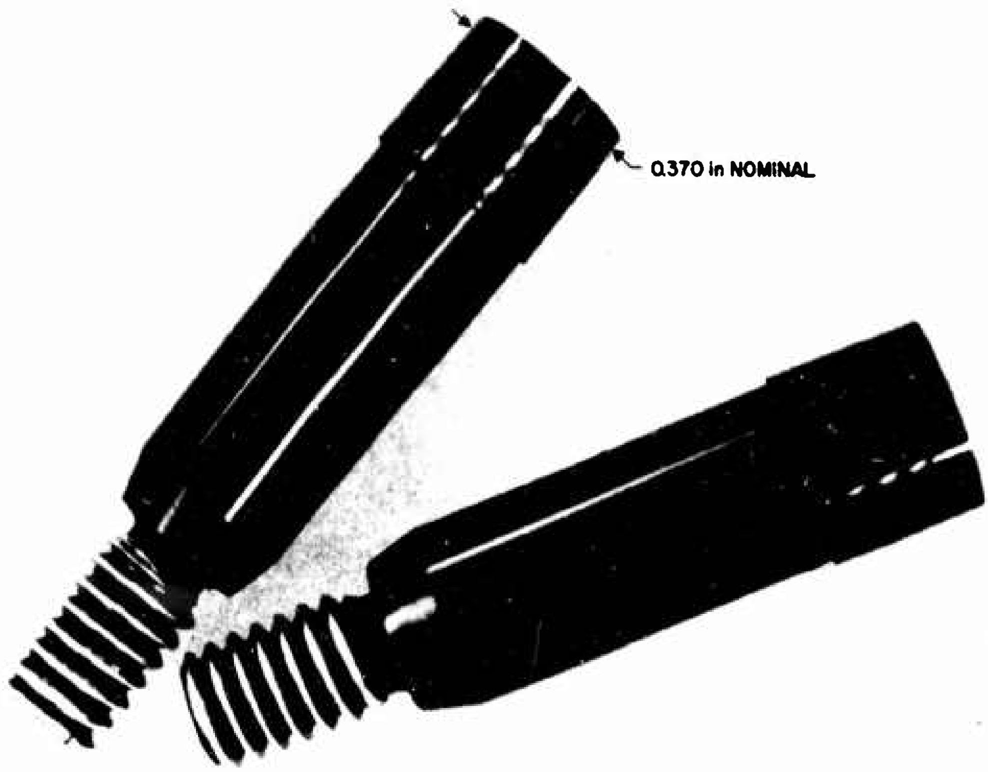

Fig. 4.2.1. Bearing pintles.

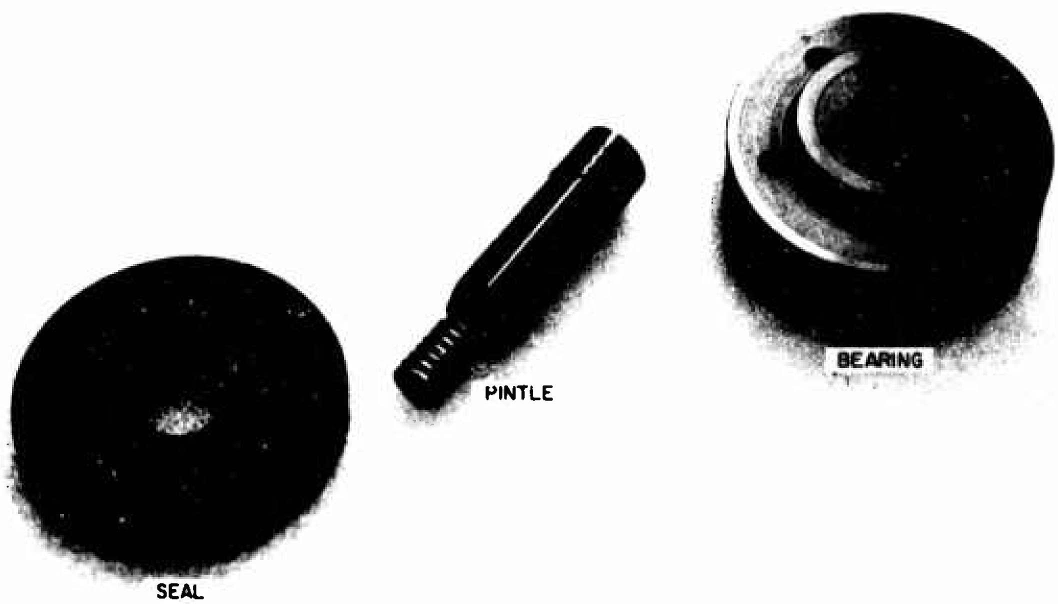

Fig. 4.2.2. Bearing, pintle, and seal.

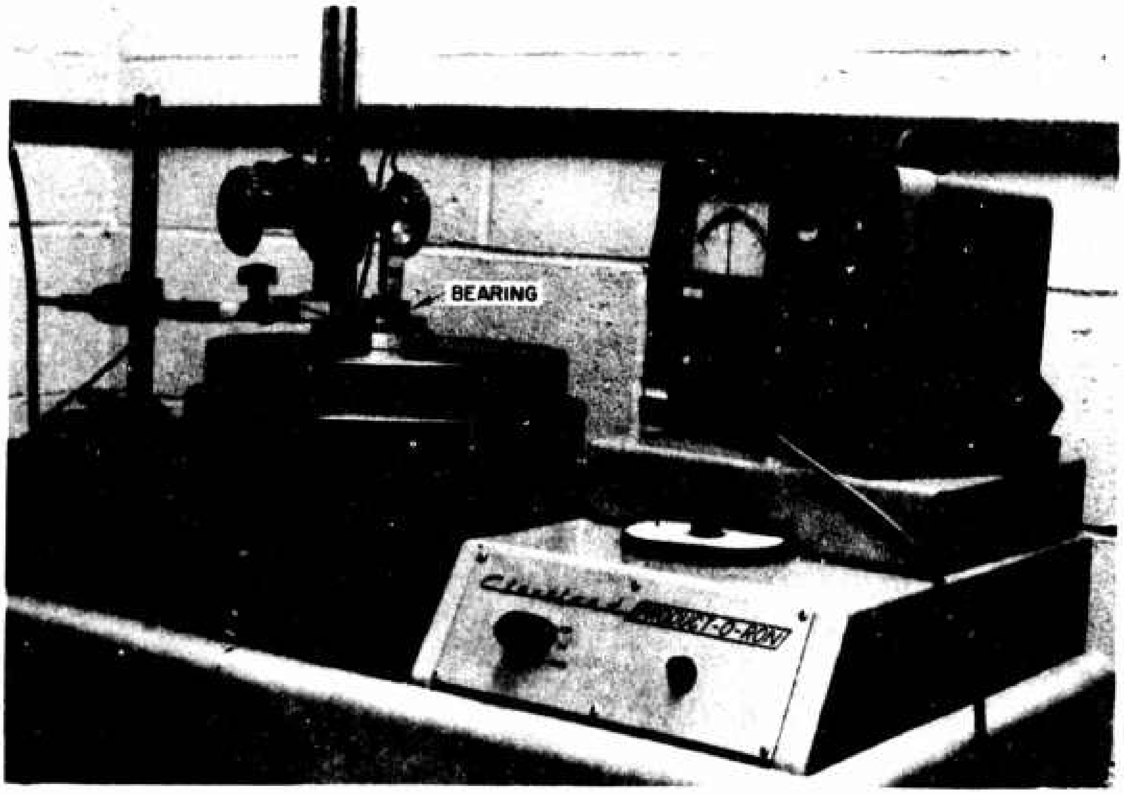

Fig. 4.2.3. Indi-Ron during inspection of bearing.

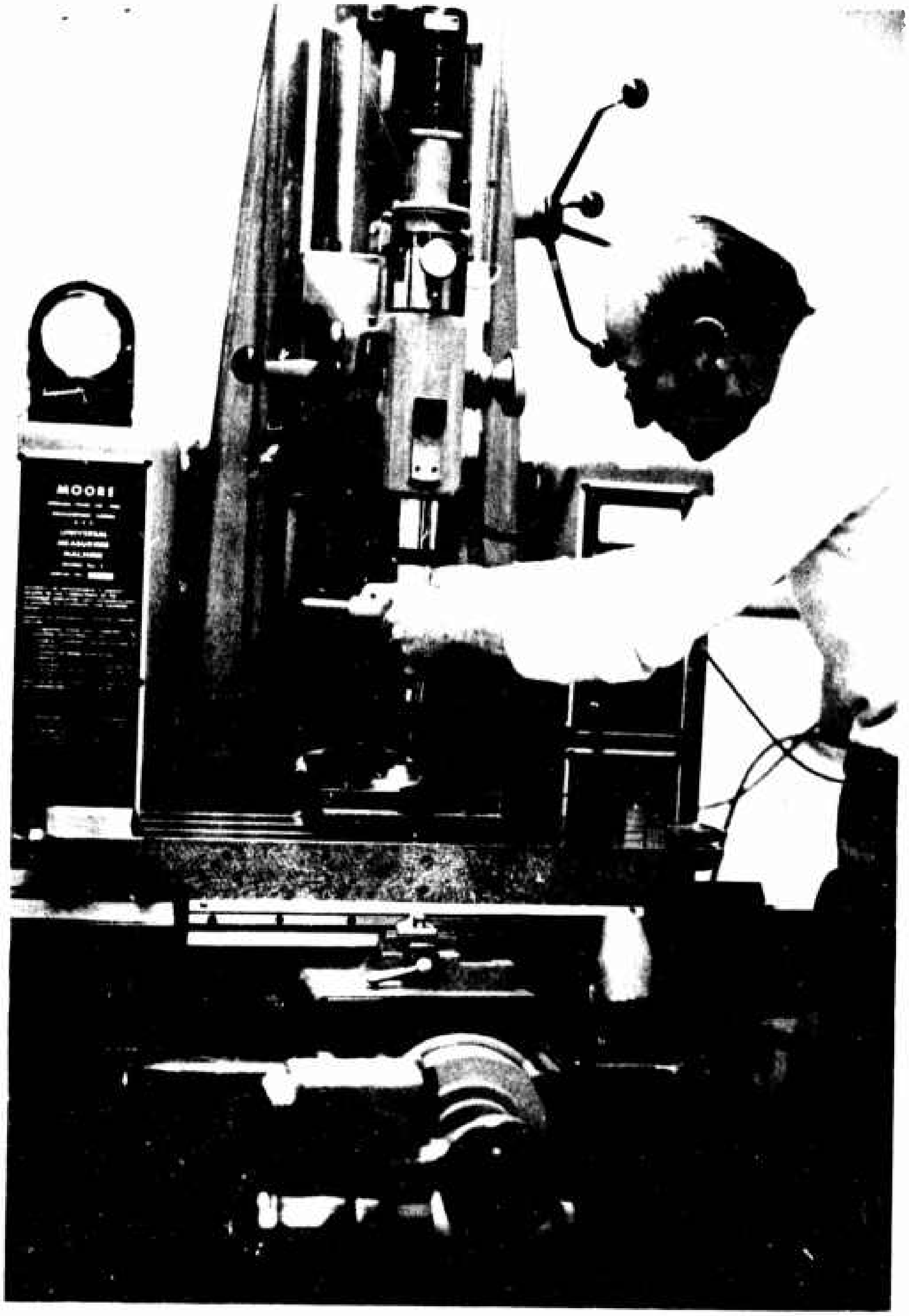

Fig. 4.2.4. Moore machine inspection of pintle.

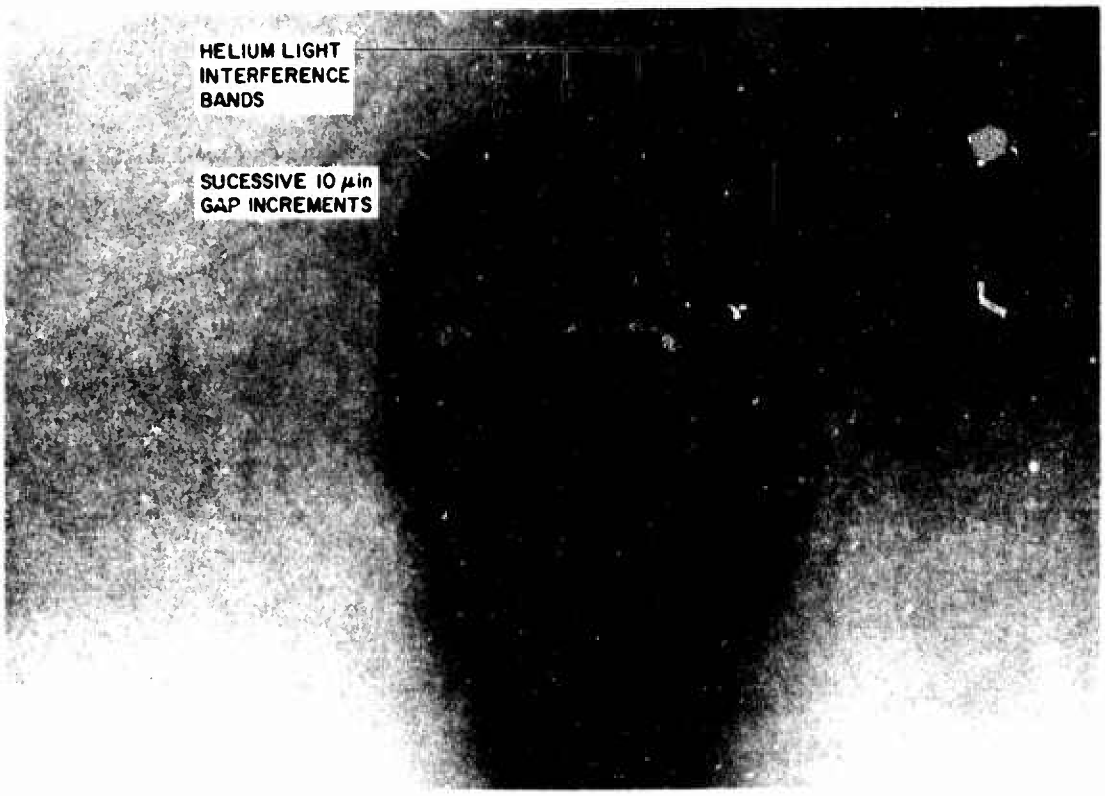

Fig. 4.2.5. Optical demonstration of pintle thrust face flatness.

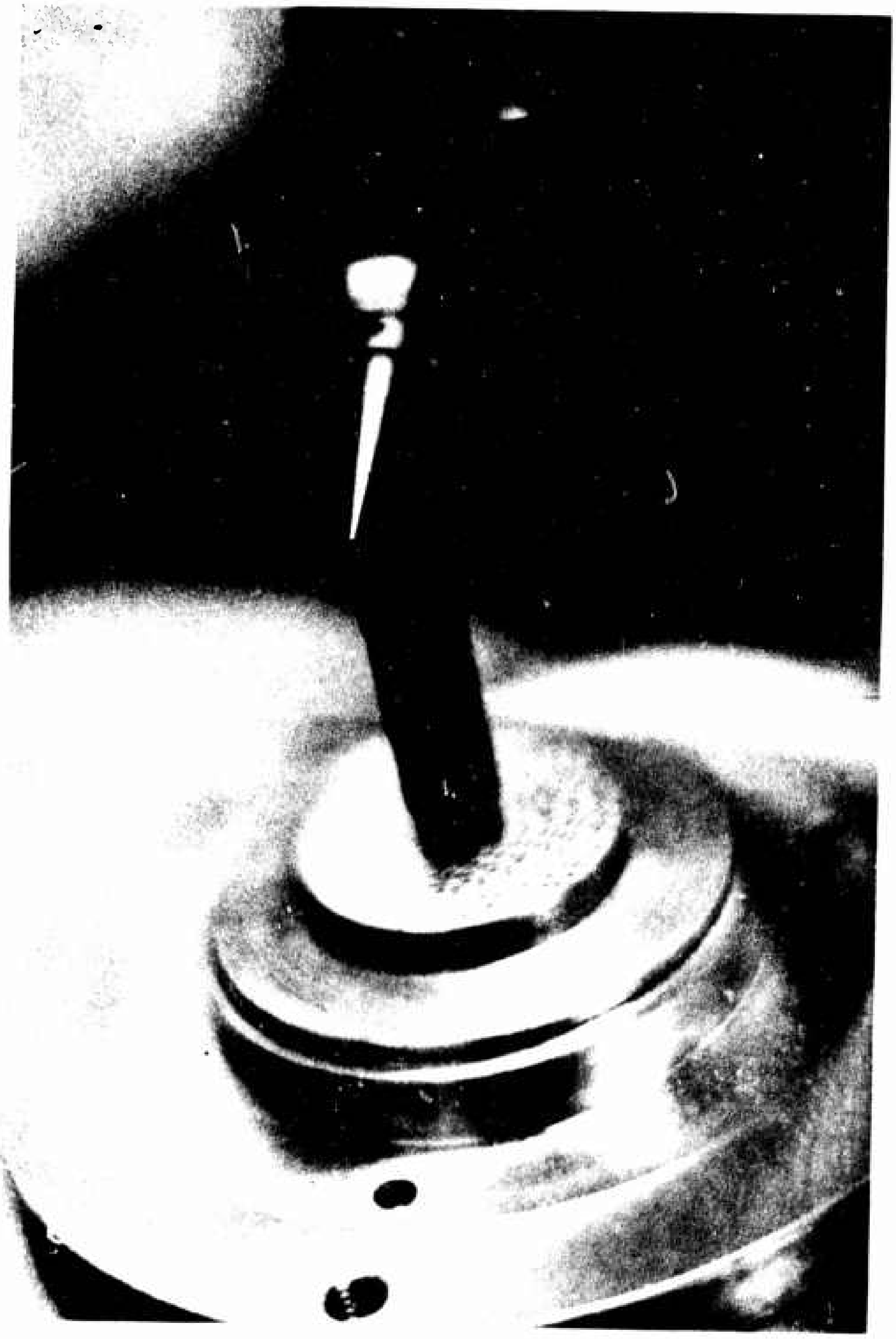

Fig. 4.2.6. Pintle spiral groove depth check.

Figures 4.2.7 and 4.2.8 are summaries of the results of the analysis of the indi-ron chart data using the overlay procedure outlined above. It is seen by these summaries that the critical bearing features met the general 5μ inch tolerance requirements with respect to roundness, flatness, squareness, and concentricity.

A similar technique was used for determining the depths of the spiral grooves. The results are summarized below.

	Groove Depth (μ inches)	
	Measured	Print
#1 Journal	201-217	130-150
#2 Journal	152-164	130-150
#1 Thrust	182-226	225-250
#2 Thrust	214-238	225-250

As is seen from these results, the control of groove depth which was produced by a sputter etching process, was not as good as desired. However, since groove depth has only a second order effect on stiffness and torque, it was postulated that the performance specification would be met even with the "out-of-print" groove depths. This was later verified by the tests described in Section 6.

4.3 Pre-Assembly

To facilitate the manufacture of the female bearing assembly, it was produced in three pieces: (101-D-02) bearing, (101-C-04) thrust runner, and (101-B-05) support plate. These pieces are bonded together with a cyanoacrylate (Eastman 910 FS).

A preliminary test of the bonding procedure was investigated to assure that flatness, and parallelism could be maintained after bonding. These bonding tests are reviewed separately in Appendix IV.

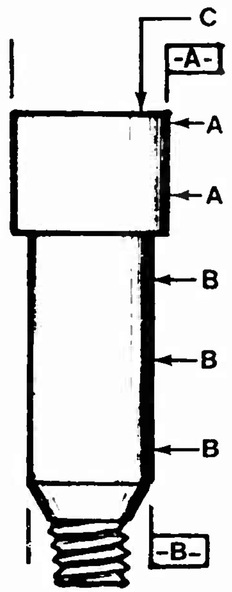

PINTLE SURFACE CHECK POINTS

MEASUREMENT	Pintle 1 (Microinch)	Pintle 2 (Microinch)
O Roundness (TIR)		
"A" Top	4	4
"A" Bottom	4	3
"B" Top	2	3
"B" Middle	5	2
"B" Bottom	3	4
⊙ Concentricity B to A	(2.5-4.5)	(3-4)
+ Squareness C Surface to A	1	2
- Flatness of "C"	2	3

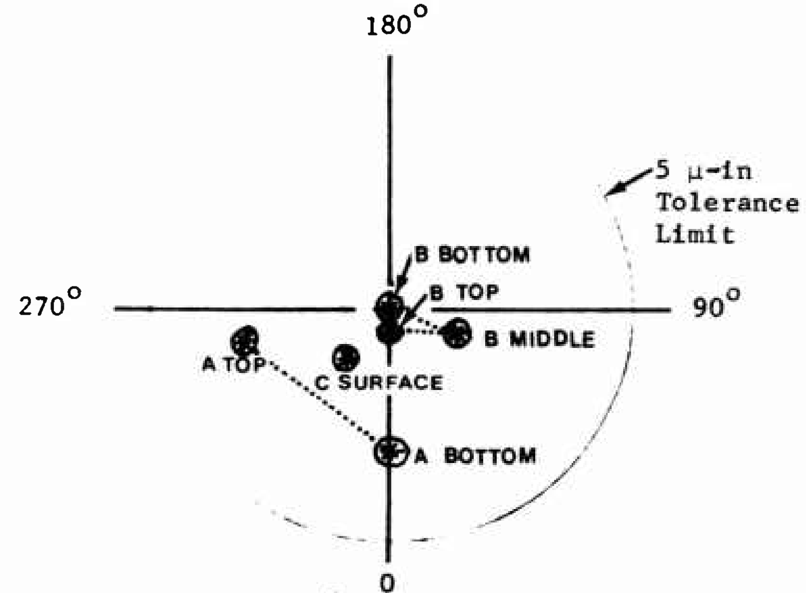

PINTLE 1 SURFACE CENTERS

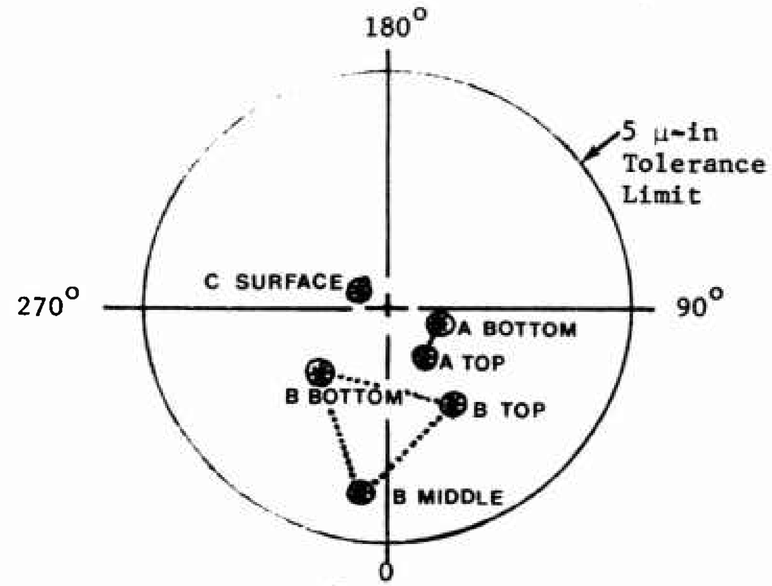

PINTLE 2 SURFACE CENTERS

Figure 4.2.7 Pintle Inspection Summary

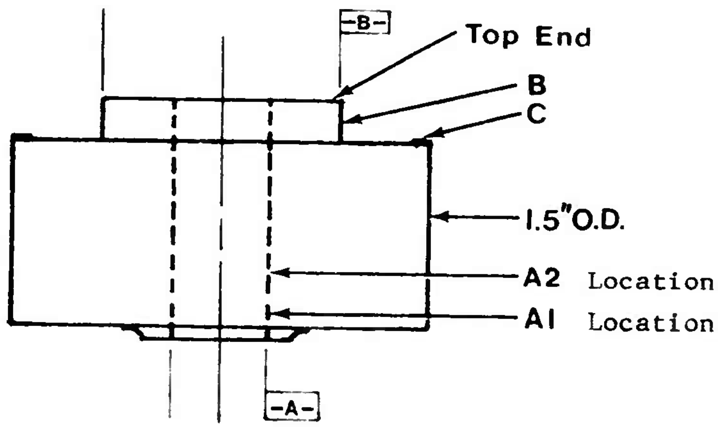

Bearing Surface Check Points

MEASUREMENT	BEARING 1 (Microinch)	BEARING 2 (Microinch)
O Roundness		
"A" Location 1	2	2
"A" Location 2	2	3
"B" Diameter	5	2
1.5" OD	5	4
⊙ Concentricity		
B to A	1.5	(1- 4)
+ Squareness		
C to A	2.5	(1.5-4)
- Flatness		
of "C"	4	2
Top End	2	4

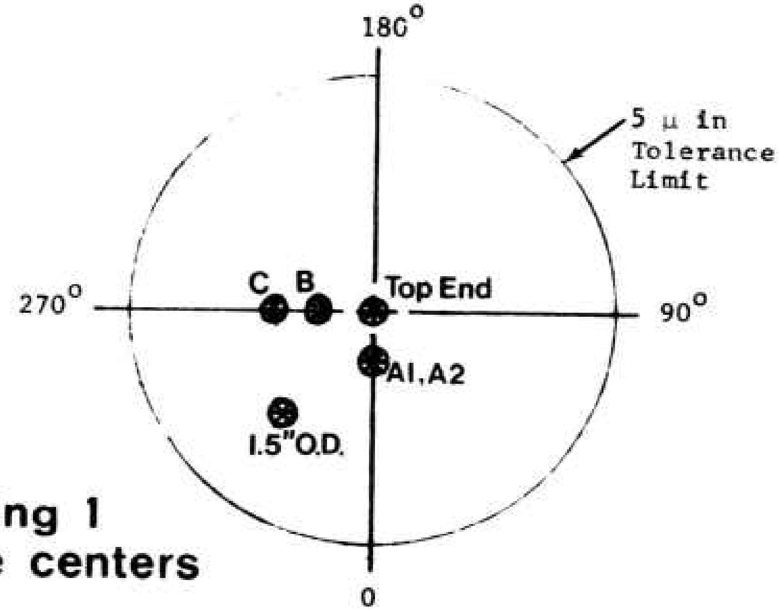

Bearing 1 surface centers

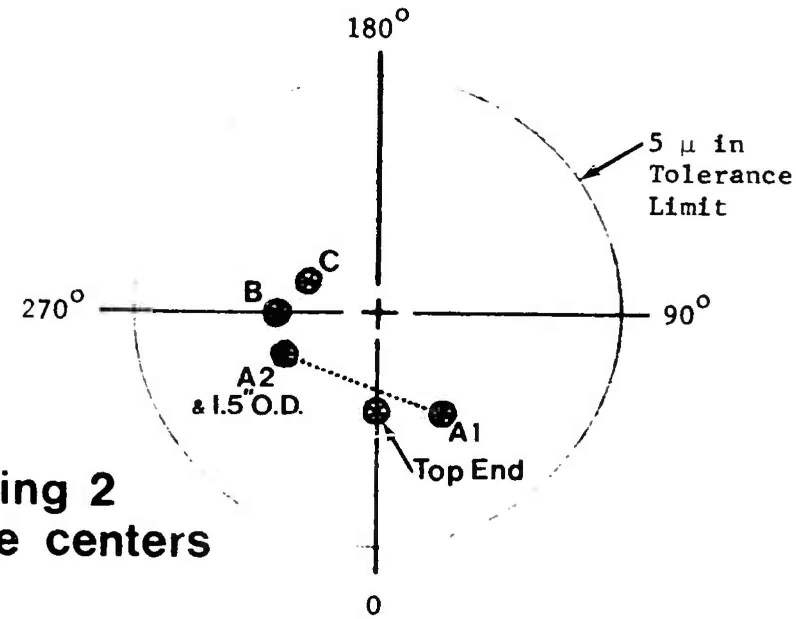

Bearing 2 surface centers

Figure 4.2.8 Bearing Inspection Summary

5.0 TEST RIG

This section describes the design and assembly of the simulated gradiometer rotor and prototype bearing test fixture. Pre-performance check-out of the mounted bearing clearances and rig alignments are also discussed.

5.1 Design

The specific details of the test rig are contained in Shaker Research Corporation drawing series number 100. A list of the drawings contained in that series is included in Appendix I.

A schematic of the test rig and related instrumentation is shown in Figure 5.1.1. The essential features are a rectangular stator support base, a cylindrical rotor, pintle bearings, bearing mounting plates, and mounted instrumentation transducers. The test rig is shown in the photograph of Figure 5.1.2.

The rectangular support base has a stress relieved welded structure which assured mounting support alignment throughout the various assembly and disassembly operations. All surfaces of the base were faced off to allow spin axis orientation in any desired orthogonal direction relative to the gravity vector.

The cylindrical rotor was center bored for mounting each female bearing component. The male bearing components were interference fit to the support structure with an intermediate carbon bushing. One end has a removable cap housing (for assembly purposes).

Additional components of the test rig include (6) six proximity transducers, (1) one thermocouple, (1) one speed pick-up, and provisions for an airjet inlet drive nozzle. The six displacement probes sensed radial and axial motion of the rotor assembly. The radial rotor motions were sensed with two pair of inductive sensors mounted to view the periphery of the female bearing components. Radial motion at each end of the rotor was sensed along mutually orthogonal axes with the viewing axis passing through the spin axis of the rotor (see Figure 5.1.3).

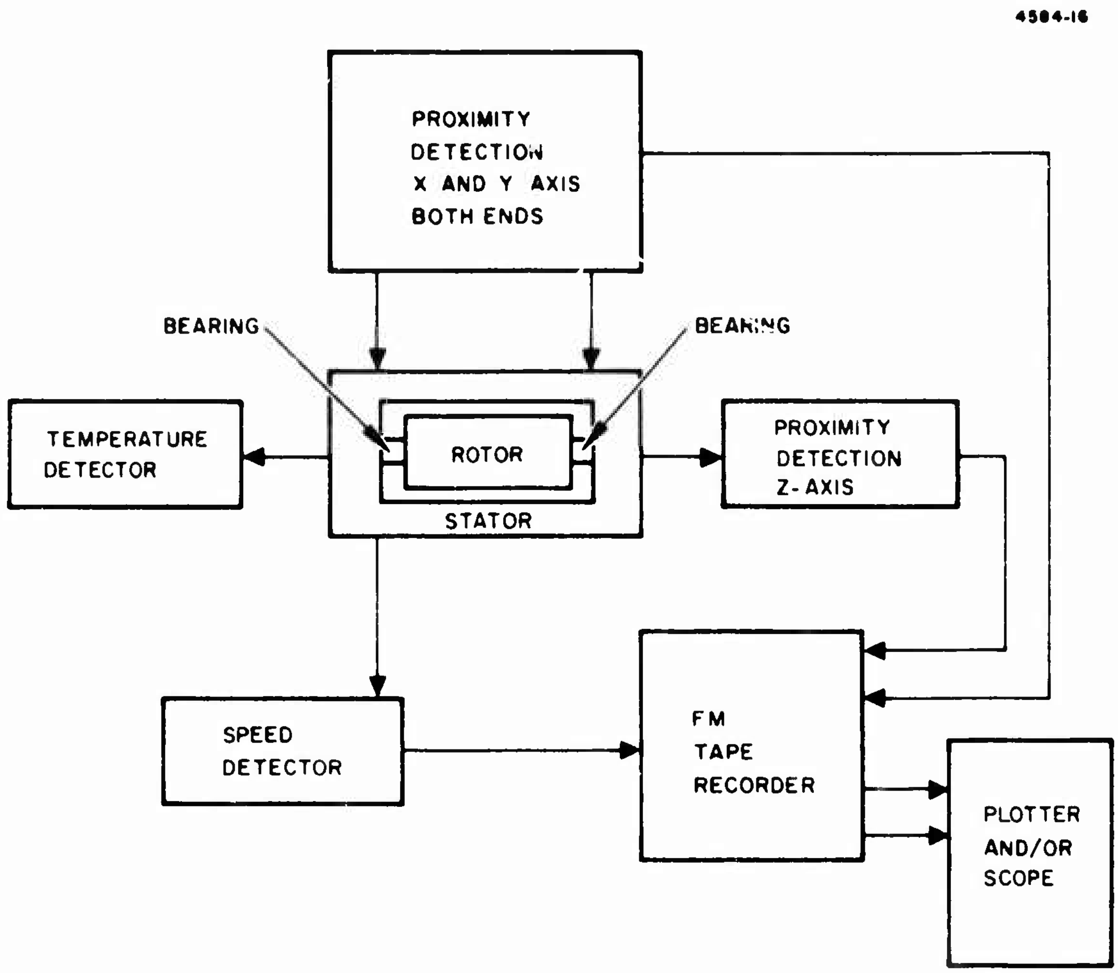

Fig. 5.1.1. Test instrumentation schematic.

4260-11

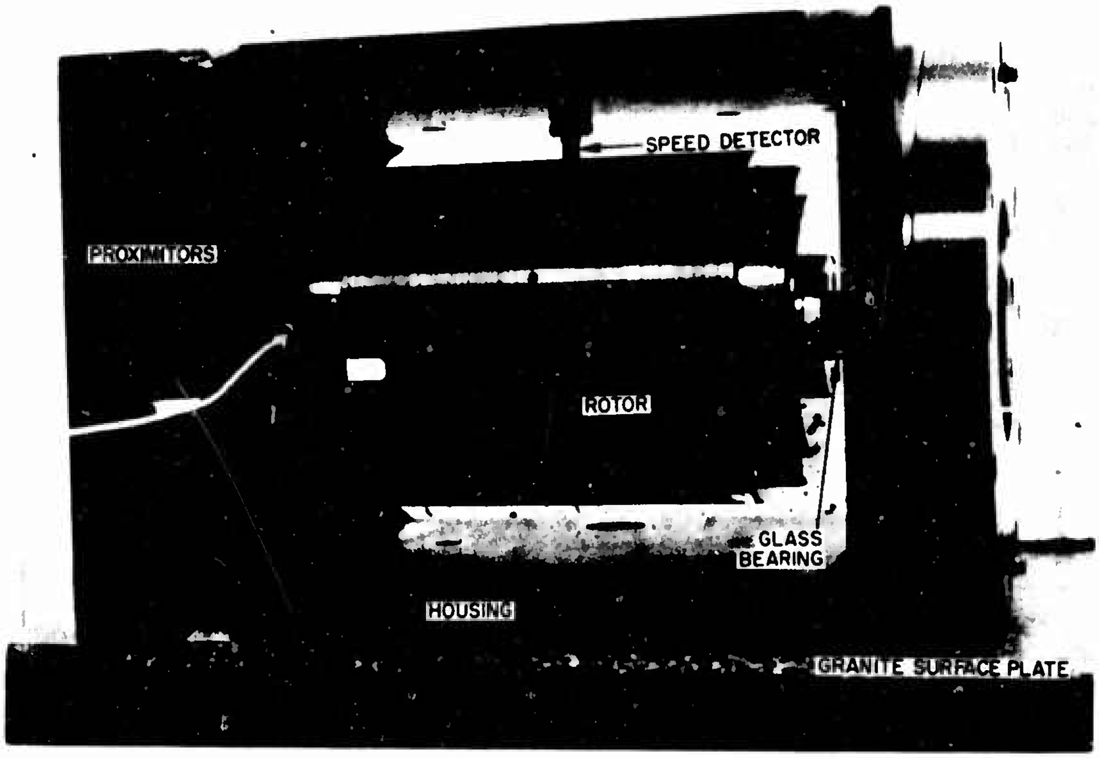

Fig. 5.1.2. Test rig photograph.

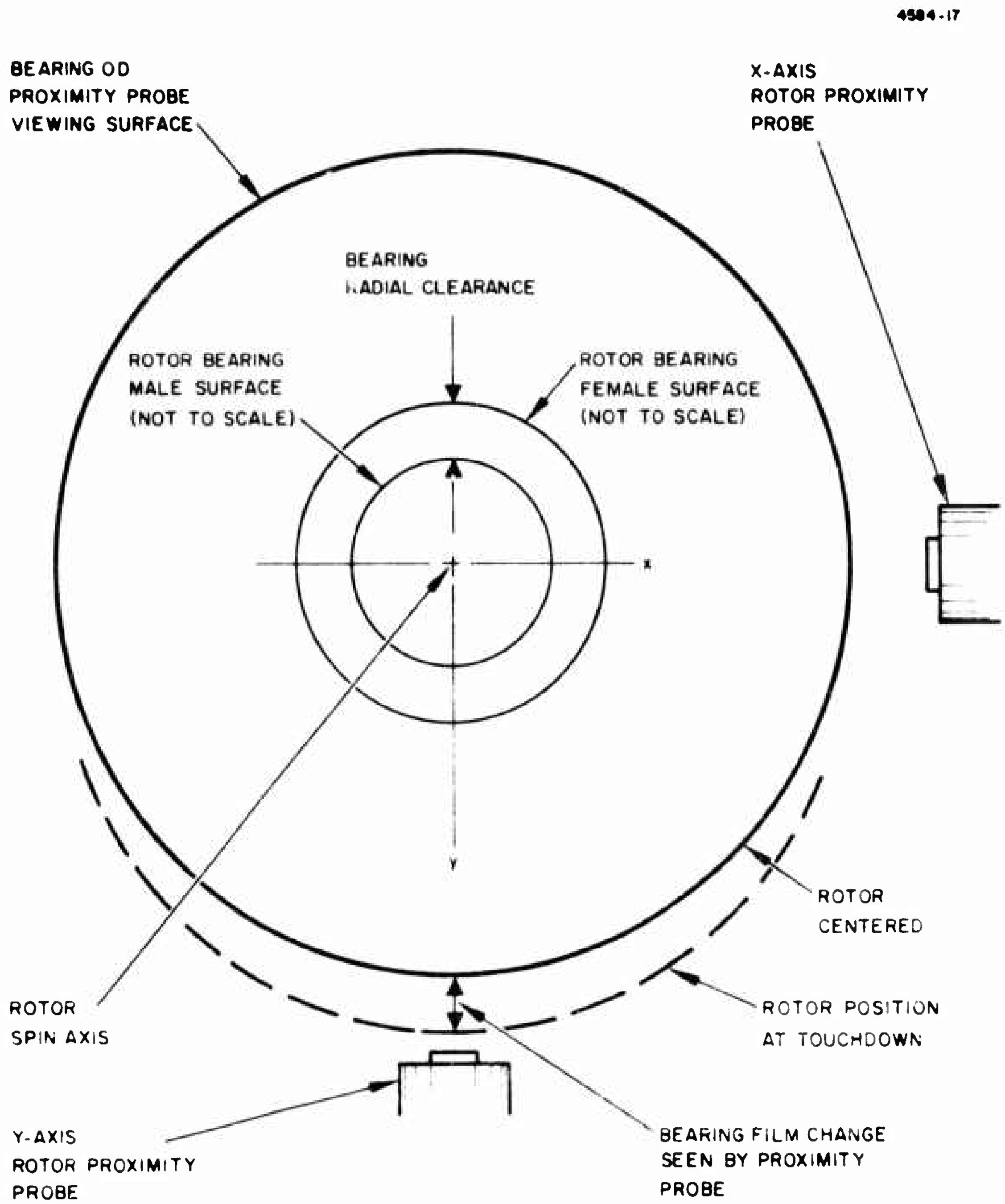

Fig. 5.1.3. Schematic of radial proximity probe placement.

Axial rotor motion was determined with a single probe at the end of the test rig which was mounted parallel to the spin axis of the rotor. This probe was mounted off the motor spin axis by approximately one inch.

One inductive sensor looking at 60 drilled holes on the rotor was used to determine rotor rotational frequency. Although 60 holes in the rotor periphery provided a convenient tachometer signal for recording the rotational speed, it was found that 120 peaks could be generated for each rotation of the rotor. Thus a double frequency signal was generated causing an erroneous conclusion as to the value of the rotational speed. It was found that increasing the probe air gap eliminated this problem.

5.2 Metrology

Misalignment of the bearings as a result of bearing and test rig mounting geometry errors cause a reduction of available bearing clearances. If the misalignment is excessive, abnormal running behavior or damage can result.

Early in the program, a design criteria establishing a maximum reduction in available clearance of 30 percent as a result of misalignment was imposed. The effect on clearance of the print tolerance of each feature having an effect on misalignment is summarized in Table I.

As might be expected, each component in the assembly due to its size and positioning has a different effect on the final bearing clearance. For instance, if the pintle thrust face (line 2, Table I) were not perpendicular to the journal surface by 5 microinches then 2 percent of the available thrust clearance for one bearing would be taken up in misalignment.

From Table I, it is seen that the maximum allowable tolerance stack-up results in an 11.7 percent reduction in journal bearing clearance and a 26 percent reduction in thrust bearing clearance.

Specific checks of each item listed in Table I during assembly revealed that the test rig and bearing were well within the allowable listed amounts.

TABLE I

EFFECT OF TOLERANCE ON BEARING ALIGNMENT

Part No.	Part	Surface	SYM.	μ"	With	Characteristic Length (Inch)	Disp. μ	Journal μ"in.	Journal % Nom. Clear (2)	Thrust μ"/in.	Thrust % Nom. Clear (3)
101-D-03	Pintle	Journal Surface(A)		5	Mounting Dia(B)	6.14	5(1)	.8	.07	.8	.12
		Thrust Surface(C)		5	Journal Surface(A)	.19	2.5	---	---	13.5	2.0
101-D-02	Bearing	Bearing Surface(A)		5	Mounting Surface (C)	.69	5(1)	7.2	.60	---	---
		Thrust Support Surface		10	Mounting Surface (C)	.34	5	---	---	14.7	2.18
101-C-04	Thrust Runner	Thrust Surface(B)		5	Mounting Surface	.19	2.5	---	---	13.5	2.0
	Bearing Components							8.0	.67	42.5	6.3
100-C-02	Rotor	Bearing Mounting Surface		50	Mounting Surface(C)	.69	12.5	18.1	1.50	18.1	2.68
		Bearing Clear(A)	Clear	100		6.14	50	8.1	.67	8.1	1.20
		Bearing Clear(B)	Clear	100		6.14	50	8.1	.67	8.1	1.20
		Bearing Mounting Surface		50	Bores(A-B)	.69	25	36.2	3.00	36.2	5.36
100-D-01	Assembly	Lower Cap Bore(C)		50	Diameter(E)	.54	25	46.3	3.84	46.3	6.85
		Diameter(E)		200	Bore(C-D)	6.15	100	16.3	1.35	16.3	2.41
	Rig Components							133.1	11.03	133.1	19.7
	All Components							141.1	11.7	175.6	26.0

(1) Total of Two Bearings
(2) Nominal Journal Bearing Radial Clearance = 180 μ inches
(3) Nominal Thrust Bearing Axial Clearance = 125 μ inches

Appendix V contains a summary of the dimension tolerances attained on the test rig. The rig is shown in Figure 5.2.1 during inspection of the pintle bore alighment. The check points used to determine test rig bore alignment are shown schematically in Figure 5.2.2. Two ground perpendicular faces of the test rig (indicator positions 3 and 4 of Figure 5.2.2) were used to place the rig squarely on the inspection machine base within 10 microinches of the vertical planes.

With the cap housing off (as shown in the photo of Figure 5.2.1) the alignment of the lower pintle mounting hole was determined relative to the reference vertical planes of the inspection machine. The bores using this procedure were found to be concentric within the 50 microinch desired limit. (Typical values of 20 μin were noted for each hole.)

The concentric alignment of the upper bore relative to the lower bore was determined to be within 50 μin, which was well within the limit of 200 μin put on the design.

Similar check with the Moore inspection machine indicated that the rotor was within the limits shown in Table I.

5.3 Assembly and Check-out

5.3.1 Rig Assembly Procedure

The test rig was assembled according to the procedure outlined below.

1. Each test component was cleaned prior to being assembled.
2. Bearings (101-D-02) were installed with match marks (red dots) on rotor (100-C-02) using screw mounting torques of two in-lbs.
3. Inspection of test rotor with mounted bearings were performed to determine the separation of the thrust faces. A value of 5.8273 was measured.
4. Pintle Number 2 (101-D-03) along with a seal (101-C-07) was mounted in the test housing (100-D-07). A protusion of the threaded side of the pintle of .3376 was set.
5. Cover (100-C-05) and plug-spacer assembly (101-B-06) and (100-B-04) were match marked (scribed) and fixed into place on the housing with 15 in-lbs torque.

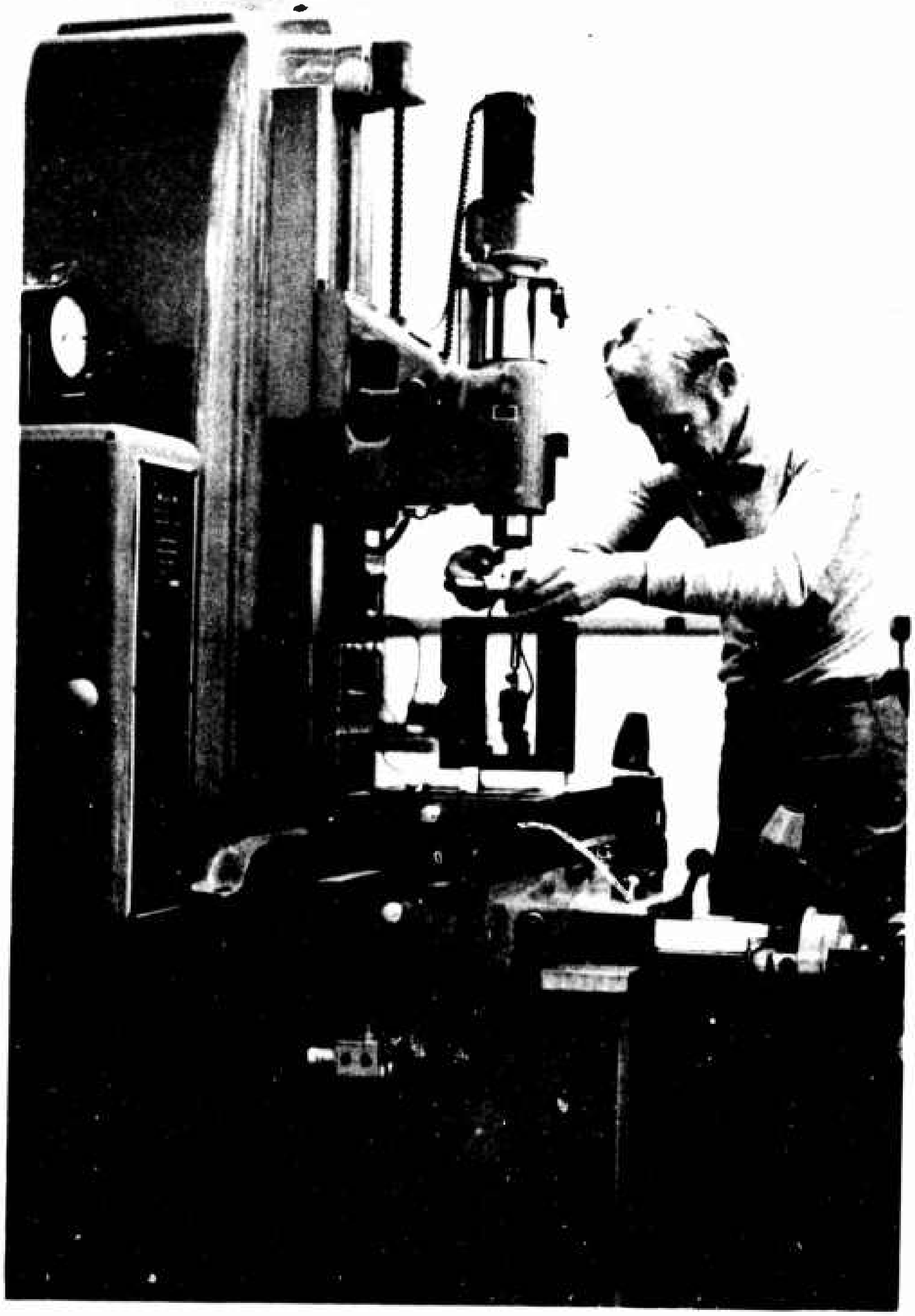

Fig. 5.2.1. Inspection of test rig alignments.

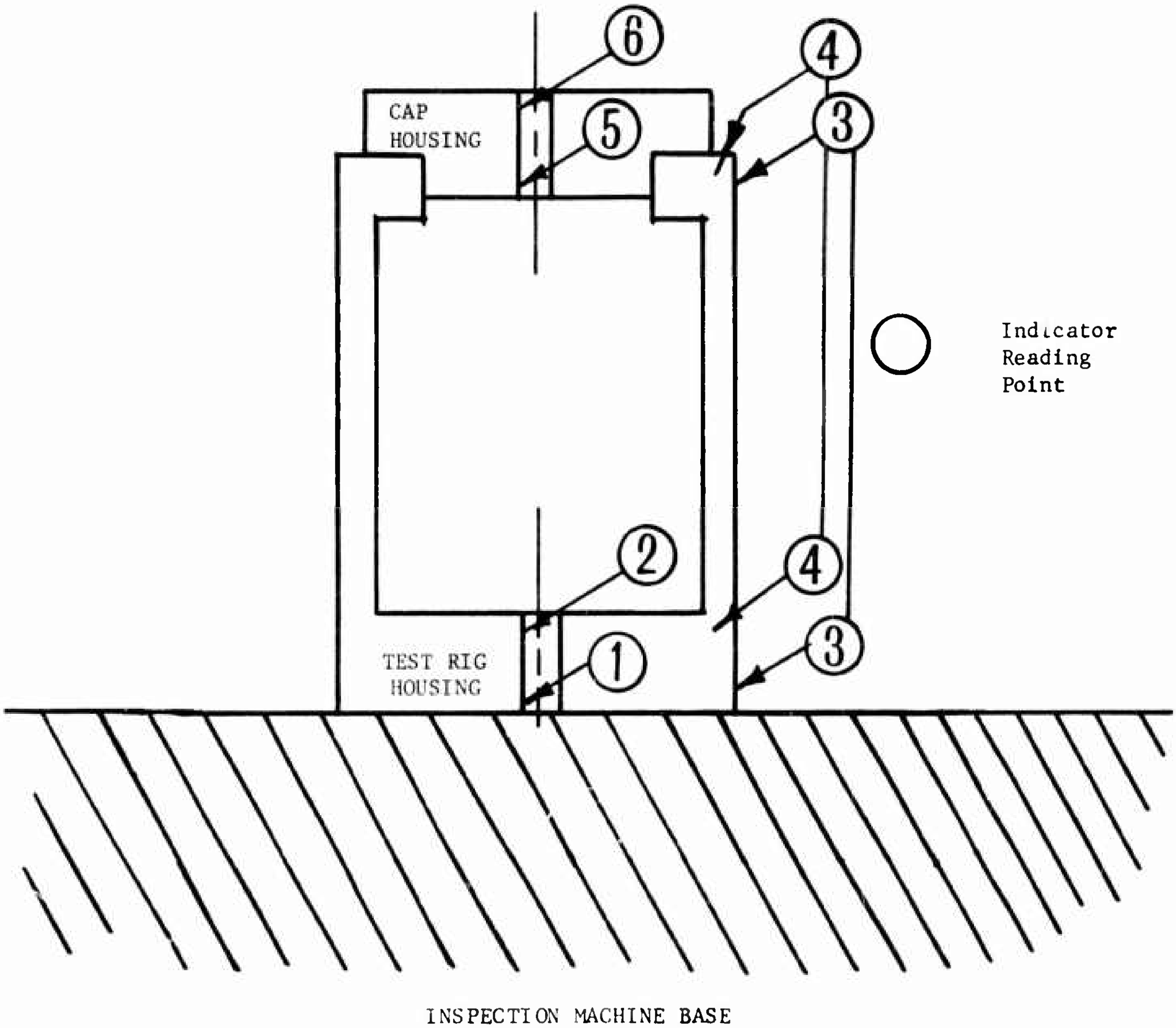

Figure 5.2.2 Test Rig Bore Alignment Check Points

6. Pintle Number 1 (101-D-03) and seal plate (101-C-07) was installed in cap housing (100-C-06) with undetermined axial positioning.
7. Cap housing (100-C-06) was mounted onto housing (100-D-07) with dowel pins and 15 in-lbs of torque applied to the fastening screws. The rotor was not installed at this point.
8. Pintle assembly fixture (100-D-20) was used to set the fact-to-face pintle distance at 250 microinches over the mounted bearing separation. This was accomplished by moving Pintle No. 1 while electronically indicating the motion of its thrust face.
9. After the appropriate separation of pintles had been attained the cap housing (100-C-06) was removed from the housing (100-D-07).
10. Probe holders (100-B-08) were installed in each end of the housing (100-C-06).
11. Non-wet barrier film was applied to the pintle and bearing surfaces (see discussion on application of Section 6.1).
12. Assembly sleeve (100-B-03) was mated with the rotor (100-C-02).
13. Housing (100-D-07) was placed on its side with the ground face down. Each open side of housing available for handling rotor. (See orientation in Figure 5.1.2).
14. Dowel pins with .422 and .413 diameter were laid on the lower inside surface of the housing (100-D-07). One for each end of the rotor to rest upon when positioned into housing.
15. Rotor (100-C-02) was placed through opening in housing (100-D-07) with spin axis horizontal and rested upon dowel pins which were positioned at right angles to the rotor spin axis.
16. Final mating of Bearing Number 2 (101-D-02) with pintle No. 2 (101-D-03) was accomplished by rolling and sliding by hand the rotor on the dowel pins. Final alignment in the vertical plane was accomplished by viewing the components from above through the displacement probe portal in the housing body.
17. Housing (100-D-07) was set vertically on bench with cover end up.
18. A double layer of masking tape was put around the rotor at each end in preparation for holding the rotor with screws.
19. Clamps (100-B-10) were installed on housing (100-B-07) and eight screws were placed finger tight to rotor.
20. Assembly sleeve (100-B-03) was removed.

21. Cap housing (100-C-06) was positioned by hand engaging upper pintle and bearing. The eight rotor positioning screws were removed.
22. End play of rotor was checked with a dial indicator before tightening the cap housing (100-C-06) down. After clearance of bearings was assured tapered dowel pins and screws with 15 in-lbs torque fixed cap housing in place.
23. Spacer-plug (100-B-04) was grounded to fit bewteen cap housing (100-C-06) and pintle cover (100-C-05).
24. Displacement and speed probes which had been previously calibrated were installed into holders (100-B-08).
25. Bearing seals (101-C-07) were attached to the bearings through the housing (100-C-07) and portals.
26. Pintle reservoirs were filled with oil.
27. Probes were hooked into electronic drivers, speed instrumentation and taping system for final testing.

5.3.2 Component Mounting Torques

Bearing and seal mounting screws were considered close enough to the bearing surfaces to possibly effect their roundness when tightened. A separate set of Indi-ron recordings were made to establish the distortion magnitude within the bearing bore from mechanically fixing the bearing to the rotor and the seal to the bearing.

Preliminary checks during the process of mounting the bearings on the rotor revealed that the bearing roundness depended primarily upon the orientation of the bearing relative to the rotor. Any one of five rotational orientations could be used to fix the bearing to the rotor. One of the first positions used in attaching the bearing revealed an egg-shaped distortion in the bearing which was approximately 20 μin TIR. A single subsequent rotation of 72° eliminated the prominant distorted feature of the bearing bore.

It was apparent from these preliminary mounting tests that care must be given to preparing the surface to which the bearings are to be mounted. If the mounting surface is not flat or is dirty, the bearing will be distorted when attached. It appears that the magnitude of distortion in the mounted component will be of the same order as the irregularity of the mounting surface.

Appendix VI contains twelve traces of Indi-ron charts showing the mounted roundness of the test bearings after an acceptable attachment orientation had been attained. The tracings were made with several variations in tightening torques on both the bearing and seal attachment screws. Bearing attachment torques were set in one of the two modes before taking a roundness tracing of the bearing; all five screws at the same torque level or four screws at the same level with one completely loose. The seal torque tests were made by setting all five screws at the same torque level.

A summary of the test torque levels and the resulting effect is made in Table II.

Inspection of the original tracings (See Appendix VI) under various test torque conditions revealed that:

1. Maximum distortions were less than 12 microinches TIR,
2. Distortions, when present, had a dominate elliptical nature,
3. Minor waviness of the bearing bore occurred in a ten wave pattern,
4. To minimize distortion, bearing and seal screw torques should be limited to 2.0 and 1.5 inch pounds respectively.

Additional observations can be made from the recordings.

A comparison of tracing pairs 1 and 2 and 3 and 4 shows that distortion may not always result if one screw were to be relaxed. Tracings 3, 4, and 5 reveals that distortions from a loose screw can be eliminated by retightening that screw.

A dominate elliptical character of the bearing bore is present when the seal is attached. Elevated torque levels on the seal screws do not necessarily increase the bearing bore distortion. In fact, a distortion reduction from 10 to 7 microinches was observed when the screw torque was increased from 0.5 to 1.0 in-lbs.

5.3.3 Proximity Probe Calibration

Since dimensional changes as small as 5 microinches were to be resolved during testing, each proximity probe was independently calibrated with

TABLE II

Fastening/Torque Distortion Test Conditions

Appendix VI Trace Number	Bearing Number	Bearing Mounted Torque (Nominal in-lbs)	Seal Mounting Torque (Nominal in-lbs)	Distortion Character	Distortion Magnitude TIR (Microinch)
1 initial	1	5 screws at 2 in-lbs	None	---	5
2 mounting	1	4 screws at 2 in-lbs	None	---	5
3	1	5 screws at 2 in-lbs	None	---	6
4 remounted	1	4 screws at 2 in-lbs	None	Elliptical	10
5	1	5 screws at 2 in-lbs	None	---	5
6	2	4 screws at 2 in-lbs	None	---	6
7	2	5 screws at 2 in-lbs	None	Elliptical	5
8	2	5 screws at 4 in-lbs	None	Elliptical	12
9	2	5 screws at 2 in-lbs	0 in-lbs	Elliptical	8
10	2	5 screws at 2 in-lbs	.5 in-lbs	Elliptical	10
11	2	5 screws at 2 in-lbs	1.0 in-lbs	Elliptical	7
12	2	5 screws at 2 in-lbs	1.5 in-lbs	Elliptical	12

its mating electronic driver and signal conditioning components. Each probe was then used throughout the test program with only one set of electronics in order to eliminate any possible component-to-component variations.

The calibrations revealed:

1. Probe displacement sensitivities were found to be within 2.5 percent of each other.
2. Displacement sensitivity did not depend upon the presence of the hard coat on the aluminum.
3. Probe output voltage was 2.40 times greater for the aluminum surface than the 4130 steel.
4. Each displacement probe sensitivity was determined within ± 1 percent.
5. Limiting probe displacement resolution and stability for a period of 500 seconds was established to be 1 microinch or better.
6. Output linearity of 1.75 percent per mil of displacement was established at the stand off output voltage used during testing. Since most displacement changes were smaller than .5 mils a linearity of better than 1 percent could be expected.

Calibration, resolution, and electronic overall stability tests were performed by moving and/or fixing the probe to target distances by known increments. Standard dial indicators and micrometers with appropriate scale sizes were used to establish known increments for displacement calibration purposes.

5.3.4 Bearing Clearances

By manually moving the rotor through the bearing clearances and observing the onput of the proximity instrumentation system, it is possible to obtain an "in place" clearance measurement.

The results of this clearance measurement technique as applied to the journal bearings is summarized in the table below.

Radial Clearance - μ Microinches

	Mounted			
Bearing Number	Vertical Plane	Horizontal Plane	Piece Part Inspection	Per Print
1	190-204	177-191	175	170-190
2	209-223	208-232	185	170-190

It is not surprising that the clearance measured by the technique of mechanically moving the bearing through the clearance space appears to be larger than that derived from the difference in the actual pintle and bearing diameters (piece part inspection). This is because the proximity probes see total motion of the rotor which includes both bearing clearance and pintle cantilever mode deflection. Calculated canilever mode deflection is at least 17 μ inches when supporting the rotor weight (assuming "built-in" end).

The measurement of bearing clearance in this manner did, however, confirm that the bearings were "well" aligned in that an abnormal reduction in clearance was not noted.

Axial clearance was established (using a mechanical indicator) during rig assembly to be within 50 microinches of 200 microinches total end play. A determination of the end play from electronic proximity probes put the test clearance at 190 $\pm$ 10 microinches.

5.3.5 Thermocouple Calibration

Boiling water and ice baths established the test thermocouple output to be within .1 percent of the standard published values. The output of the copper/constantan junction was fed into a floating differential amplifier with a 1000 to 1 grain. A limiting resolution of .25°F was determined from the temperature detection set-up used.

6.0 TEST RESULTS

The results of performance testing presented in this section are separated into two categories; those related to bearing performance and those related to the test lubricant. Appendix VII itemizes the equipment used to carry out the investigations.

The test lubricant used was a highly refined gyroscope bearing oil sold by Nye Inc. The super-refined oil from their SRG series are made from specially selected hydrocarbon distillation fractions. Lubricant viscosity, volatility, lubricity, oxidative stability, and metal corrosion characteristics have been closely controlled to permit long term operation of high performance gyros. The operating temperature range of these oils extend from $0^{o}C$ to $125^{o}C$.

The viscosity of the SRG-20 oil used in testing was 15 centistokes at room temperature of $70^{o}F$. Figure 6.1.1 is a temperature-viscosity plot on standard ASTM viscosity paper. One reason for using the SRG series oils is that it is available in many different viscosity blends. Since the gravity gradiometer bearings will probably be operated at $110^{o}F$, the ability to select the oil viscosity at any operating temperature is desirable.

The results of the bearing performance tests described in this section indicated that an oil with 20 percent lower viscosity could be used while still meeting the minimum stiffness requirements while an oil with a 33 percent higher viscosity could be used and still meet the maximum running torque requirement.

Thus from an operating performance requirement standpoint, a viscosity range between 12.5 cs and 20.7 cs at the desired operating temperature should be specified. However, if prolonged operation at the 3g condition specified in Paragraph 2.2.5 of HRL DS-1-473 is anticipated, the higher viscosity oil would be recommended to give a little more margin to the thrust bearing. (Test results indicate that the thrust bearing touchdown point is near 45 pounds at design speed with the 15 cs oil. Increasing viscosity will increase the load capacity directly.)

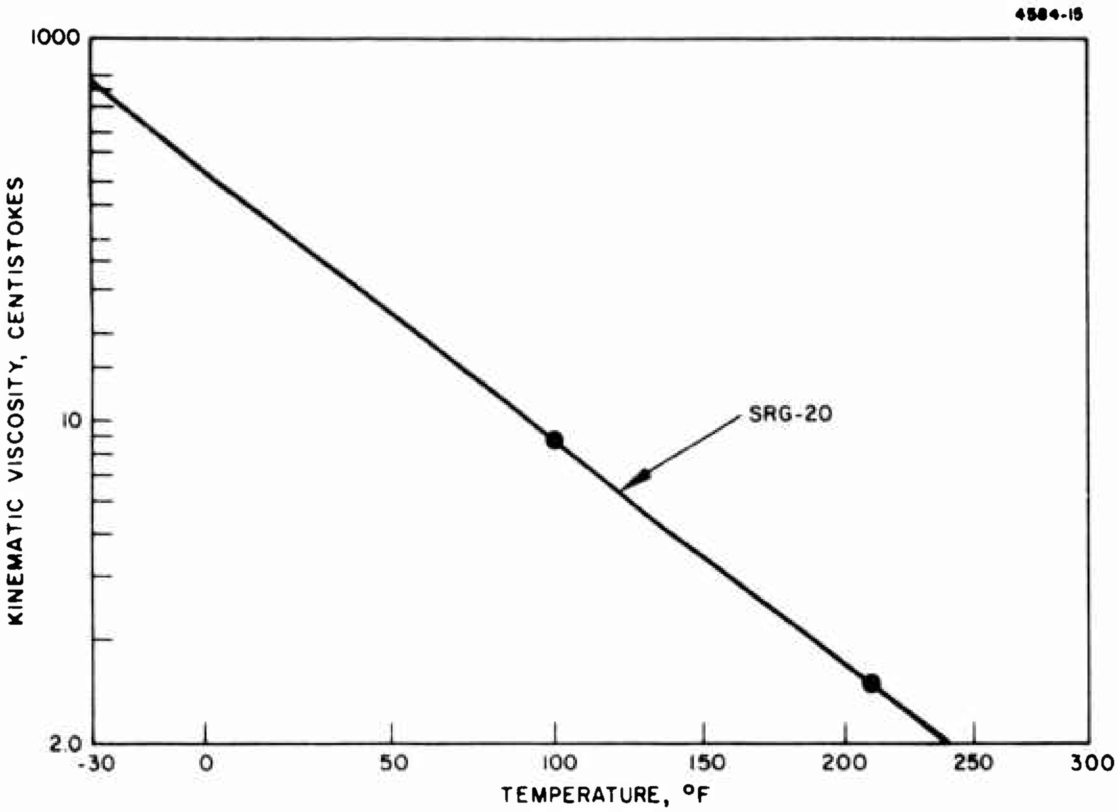

Fig. 6.1.1. Temperature — viscosity plot.

6.1 Bearing Performance Tests

Three types of performance tests were made on the prototype gradiometer test bearings: Torque, stiffness, and thermal evaluations.

Starting and operating torques were established with the rotor spin axis in each of the two intended operating orientations; vertical and horizontal. Starting torques were established by applying a force to a cord wrapped around the rotor. Running torques were obtained from rotational frequency versus time plots obtained during rotor coast down.

Stiffnesses of the bearings were determined from film thickness data taken as a function of rotation frequency. Film thicknesses were recorded with the spin axis at several tilt angles between, as well as, at the horizontal and vertical position.

6.1.1 Torque

The nominal measured and specification maximum starting torques are summarized in the following table.

Measured with Axis Vertical	3.01×10^5 Dyne-CM (4.26 in-oz)
Measured with Axix Horizontal	4.07×10^5 Dyne-CM (5.77 in-oz)
Max per Para 3.4.3 of HRL DS1-473	4.94×10^5 Dyne-CM (6.99 in-oz)

The above nominal measured starting torques were determined from at least twenty trials for each spin axis orientation. Maximum and minimum forces required to "break" the bearing away from its stationary position varied by about 10 percent from the nominal.

This variation is not unusual, since the amount of surface asperity contact which determines the friction coefficients between the bearing interfaces, changes as the rotor is turned from one angle to another.

Operating running torques were found from coast down curves and a knowledge of the rotor inertia. The assembly bearing torques are given by

$$\text{TORQUE} = I\dot{\omega}$$

where $\dot{\omega}$ is equal to the rate of change of the rotor speed evaluated at the design rotational frequency. The rotor inertia (I) was constant and calculated to be 0.0698 in-lb-sec^2 from the detail drawing dimensions. Figures 6.1.2 to 6.1.4 are the typical coastdown plots for the test rotor. The spin-axis orientation of the assembly during each recorded plot is indicated on each figure. The numbers indicate, for vertical orientations, whether bearing number 1 or 2 is either up or down. Each plot has two tracings; one for the complete coastdown period and a second with an expanded scale near design speed. Since the raw data was recorded on magnetic tape, a replot of any segment of the coastdown could be obtained for better resolution (as shown in the expanded scale output). Slopes calculated from the expanded tracing portion of each test curve were used to calculate running torque. The results are summarized below.

With Number 1 Bearing Up	3.359×10^4 Dyne-CM (.474 in-oz)
With Number 2 Bearing Up	3.345×10^4 Dyne-CM (.472 in-oz)
With Axis Horizontal	3.636×10^4 Dyne-CM (.514 in-oz)
Max Per Para 3.5.1.1 of HRL DS 1-473	5.000×10^4 Dyne-CM (.706 in-oz)

Variation of the running torque, if any, with the end-shake, is within 3 percent, which is about the resolution of the coastdown displacement data.

6.1.2 Bearing Stiffness

Measurements of bearing stiffness were obtained by analyzing rotor coast down data in the form of displacement vs. speed plots which were produced on an X-Y Plotter, either "on line" or from magnetic tape recorded data. These coast down curves were generated with the spin axis oriented at several different angles between the horizontal and vertical so as to impose different loadings onto the bearings.

Unfortunately, the design speed displacement data at different loading (orientation) conditions could not be directly evaluated for stiffness because of the uncertainty of the zero or touch down position. This uncertainty arose from the irregularities of the proximity probe measurement surfaces. At low speeds, these irregularities (out-of-roundness or flatness) produced output signals having band widths of approximately 25 μ inches and 100 μ inches on the journal and thrust bearing displacement measurements respectively. These band widths represented the un-

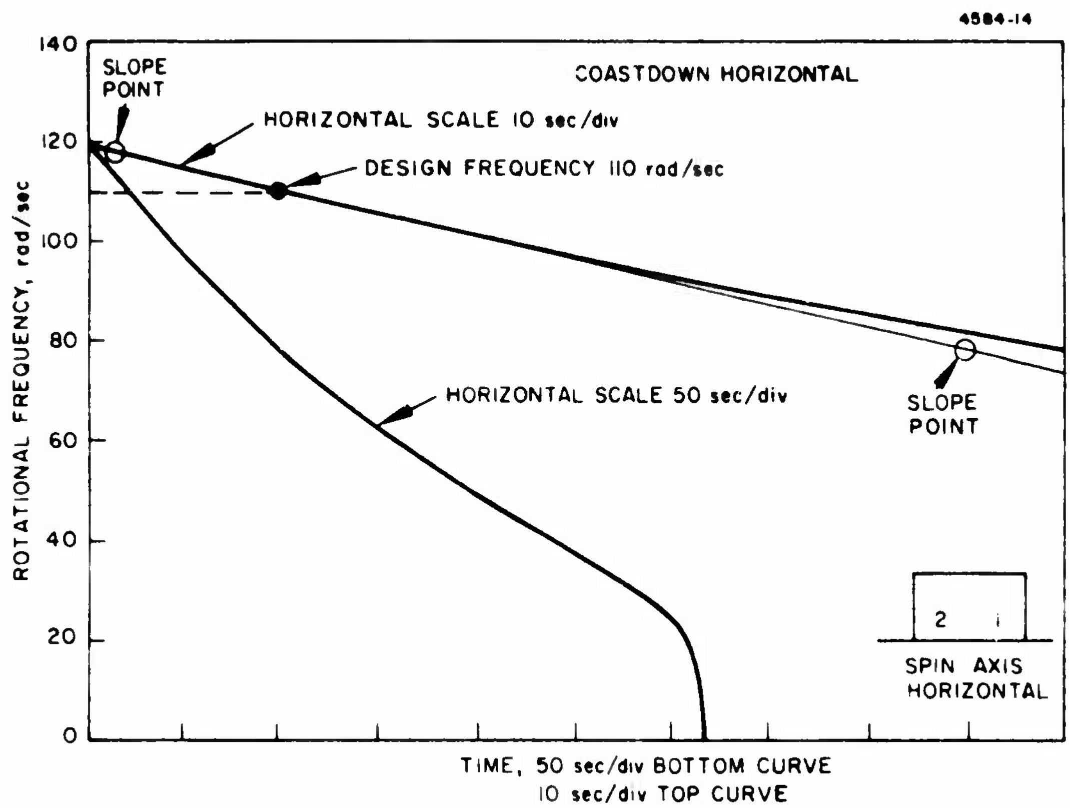
4584-14
140
120
100
80
60
40
20
0
ROTATIONAL FREQUENCY, rad/sec
SLOPE POINT
COASTDOWN HORIZONTAL
HORIZONTAL SCALE 10 sec/div
DESIGN FREQUENCY 110 rad/sec
HORIZONTAL SCALE 50 sec/div
SLOPE POINT
2
1
SPIN AXIS HORIZONTAL
TIME, 50 sec/div BOTTOM CURVE
10 sec/div TOP CURVE

Fig. 6.1.2

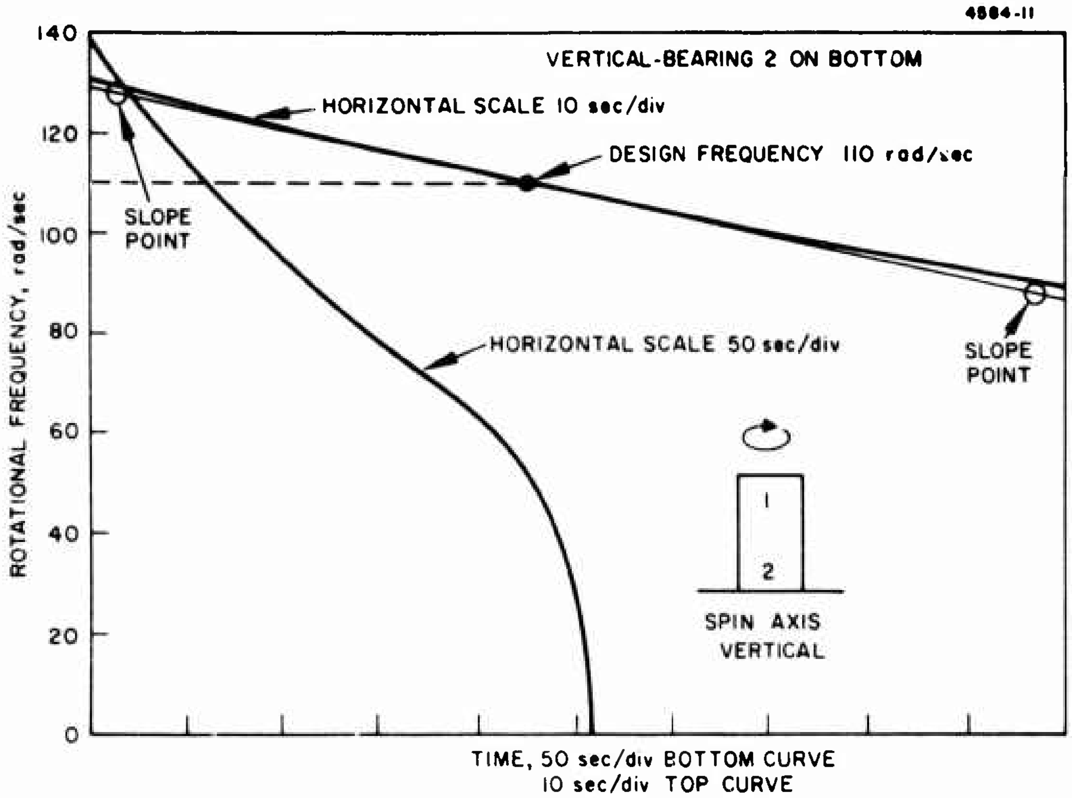

4584-11
VERTICAL-BEARING 2 ON BOTTOM
HORIZONTAL SCALE 10 sec/div
DESIGN FREQUENCY 110 rad/sec
SLOPE POINT
HORIZONTAL SCALE 50 sec/div
SLOPE POINT
1
2
SPIN AXIS VERTICAL
ROTATIONAL FREQUENCY, rad/sec
140
120
100
80
60
40
20
0
TIME, 50 sec/div BOTTOM CURVE
10 sec/div TOP CURVE

Fig. 6.1.3

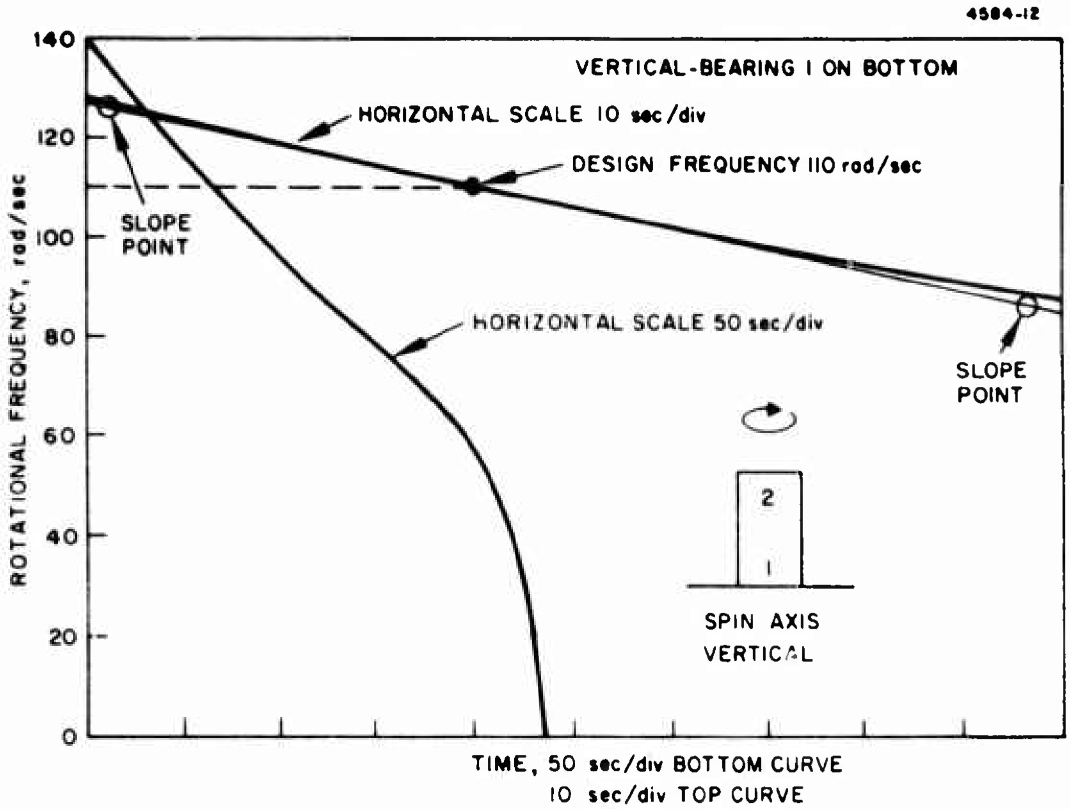
4584-12
VERTICAL-BEARING 1 ON BOTTOM
HORIZONTAL SCALE 10 sec/div
DESIGN FREQUENCY 110 rad/sec
SLOPE POINT
HORIZONTAL SCALE 50 sec/div
SLOPE POINT
2
1
SPIN AXIS VERTICAL
ROTATIONAL FREQUENCY, rad/sec
140
120
100
80
60
40
20
0
TIME, 50 sec/div BOTTOM CURVE
10 sec/div TOP CURVE

Fig. 6.1.4

certainty in the touch down or zero film thickness point. At high speeds, this problem went away because the X-Y Plotter could not respond to the surface irregularities.

Thus, a method of evaluating the clean signal high speed data was employed to establish the center (zero load or infinite speed) position and the stiffness of the bearing at that position. The center position was used because that is the point of minimum stiffness. The method used is described in Appendix VIII. It should be noted that Appendix VIII treats the case of the journal bearing which has four stiffness coefficients (K_{xx}, K_{yy}, K_{xy}, K_{yx}). Although the thrust bearing posesses only one stiffness coefficient (K_{zz}), the same analytical technique, though simpler in detail, is used.

6.1.2.1 Thrust Bearing Stiffness

Thrust bearing displacement vs speed plots are shown in Figures 6.1.5 and 6.1.6. It is seen from Figure 6.1.6 that the rotor has a tendency to run closer to bearing number 2 than to bearing number 1. The most likely reason for this unequal thrust bearing performance characteristic is that the number 1 journal bearing has a smaller radial clearance than number 2 journal bearing. This results in a larger preload imposed upon the number 2 thrust bearing because of the larger pressure developed by the number 1 journal.

A larger total axial clearance, if acceptable to the gradiometer design, would tend to minimize the dependence of the thrust bearing performance on journal bearing clearance.

The stiffnesses of the thrust bearings at the centered* position (using the data analysis technique described in Appendix VIII) are summarized below.

Bearing Number 1	58,854 lb/in
Bearing Number 2	163,835 lb/in
Minimum per Paragraph 3.5.3 of HRL DS1-473	57,000 lb/in

* "Centered" position means position at zero thrust load -- not geometric center.

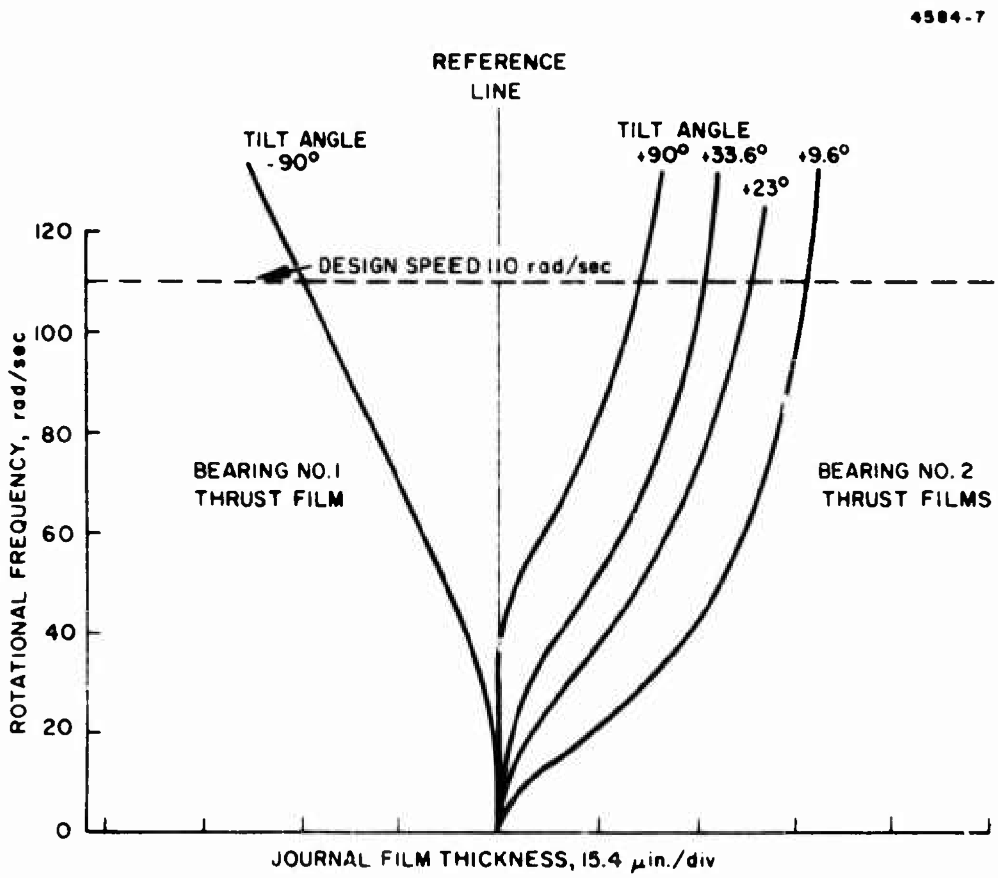

Fig. 6.1.5. Axial film thickness.

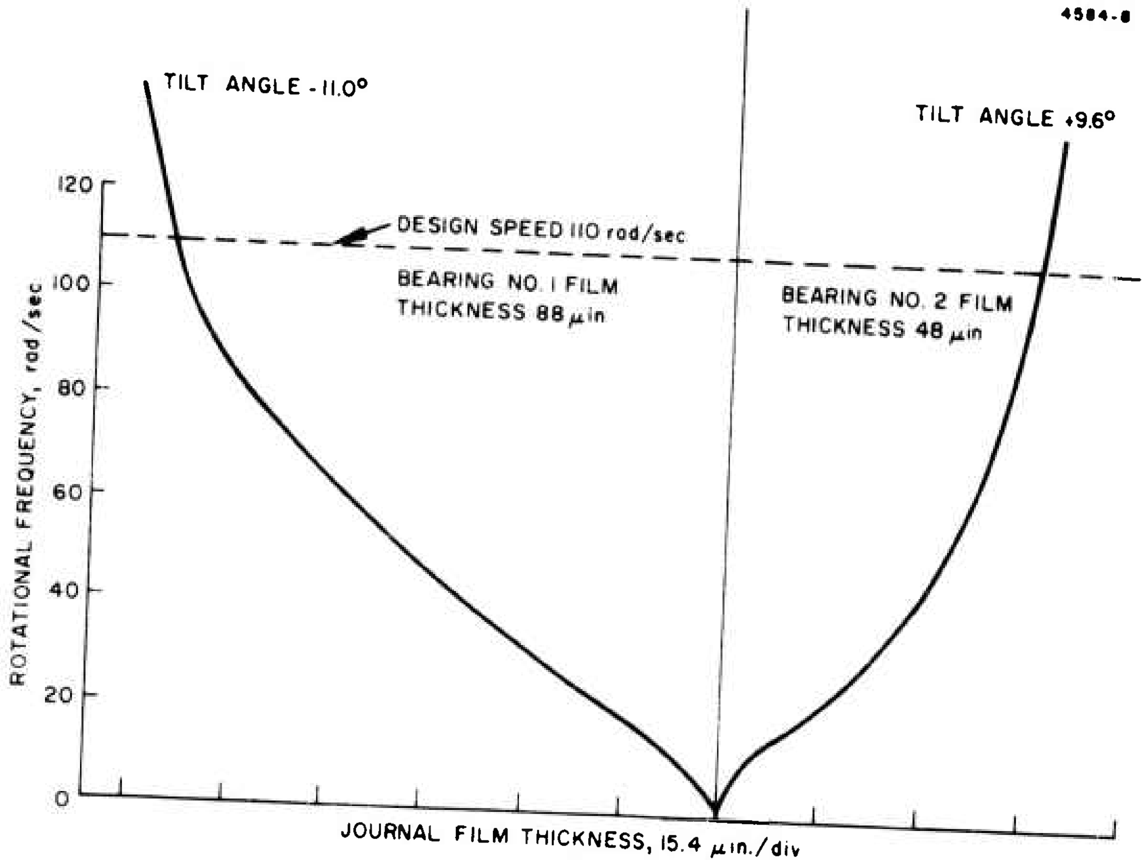

Fig. 6.1.6. Axial film thickness.

In reality, the actual stiffness of the double acting thrust bearing system at the zero load condition is somewhere in between the stiffnesses cited above. The discrepency arises from the fact that the data analysis technique utilizes speed data at some finite load near zero to extrapolate to the zero load condition. Unfortunately the non-uniformity of the two film thicknesses (caused by the aforementioned unequal preload) forced the number 2 thrust bearing to operate in a more non linear mode near the zero load condition than bearing number 1. The data analysis technique assumes linearity at zero load and similar non linearity characteristics for each bearing as the loads depart from zero.

Although the raw data was not as "clean" as desired which caused a relatively wide descrepancy in "measured" stiffnesses, it has been concluded that the thrust bearings will perform their intended function, i.e. to accurately locate the rotor in the axial direction. Probably a more meaningfull stiffness value in this respect is the average stiffness over the $\pm$ 1 g load range, which is defined as:

$$\frac{\text{Total Load Change}}{\text{Total Measured Axial Travel}} = \frac{30 \text{ lb}}{136\ \mu \text{ inches}} = 220{,}588\ \frac{\text{lb}}{\text{in}}$$

If it is true that the specification axial stiffness was established to limit total rotor travel over a $\pm$ 1 g load range for encoder optics or other mechanical reasons then the allowable total end play can be increased to a value near:

$$\frac{2 \text{ g load}}{\text{Specification Stiffness}} = \frac{30 \text{ lb}}{57{,}000 \text{ lb/in}} = 526\ \mu \text{ inches}$$

As compared to the current design clearance of 150 to 250 μ inches. By increasing the total end play to a maximum of 526 μ inches, the actual rotor travel under $\pm$ 1 g load variations would still be less than that value of the sum or the two operating film thicknesses at 15 lb load (approximately 54 μ inches).

Increasing the total end play would have the following advantages:

1. Ease assembly
2. Lessen differential thermal expansion problems
3. Minimize effects of different journal bearing geometries on thrust bearing performance

6.1.2.2 Journal Stiffness

Journal stiffnesses were also determined using the technique described in Appendix VIII. Displacements of the journal bearing taken over the full operating speed range and at three test angles were used to calculate stiffness of the bearings. A typical plot of observed journal displacement vs rotational frequency is presented in Figure 6.1.7. A full set of plots for each bearing at 45^{o}, 30, and 0^{o} tilt relative to the horizontal plane are reproduced in Appendix IX.

As is indicated in Appendix VIII, the journal bearing stiffness is actually derived from combined motion along mutually perpendicular axes. The typical combined movement for bearing 1 is shown in Figure 6.1.8.

The weighted average of the data presented in Figures 6.1.7 and 6.1.8 along with that included in Appendix IX were used in the calculation of journal bearing stiffness. The weighting factor used was based upon the magnitude of the film thickness plot sensitivity. That is, data plotted with a 10 MV/inch sensitivity was weighted five times as heavily as data plotted with a 50 MV/inch sensitivity.

The results of the data analysis in terms of zero load stiffnesses are summarized below:

Bearing Number 1	68,107 lb/in
Bearing Number 2	68,599 lb/in
Total	136,701 lb/in
Per Paragraph 3.5.3 of HRL DS 1-743	114,000 lb/in

From the data shown on Pages 45 and IX-4 the 1 g load attitude angles for bearings 1 and 2 are $32^{o} \pm 4^{o}$ and $22^{o} \pm 3^{o}$ respectively. The range ($\pm 4^{o}$ and $\pm 3^{o}$) is a result of the uncertainty of the actual bearing center.

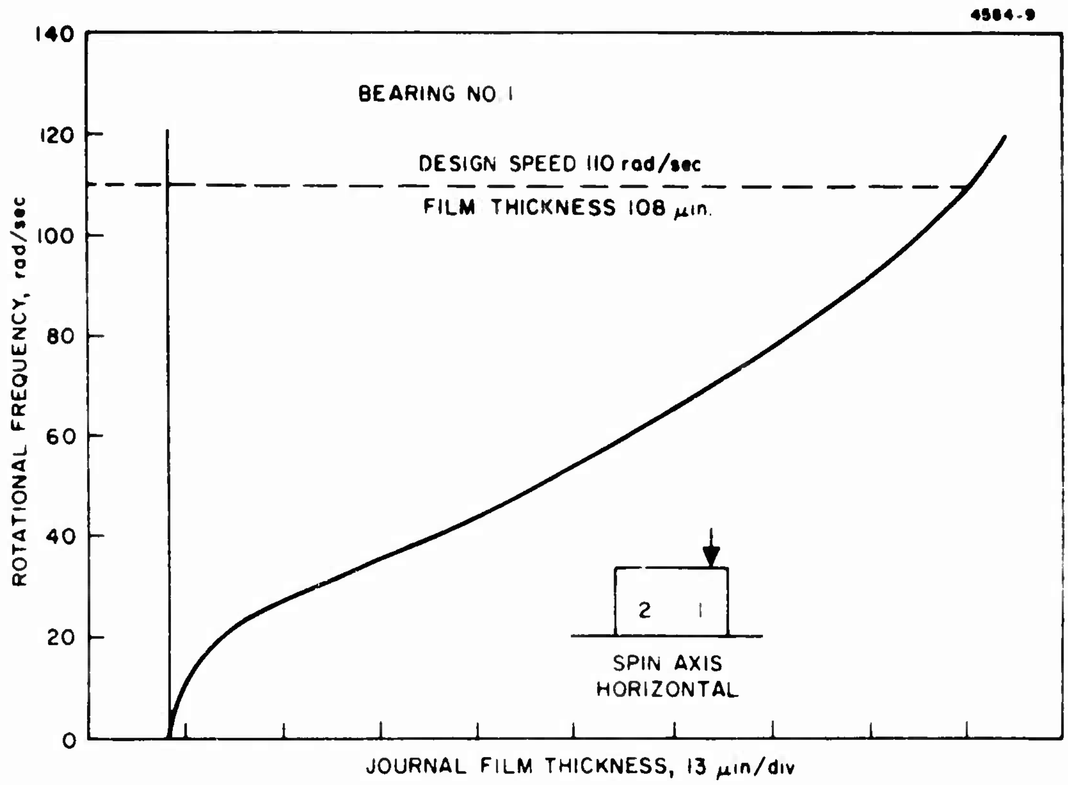
4584-9
BEARING NO. 1
DESIGN SPEED 110 rad/sec
FILM THICKNESS 108 μin.
2
1
SPIN AXIS
HORIZONTAL
ROTATIONAL FREQUENCY, rad/sec
140
120
100
80
60
40
20
0
JOURNAL FILM THICKNESS, 13 μin/div

Fig. 6.1.7

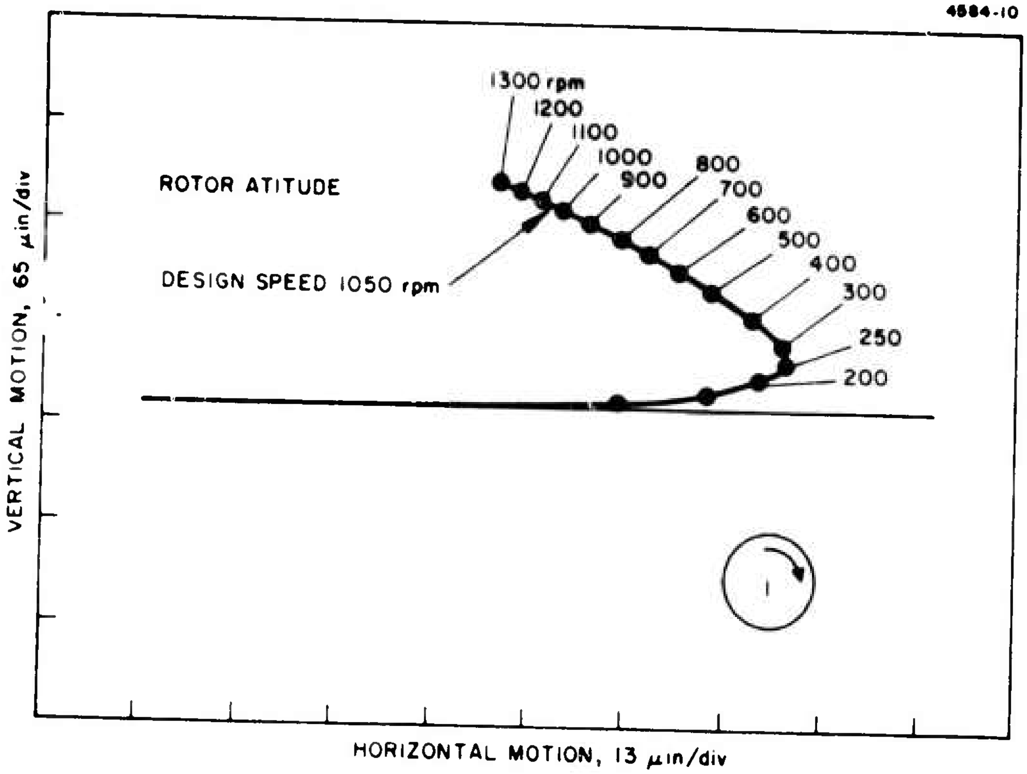

4584-10
1300 rpm
1200
1100
1000
900
800
700
600
500
400
300
250
200
ROTOR ATITUDE
DESIGN SPEED 1050 rpm
VERTICAL MOTION, 65 μin/div
HORIZONTAL MOTION, 13 μin/div

Fig. 6.1.8

6.1.3 Bearing Temperature

A small thermocouple junction was inserted into the center bore of each pintle and positioned within one-tenth inch of the rotor thrust face. Records of temperature changes caused by operating the bearing in each of three orientations; spin axis up, spin axis down, and horizontally. In addition, the temperature of the glass bearing was checked for comparison with the prototype aluminum component.

The power disipated within the bearing from frictional drag is quite low--approximately 28 in - oz/sec or .2 watt at the design rotor spin frequency of 110 rad/sec. As a result the bearings had no detectable steady-state rise in temperature over and above the limiting resolution of the thermocouple which was $\pm .1^{\circ}F$. This result was true for both the glass and aluminum test bearings.

6.2 Lubricant Studies

Several investigations related to the performance of the lubricant were carried out during the test program. Long and short term retention studies were made on simulated and actual bearing components. Non-wetting barrier films were evaluated for their ability to reduce creep and minimize loss of lubricant from the bearings. A suitable filling procedure and recommendation for reducing the possibility of getting oil onto undesired components of the gradiometer were established and presented in this section. Lubricant flow patterns observed with the aid of the optically clear glass bearing are also shown.

6.2.1 Retention and Spreading

Although spiral grooved spin bearings of the rotating gravity gradiometer can in theory be permanently lubricated, prolonged operation of this type of bearing, before the present program was demonstrated only in submerged designs. The present configuration of bearing design, along with the application of barrier films over suitable surfaces, was shown to retain the lubricant for the short test period under the actions of earth gravity, acceleration, and surface tension forces. Experimentation to establish the "best" arrangement of seal geometry and non-wetting agent consistent with the established bearing design was undertaken.

The results of the present lubricant investigation reveal that some problems of maintaining the lubricant within the bearing and seal periphery may result if proper procedures of filming and maintaining barrier film integrity are not carried out. The following discussion will attempt to point out where possible difficulties may arise related to lubricant loss.

A basic spreading test was performed to establish the rate at which the SRG-20 oil creeps along a clean, aluminum, machine turned surface.

The results of the spreading of one syringe needle droplet (.010 gm) after three days is shown in Figure 6.2.1. The surface area covered in that time was 11.01 square centimeters. Although the continued rate of coverage (3.7 cm^2/day) would depend upon the actual area available, the surface geometry, ambient temperature, and a sufficient supply of oil; it is indicative of what might occur to a droplet of oil placed on a clean aluminum surface. Coverage of untreated aluminum surfaces with SRG-20 appears to be rapid.

A second spreading test to evaluate the non-wetting agent NYEBAR has proven the effectiveness of this product. Three oil drops were placed on an identical clean aluminum, machine turned surface which had been coated with NYEBAR. After four weeks the drops had not spread beyond their original boundaries. Two drops (see Figure 6.2.2) were placed on areas which were completely surrounded by NYEBAR. Note the irregular shaped droplets. They have spread up to the barrier film and stopped.

One drop was placed directly on the NYEBAR (see the round droplet of Figure 6.2.2. It did not changed size in four weeks. Subsequent inspection of the same droplets after eight months have shown very little migration of the original oil drop. Changes which have occurred may be the result of periodic handling during the past eight months.

With basic spreading results in hand six test bearing components were set-up under the following conditions:

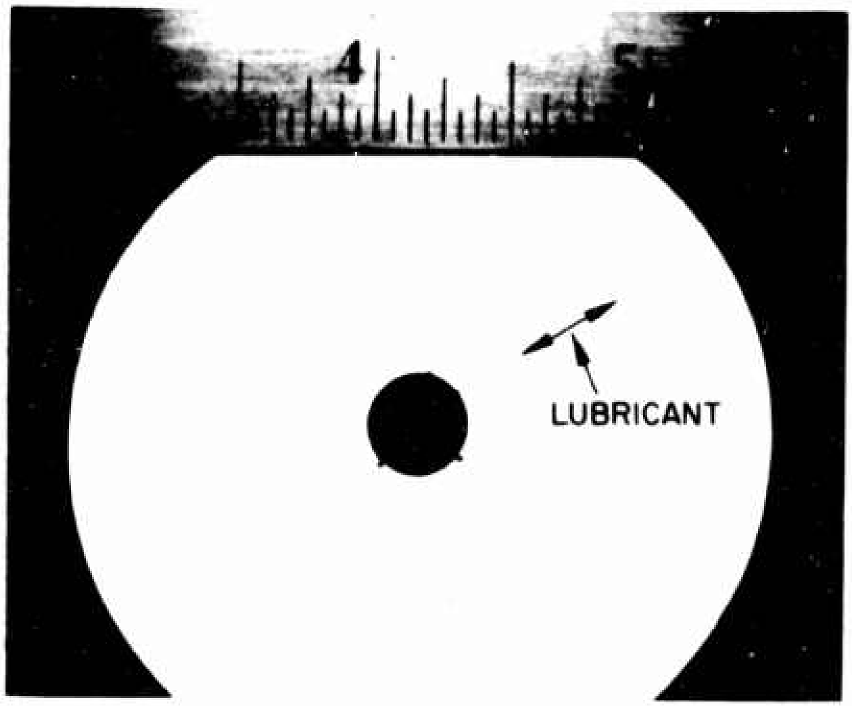

Fig. 6.2.1. Lubricant spreading on clean aluminum.

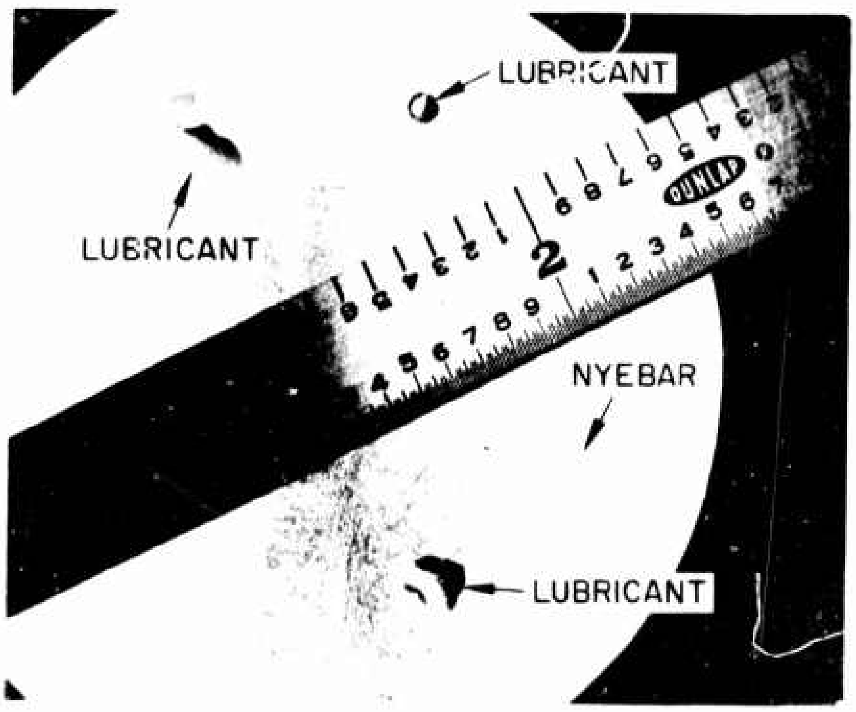

Fig. 6.2.2. NYEBAR coated aluminum.

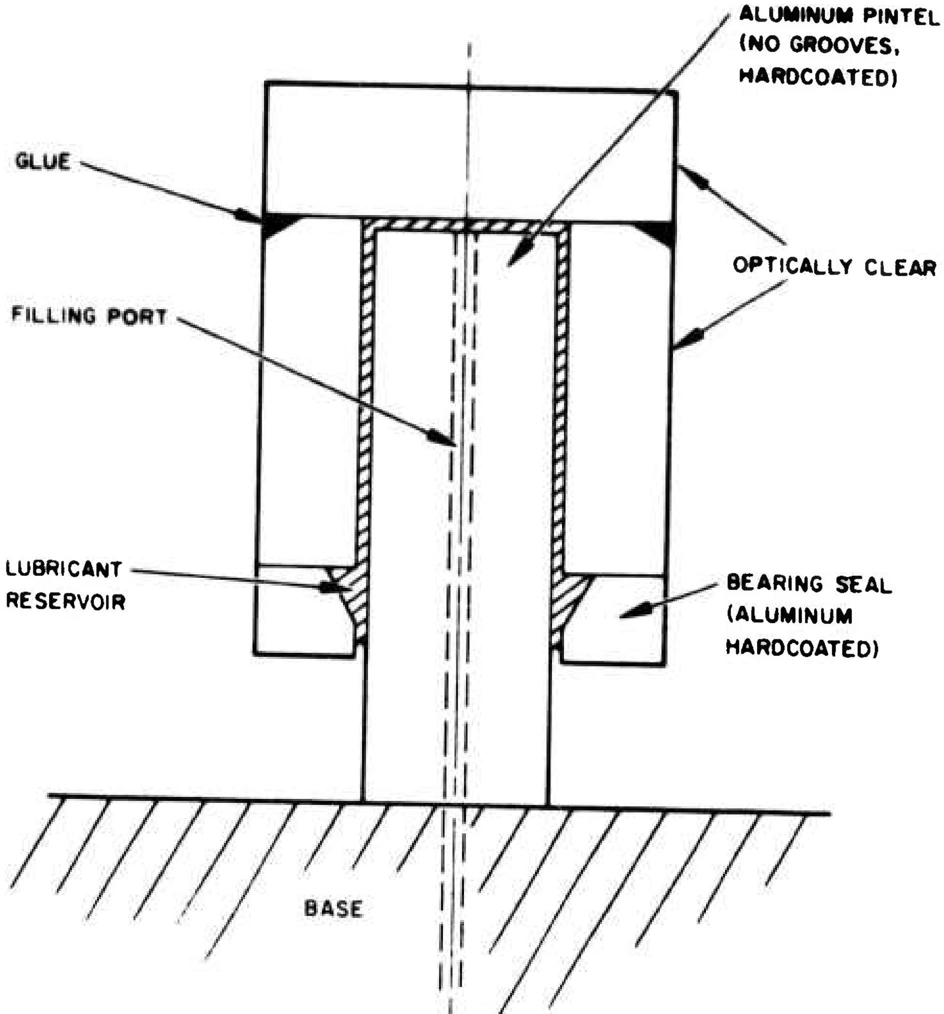

Fig. 6.2.3. Bearing simulator.

Fig. 6.2.4. Lubricated test bearing simulators.

BEARING SIMULATOR TEST CONDITIONS

BEARING NUMBER	SEAL RADIAL CLEARANCE	NYEBAR COATED
1	2 mil	No
2	2 mil	Yes
3	4 mil	No
4	4 mil	Yes
5	6 mil	no
6	6 mil	Yes

A cross sectional sketch of the test pintle with its optical components and seal is shown in Figure 6.2.3. The completely mounted set of six simulators is displayed in the photograph of Figure 1.2.4. All pintles have been hard-coated along with three of the support bases. The coating when present is dark as displayed on bases 2, 4, and 5 of Figure 6.2.4.

Observation of the simulated test pintles for the first three months indicated a gradual wetting of the shaft support of the test pintle of those components which were not treated with NYEBAR. The leading edge of the film, however, reached the base plate making further rate analysis difficult. Similuators 3 and 5 without NYEBAR coating showed initial oil creepage down the stem of the pintle at a rate of .069 cm/day. Bearing simulator number 1 displayed a slightly higher rate of .127 cm/day. In addition, simulator 1 displayed a highly "wetted" region near the seal.

Inspection of the simulators after eight months has revealed that none of the pintles have lost enough oil to create voids between the bearing surfaces. A conservative estimate of lubricant lost during this period is the amount contained in the simulator reservoir, which was about half the volume of the prototype bearings. Thus, even without the NYE-BAR treatment, a storage life of 16 months at room temperature should be realized.

None of the simulators coated with NYEBAR appear to have lost any oil since the beginning of the study.

The rig assembly provided information on the retention of lubricant in the prototype test bearings under actual operating conditions of starting, running, and stopping. No significant changes in coast down torques during the test period were observed from oil loss. Loss of lubricant from the bearing (if it occurs as it did during glass bearing testing) results in the operating torque of the system approaching the value of the starting torque of the bearing.

A significant point related to lubricant loss from around the bearing seal should be mentioned. If droplets, resulting from over filling, are present on the flat portion of the bearing seal before start-up, they may be "slung" off during rotation. The rate of movement of a particular droplet in the radial direction on the seal, and whether it will be slung off depends upon many factors. The size of the droplet, the rotation speed of the rotor, the radial position of the drop on the rotor, and the condition of the barrier film will all effect whether a particular drop will slide off the seal in any given start-up of the rotor. A technique of retaining or absorbing droplets which might get on the outside of the seal may be desired. During rig tests, it was found that excess oil could be readily absorbed by placing (and then removing) a paper towel or other absorbanant material adjacent to the seal-housing gap under the bearing O.D. (when the rotor was horizontally oriented).

Temperature variations of the lubricant could cause oil to be extruded from the bearing. Oil has a typical volumetric expansion coefficient of .00045 per $^{\circ}$F. This is approximately 11 times that of aluminum. The oil contained in the bearing peripheral reservoir and pintle body is larger than the amount required to fill the bearing by factors of 12 and 27 respectively. It is possible for a 100°F temperature change to displace nearly 13.7 percent of the reservoir volume.

With the spin axis vertical this may not present a problem since molecular cohesion would tend to pull the extruded oil back toward the seal when the temperature of the system was reduced. Tests with the filling syringe showed that oil from the extreme periphery of the seal could be drawn slowly back into the bearing by creating a partial vacuum inside the pintle.

The horizontally oriented system did not respond, however, in the same manner. Oil intentionally extruded from the seal in that orientation, due to gravity, wanted to collect on the lower side of the pintle between the seal and rig housing. If a certain volume were exceeded outside the seal, then the droplet could break away from the seal—bearing inlet region. Once oil had filled the gap between the seal and housing with the spin axis tilted from the vertical, there was a reduction of the non-wet capillary forces which tends to hold oil inside the bearing. The reduction of oil containment was so severe th even a 20° elevation of the back end of the pintle was too large for proper filling

6.2.2 Filling Procedure

A filling procedure was established early in the program on the bearing test simulators discussed in the previous section. That procedure was carried out and refined on the test rig with the aid of the optical bearing. An outline of the pertinent steps for filling by hand in air along with a discussion of each step follows:

1. Place assembled bearing spin axis in vertical direction.
2. Place small quantity (1 to 2 drops) of lubricant into opening of pintle center bore with syringe.
3. Tilt spin axis from vertical (70°-80°).
4. Insert syringe to cross holes in pintle.
5. Slowly fill volume until lubricant begins to appear around needle at the back end of pintle.
6. Withdraw needle while continuing to add oil. Needle volume must be replaced while withdrawing needle.

7. With needle fully withdrawn, the center bore of the pintle should remain filled. (see photos of Figure 6.2.5)
8. Position spacer-plug assembly (100-B-04) into pintle bore.
9. Secure pintle cover (100-C-05).
10. Invert assembly and repeat procedure on second bearing.

Comments on Above Outlines Procedures

Step 1: Before assembling the bearing mating components the appropriate male, female, seal and mounting surfaces must be coated with NYEBAR type F solution. The desired surfaces to be coated are indicated in Figure 6.2.6. In addition, the threaded portion of pintle should be coated, as well as the spacer assembly (100-B-04). It has been determined that jointed male and female bearing component interfaces may be either "wetted" with a small amount of lubricant or dry before starting with filling procedure. With the bearing in the vertical position capillary action is sufficient to completely fill without voids in the bearing interface.

Spacer assembly O-ring, and plug were preassembled as indicated on Drawing (100-B-04) with an appropriate adhesive such as Eastman 910.

Step 2: One to two drops of oil were placed into the pintle bore and allowed to "wet" the bearing interfaces. If no oil has been placed in the bearing, wetting will occur within 60 seconds of placing an initial drop of oil in the bearing. Thus, a waiting period of one to two minutes before proceeding with Step 3 should be sufficient. Slow rotation of the rotor at this point would aid the action of wetting the bearing.

Step 3: It has been observed experimentally that flow from the seal is inhibited by the barrier film on the seal and pintle. Hydrostatic pressure, however, from fluid inside the pintle at a sufficient height above the seal can force fluid from the seal clearance. The maximum no-flow stand pipe fluid height with the 2 mil clearance was experimentally found to be .75 inches. By tilting the spin axis of the bearing to

Drop left after withdrawing syringe.

10 Minutes later.

Fig. 6.2.5. Filling end of pintle.

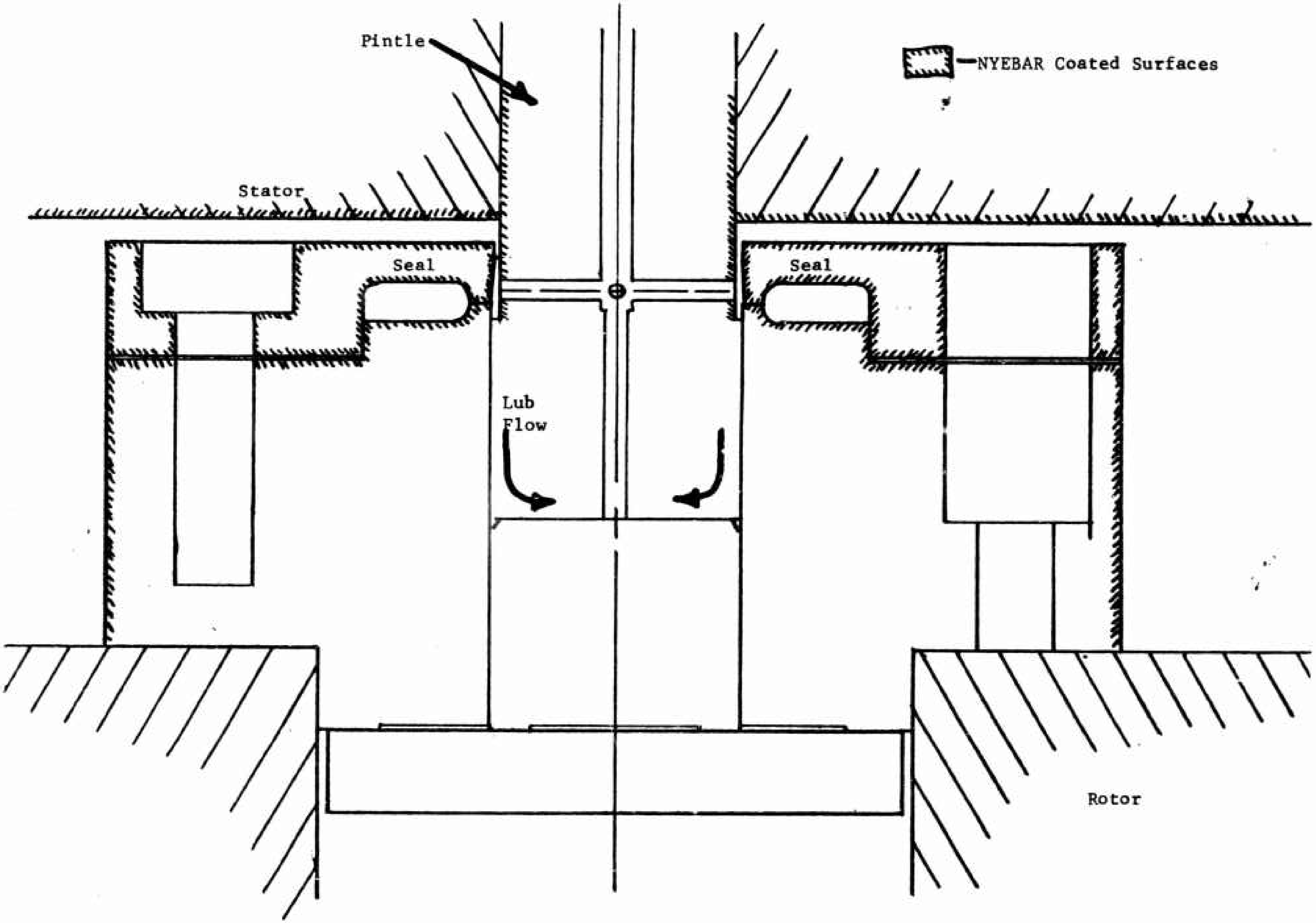

Figure 6.2.6 Bearing Surfaces to be Coated with NYEBAR

more than 70° but less that 80° from the vertical, flow from the open bearing and portals can be prevented. The minimum angle of 70° is required to reduce the fluid height from a hydrostatic pressure standpoint. The maximum of 80° should not be exceeded in order to prevent flow from the filling end of the pintle. If the threaded portion of the pintle is also coated with NYEBAR flow from around the filling hole will also be prevented due to the meniscus at the inlet. This is recommended.

Steps 4, 5 and 6: Needle insertion is necessary to prevent small bubbles from being formed within the pintle bore creating a "false" filling of the bearing. The amount of lubricant contained within the pintle, reservoir, and bearing is approximately .00314 in^3. This is approximately 6 - 7 drops of SRG-20 oil from a 22 gauge hypodermic needle. The actual amount can be determined by observing when the meniscus reaches the opening of the filling portal at the back of the pintle.

Step 7: The photos of Figure 6.2.5 display the meniscus at the back end of the pintle in a properly filled bearing.

As discussed in Section 6.2.2 overfilling, from hydraulic action of the needle can "break" the bearing seal in the tilted orientation; resulting in a slow depletion through the pintle of residual oil at the filling inlet of the pintle (such as shown in Figure 6.2.1).

Steps 8 and 9: The objective here is to seal the inner bore of the pintle. Failure to seal would allow excess oil to run out of the bearing when it is placed into the operating position. The hydrostatic pressure of the fluid column within the vertical pintle is sufficient to cause overflow at the bearing seal clearance. If flow is not prevented by caping, an excess of fluid could build up around the periphery of the edge of the bearing-seal interface.

As discussed previously, excess oil in the vertical position, may be no problem, but in the horizontal direction the lubrican may run off due to gravity.

6.2.3 Operational Glass Bearing

The operation of the test rotor with a clear glass bearing was intended to dispel certain questions about the operating bearing. Do voids once introduced into the bearing get removed or do they pass through the bearing? What happens to the oil during filling? Will bubbles around the reservoir create difficulties in bearing performance? The answers to these and many other questions which could only be satisfied by "watching" the bearing were sought.

The results of the optical studies have resolved many questions, but have also provoked some new ones. A large number of photographs were taken of the assembled unit. The majority of the photographs have been grouped in Appendix X for reference. The photographs of Appendix X have been lettered (A) through (X) for convenience of the discussion which follows.

The glass test bearing is shown before assembly mounted on the test rig rotor in the upper photo of Figure 6.2.7. The lower photo of the same figure shows the mating pintle after mounting, along with the seal, on the cap housing. The assembled bearing is shown in photograph (A) of Appendix X. It will be noted in most of the photos in Appendix X what appears to be a dark square spon on the land portion of each groove. These are believed to be caused by a chemical reaction between the sputter etching mask material and the pintle which occured during etching. These spots, or surfaces discolorations, are more pronounced in this series of photographs than in others in this report because of the pecularities of the glass bearing and lighting technique used.

The bearing is shown with the spin axis vertical and fully filled with lubricant. The sequence of photos (A) through (F) shows the bearing before operating, at four speeds near the design value of 1050 RPM and

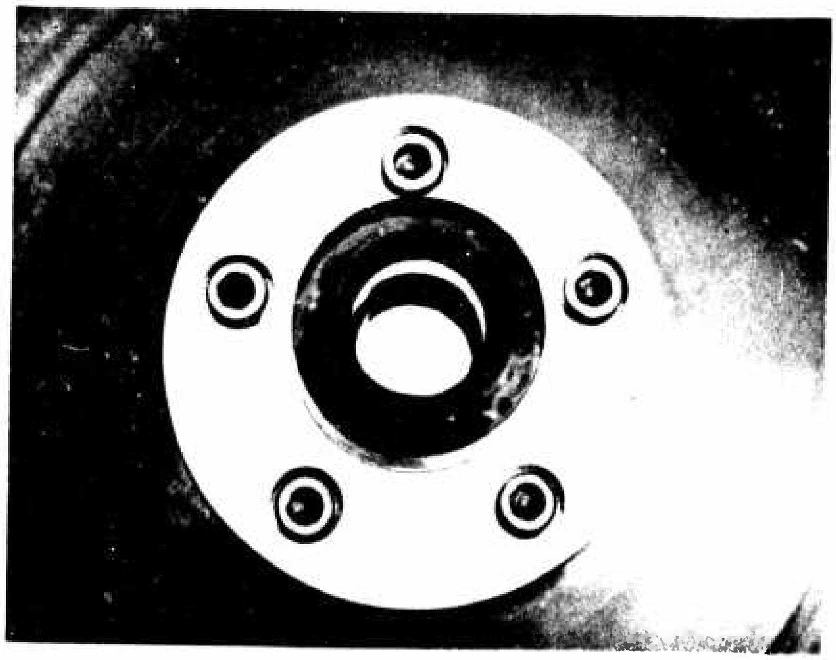

View of open bore of glass bearing attached to rotor.

Mating pintle with seal.

Fig. 6.2.7. Glass bearing and mating pintle.

after it has come to a stop. No significant changes within the bearing in this orientation occur during operation as opposed to when it is stationary.

Voids could be placed into the bearing interface by hand turning the bearing in the reverse direction and limiting the amount of lubricant placed in the reservoir. A typical trapped air space is shown in Photograph (G) in Appendix X. Fluid with entrained air before rotation is cleared of the gas when rotation is begun. This is demonstrated in Photos (G), (H) and (I) of Appendix X. Photo (G) taken with entrapped air before start-up shows no air encased at running speed or after coastdown as in Photos (H) and (I).

Operation in the inverted direction with the glass bearing down and the spin axis vertical shows that the lubricant remains in the bearing before, during, and after spin-up. Photos (J), (K), and (L) were taken under those conditions before spin-up (J), at speed 1050 RPM (K), and after coastdown (L).

Bearing fluid flow when operated with the spin axis horizontal reveals a different internal set of conditions inside the bearings. With no obvious void or air present in the bearing before start-up, an entrained volume devoid of fluid was generated after rotation had begun. The entrainment was produced at a very low speed (less than 100 RPM). Appendix Photos (M) through (X) shows the bearing oriented with the spin axis horizontal. The horizontal photos are taken over a period of three days without changing the lubricated state of the bearing. Photos (M) through (R) are taken during the first day. The fully filled bearing before start-up is shown in Photo (M). Between rotational speeds of 1200 and 1000 RPM, Photos (N) through (Q), the entrainment in the lower unloaded region of the bearing appears to remain constant. After stopping some bubbles and voids in the grooves on the lower side are present. Photos taken on successive second (S - U) and third days (V - X) display similar voids in the lower portion of the bearing.

It is not known whether the voids which persist in horizontal operation are from desolved gases in the oil or air being drawn into the reservoir from the seal. In any case, if the bearing were to be operated in a vacuum neither source of entrainment would be possible, if out-gased oil were used to fill the bearing.

The entrainment characteristic, though present in horizontal operating orientation in air did not detrimentally affect bearing performance or appear to "starve" the loaded zone. It is apparent, however, that it would be unwise to pull a vacuum on a bearing which has already been run in air.

One problem which persisted on the glass bearing but did not occur on the aluminum components, was the releasing of the bond tetween the glass and the aluminum support plate which carried the thrust runner in the bearing. This was attribuced to the differences between the coefficient of expansions of the two materials used for these special tests.

Aluminum has an expansion coefficient which is nearly 25 times as great as the glass used to make the alternate bearing. Small changes in temperature ($10^{o}F$) could easily create large enough shear stresses at the component interfaces to overcome the 910 strength. No damage to the prototype bearing components has resulted from this problem.

The bond release occurance (although only on the glass bearing) has, however, brought to light a possible overloading safety feature which might be desired in the final gradiometer design.

Figure 6.2.8 depicts a mounted bearing with a back-up spring which would preload the support plate and decrease any chance of overcoming the bond which holds the thrust plate of the bearing in position.

The removal of the bearing thrust face caused by a release of the glass-to-aluminum bond, did provide unanticipated data from the bearing with a reduced amount of oil in the system. Although bearing operation without oil is not recommended, the boundary lubricant available after loss of oil from the system is sufficient to prevent damage of the components.

Coastdown curves with insufficient lubricant reveal bearing torques identical to the "break away" starting torques reported in a previous section. Visual examination of the glass bearing with insufficient oil shows the land area at the end of the pintle to remain "wetted" with lubricant even though the spiral region has been depleted. Subsequent lubricant refilling and rebonding of the glass provided "post failure" data which revealed no change in the operation of the bearings.

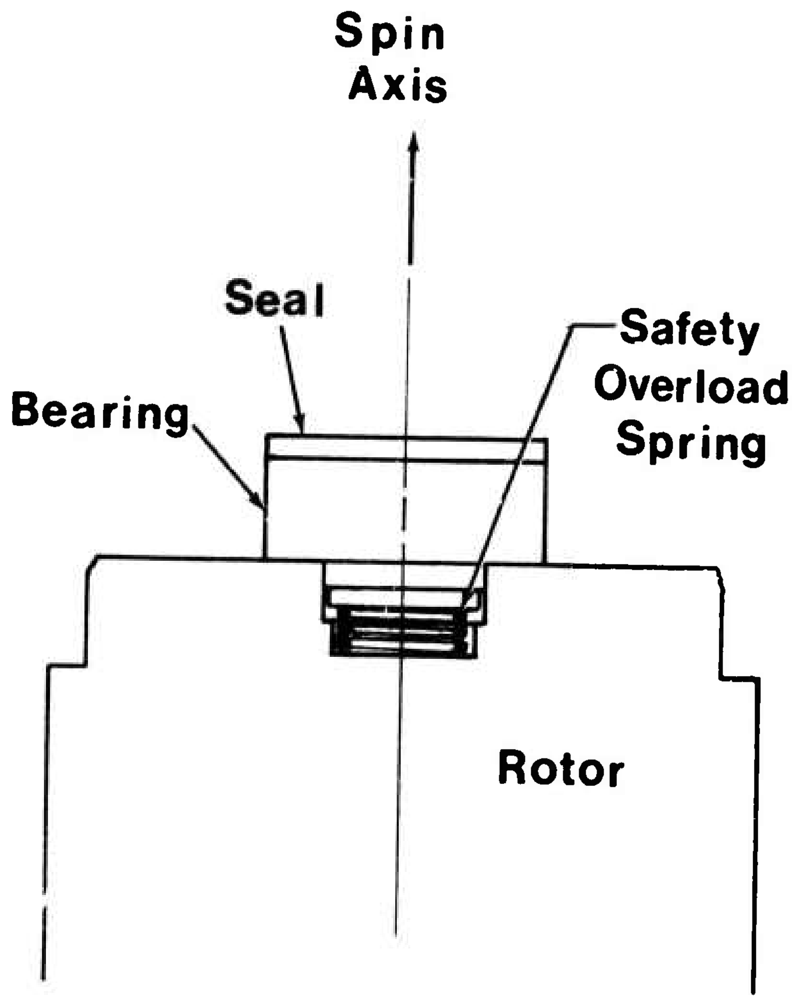

Figure 6.2.8 Overload Safety Spring

APPENDIX I

BONDING TESTS

BEARING COMPONENT BONDING

Thrust bearing squareness of five micro-inches or better was desired in the assembled gravity gradiometer test rig. Since the bearing components have (support plate; 101-B-05; thrust runner, 101-C-04; and bearing, 101-D-02 in the female portion) more than one piece of metal bonded to form an integral unit; a bonding test was performed to insure unit assembled quality.

The purpose of test bonding was to:

(a) establish whether squareness could be maintained throughout bonding and,

(b) develop a preferred technique of placing the adhesive between the components to be bonded.

The test components consisted of several optical flats (quartz) and chrome plated gage blocks. Optical flats and gage blocks have surfaces which are typically within two microinches of flatness and were observed optically to be so over their center portions.

INTERFACIAL ADHESIVE BONDING TECHNIQUES

The first test involved bonding two quartz optic flats together in order to establish:

(a) glue line thickness obtainable,

(b) typical parallelism of glud-line, and

(c) distortion obtained (if any) in bonded pieces.

One flat had a .0005 inch step lapped into it as shown in Figure I-1 for trapping the adhesive. After lapping, the center surface of the flat was shown by inspection to be flat within 2.5 microinches.

A drop of Eastman 910 adhesive was placed between the two flats and a slight pressure applied. Solid filling of the adhesive was obtained except near a portion of teh extreme edge. As shown in Figure I-1, a wedge shape on the glue line was obtained and found to be unacceptably large (sixty micorinches).

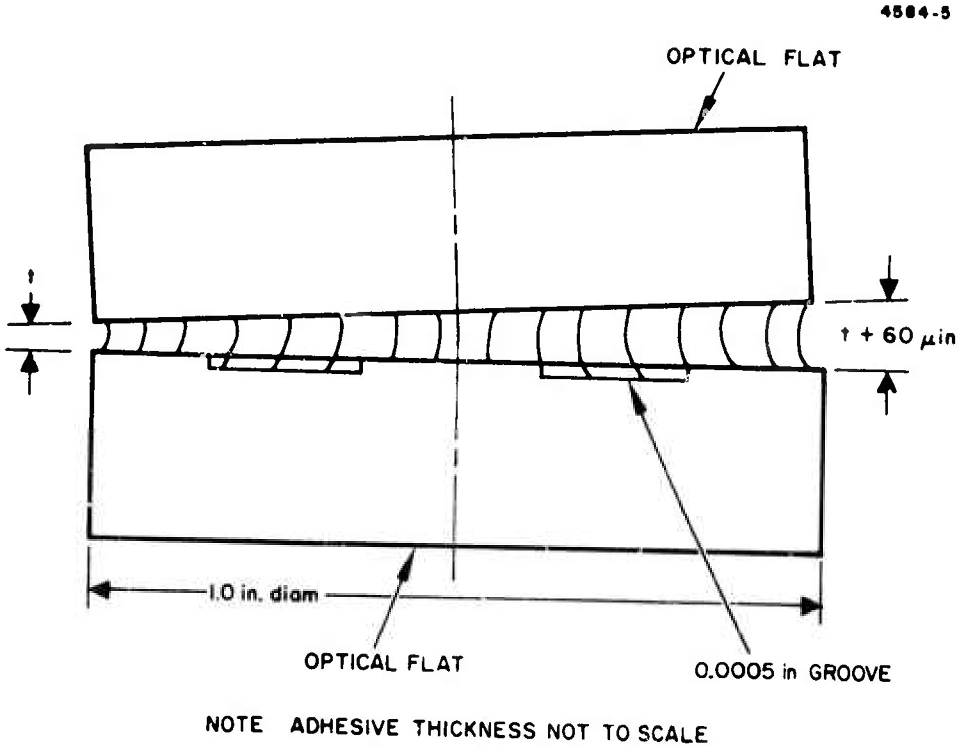

Fig. I-1. Flat on flat bond (initial results).

A second set of flats bonded with a drop of Eastman 910 was clamped during curing. This component was found to be highly distorted after the bond had set-up. The outer surface of each flat was found to have an irregular wavy nature with peak to valley differences as much as 100 micro-inches. This distortion was a result of stresses being fixed in the glue-line of the bonded components during set-up of the adhesive. As in the first test, a thick wedge of glue (larger than desired) was contained between the bonded components.

These preliminary bonding tests showed that adhesive between the bonding surfaces could result in a taper in the adhesive layer upon setting which would be highly undesirable in the final assembly of the bearing components. An additional set of tests were performed in order to dircumvent the observed uncontrollable wedge producing action.

SURFACE-CONTACT BONDING TECHNIQUES

A set of commercial gage blocks as shown in Figure I-2 were prepared for bonding. Steps ranging in depth from .5 to 3.5 mils were chemically etched into the flat gage block surfaces. After etching, the gage blocks could be mated with optical flats and showed continuous uniform contact around the periphery of the etched step. A gage block in intimate contact with an optical flat (with surface separations of less than five microinches over the majority of interface) is shown in the photo of Figure I-3. The Newton ring displayed is at approximately ten micorinches of separation in the components.

This technique allows one to "Ring" the desired mating surfaces together temporarily without adhesive. It will also allow inspection confirmation of flatness and parallelism of the combined components before the adhesive is applied. A typical pair of test components is shown in Figure I-4 with the etched step in the gage block.

Two types of adhesives were considered, epoxy resins and cyanoacrylates. The final choice was made in favor of the quick setting cyanoacrylates on the basis of:

(a) obtainability in low viscosity 1-10 cps.

(b) high contact supportive stress

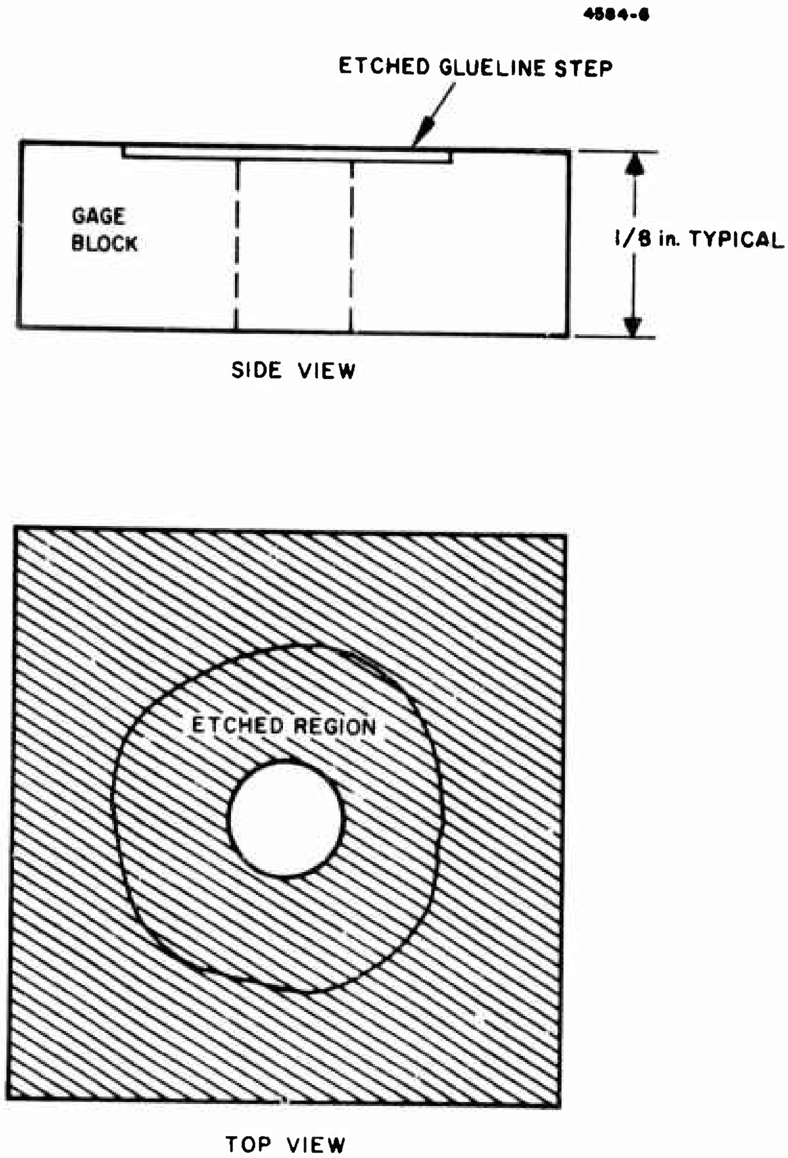

Fig. I-2. Etched gage block schematic.

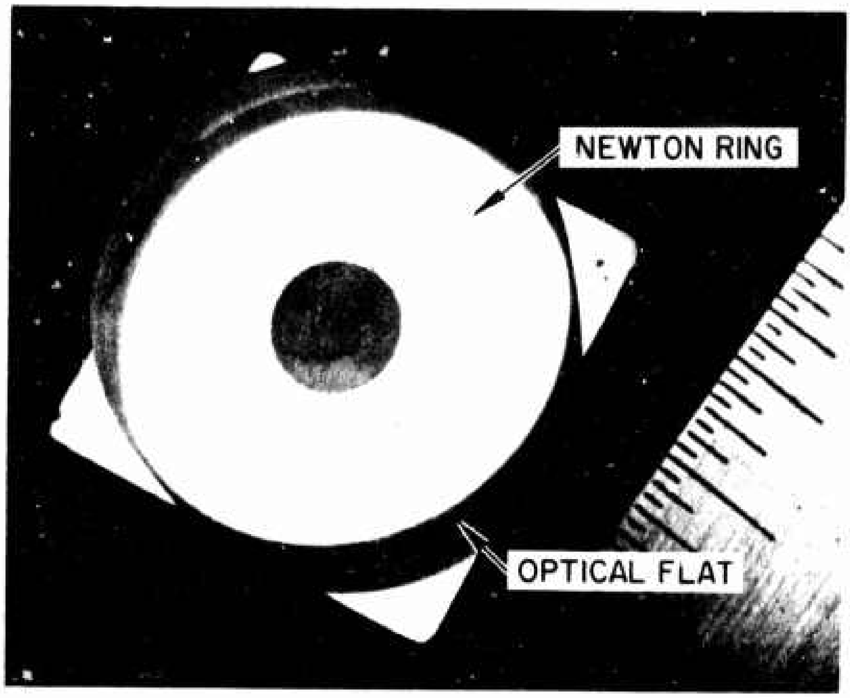

Fig. I-3. Optical flat and gage block before etching.

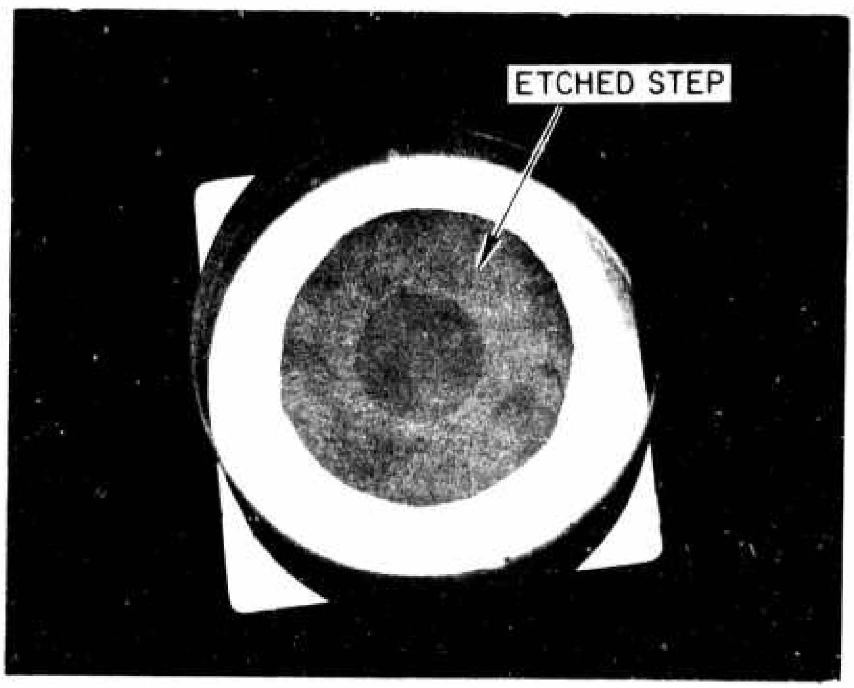

Fig. I-4. Test components with etched step.

(c) thermal release feature (can be separated by boiling in water for approximately 1 hour), and

(d) ability to remove adhesive by solvent action from components after separation.

Once the components to be bonded were shown to have the appropriate flatness and parallelism the adhesive was introduced (via the open port-hole in the gage-block) into the etched step region between the test flats. It was found that etched interfaces of .5 to 3.5 mils bond well.

Eastman 910 FS was found to be satisfactory for the purpose. A typical satisfactory bond is depicted in photograph of Figure I-5 which shows intimate contact around the periphery of the .5 mil step and flatness within 5 microinches up to the diameter of the bright band indicated.

The separate step thicknesses evaluated provided data on the shrinkage of the adhesive. Bonding can be observed to be complete after 24 hours by placing an optical flat on the back side of the etched, cemented gage-block. Changes in the back-side flatness do not occur after 24 hours of set-up time. Block distortion caused by shrinkage in the adhesive were found to be approximately 5 percent of glue line thickness used to bond. This distortion does not appear to be unacceptable for several reasons.

The adhesive acting on the test conponent created a 25 microinch center point concavity on the back-side of the test component. Since the bond acts on a rim support at the component edge the center distortion can be expected to follow the reaction given by

$$y \propto \frac{d^2}{Et^3}$$

where y equals the center point deflection, d is the rim support diameter, E is Young's Modulus of the material, and t is the thickness for the plate. Since the final bearing component thrust runner has 2.8 times the thickness, .56 times the diameter, and .36 times the modulus of the glass test component; the concavity distortion magnitude should be approximately 0.39 times what it was in the test piece. The thrust runner may be expected from bonding to distort in flatness about on microinch from this argument.

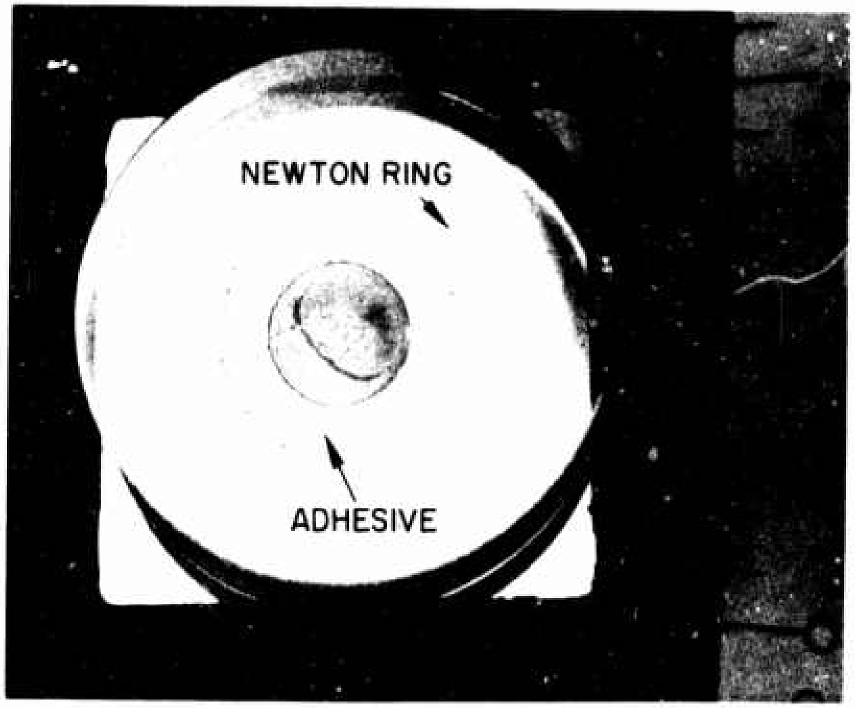

Fig. I-5. Bonded flats.

This distortion, although of one microinch magnitude, is axisymetric. In operation this means there will be no angular dependent distortion in the thrust face from bonding which could cause undesirable torque or axial rotor variations.

Figure I-6 shows two conditions of bonding which can occur if filling is improper. In each case shown, the capillary action of the cement introduced to the step region was incomplete, leaving voids in the interface. In each case the inlet hole was "wet" around the rim before the adhesive had fully filled the cavity available. Although voids were apparent in the interface no non-uniform distortion appeared in the bonded elements.

Since the bonded region in the bearing assembly covers two regions, a special test component simulating the support plate (101-B-05) was made. The unit is shown attached to an optical flat in the photo of Figure I-7. Two stepped regions; one with a single concentric port hole and one with four ports were made for introducing adhesive. Each region again was filled with Eastman 910 FS as shown.

The bond strength is typically 2500 psi in tension over the area of attachment of the outer stepped region and should be sufficient to support the RGG rotor since,

$$\begin{aligned} \text{Load Carrying Capacity} &= \text{Bond Pressure X Bond Area} \\ &= 2500 \ \tfrac{\pi}{4} (.690^2 - .370^2) - \pi (.125^2) \\ &= 543 \text{ lbs} \end{aligned}$$

The voids, if they occur in bonding, can be expected to decrease this capacity. In the case of the bond shown in Figure I-7, the reduction would be approximately 30 pounds.

The conclusions drawn from the adhesive bonding tests were:

(1) Satisfactory non-distortive bonds can be made with .5 mil interfacial clearances,

(2) Eastman 910 FS is an appropriate adhesive for the technique used,

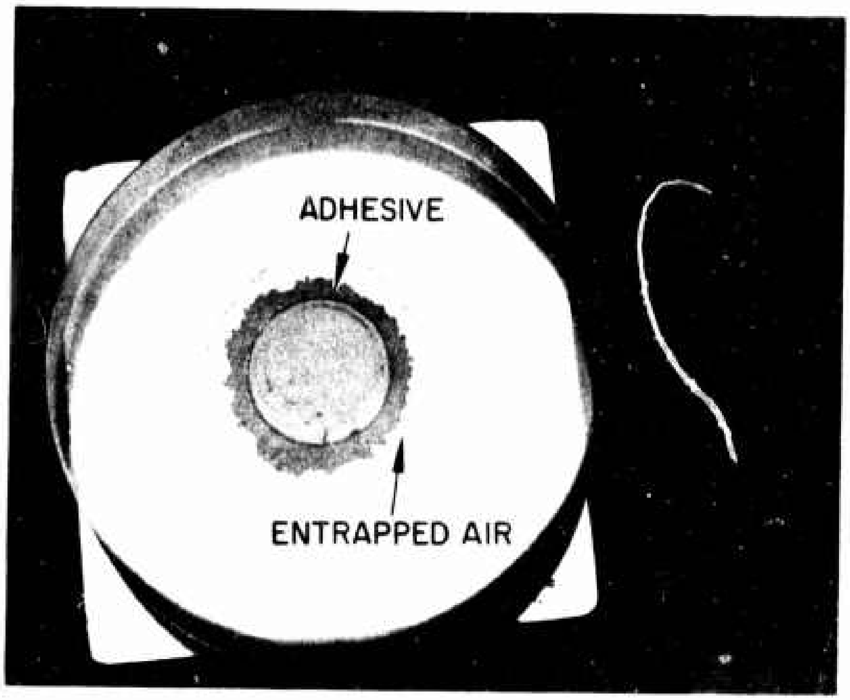

a Circular partial.

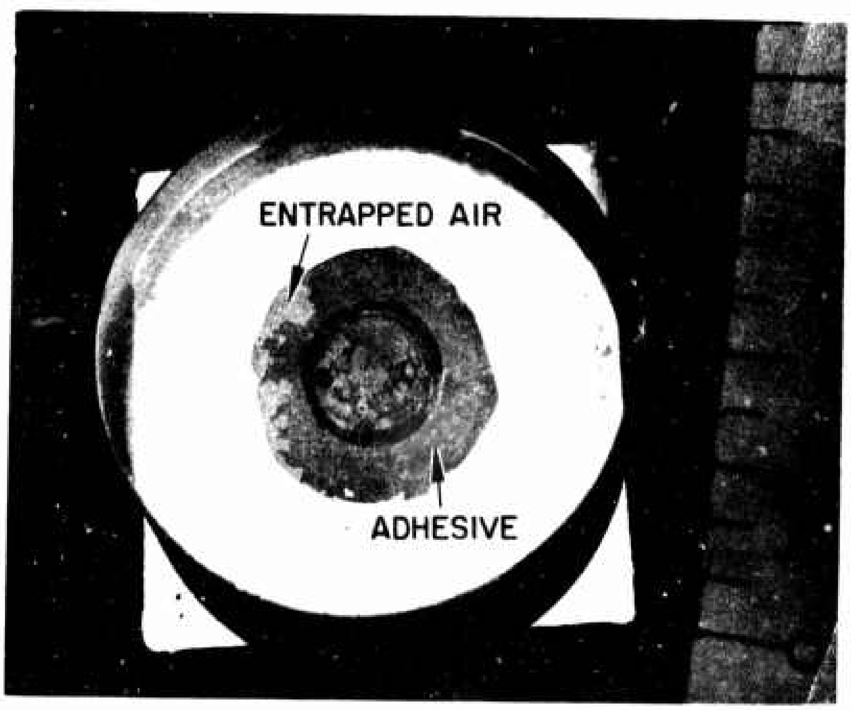

b One sided partial.

Fig. I-6. Incomplete bond conditions.

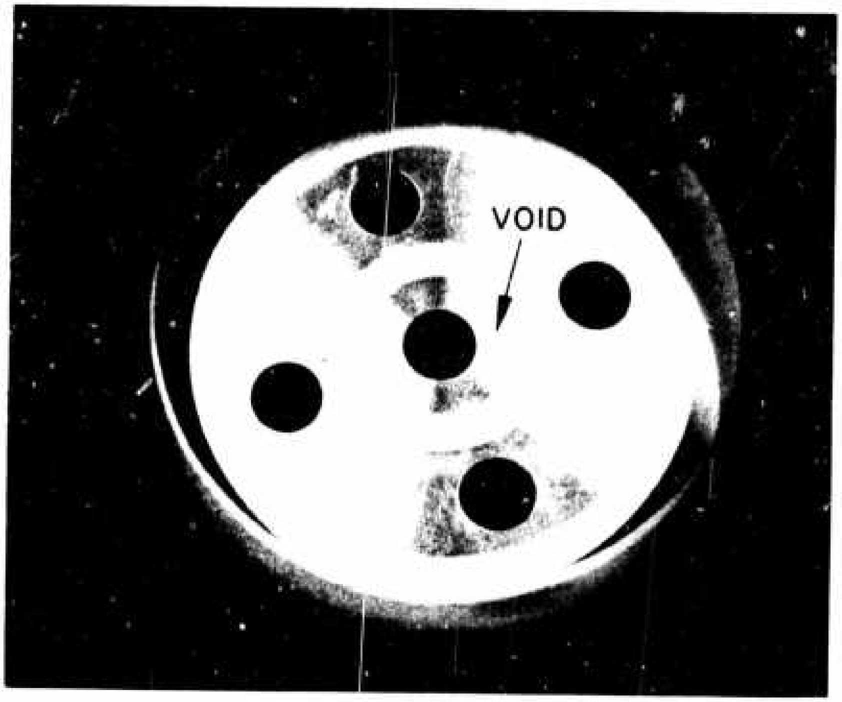

Fig. I-7. Double step bonded specimen.

(3) Intimate flat surface contacts can be maintained throughout bonding procedure,

(4) Bond can be broken by boiling in water for 1 hour or more (the usable temperature range of the 910 is from -65° to $+175^{\circ}F$),

(5) Separated parts having adhesive on them can be cleaned by scrubbing in nitro methane solvent.

APPENDIX II

BEARING STIFFNESS AND MEAN SQUARE ERROR ANALYSIS

The general load-displacement relationship of a fluid-film journal bearing is

$$F_x = K_{xx} e_x + K_{xy} e_y \tag{II-1}$$

$$F_y = K_{yx} e_x + K_{yy} e_y$$

Inverting, one finds

$$e_x = \frac{K_{yy} F_x - K_{xy} F_y}{K_{xx} K_{yy} - K_{xy} K_{yx}}$$

$$e_y = \frac{-K_{yx} F_x + K_{xx} F_y}{K_{xx} K_{yy} - K_{xy} K_{yx}} \tag{II-2}$$

It is convenient to choose the coordinate system such that

$$F_y = 0 \tag{II-3}$$

Consequently, Equation (II-2) is reduced to

$$e_x = \frac{K_{yy} F_x}{K_{xx} K_{yy} - K_{xy} K_{yx}}$$

$$e_y = \frac{-K_{yx} F_x}{K_{xx} K_{yy} - K_{xy} K_{yx}} \tag{II-4}$$

If the lubricant is incompressible, the coefficients (K_{xx}, K_{xy}, K_{yx}, K_{yy}) obey the Sommerfeld scaling law:

$$K = \frac{\mu \omega D^4}{C^3} \bar{K} (S) \tag{II-5}$$

where,

μ = lubricant viscosity

ω = rotational angular speed = $2\pi N$

D = bearing diameter

C = radial bearing clearance

S = Sommerfeld number

$$= \frac{\mu N L D}{\sqrt{F_x^2 + F_y^2}} \left(\frac{R}{C}\right)^2$$

In (II-5), $(K, \bar{K})$ are abbreviations for the respective symbols with double subscripts.

If the Sommerfeld number is sufficiently large, (e_x, e_y) would be sufficiently small in comparison with C, then $\bar{K}$'s would assume the limiting asymptotic values of

$$\lim_{S\to\infty} \bar{K} = (\bar{K})_\infty \tag{II-6}$$

For bearings with rotationaly symmetrical geometry, or if its geometrical pattern repeats in the circumferential direction three times or more (in integral times), then its stiffness characteristics are isotropic as defined in the following:

$$(\bar{K}_{xx})_\infty = (\bar{K}_{yy})_\infty \quad ; \quad (\bar{K}_{yx})_\infty = -(\bar{K}_{xy})_\infty \tag{II-7}$$

Substituting the above two conditions into Equation (II-4) it is found

$$\lim_{S\to\infty} \begin{cases} e_x = \left(\dfrac{C^3 F_x}{\mu\omega D^4}\right) \dfrac{(\bar{K}_{xx})_\infty}{(\bar{K}_{xx})_\infty^2 + (\bar{K}_{xy})_\infty^2} \\[2ex] e_y = \left(\dfrac{C^3 F_x}{\mu\,\omega\, D^4}\right) \dfrac{(\bar{K}_{xy})_\infty}{(\bar{K}_{xx})_\infty^2 + (\bar{K}_{xy})_\infty^2} \end{cases} \tag{II-8}$$

In an experimental setup, for a given bearing-lubricant system, the condition $(S \to \infty)$ can be approached by letting $(F_x/\omega) \to 0$. For this reason it is useful to write

$$A = \left(\frac{C^3}{\mu D^4}\right) \tag{II-9}$$

Such that

$$\lim_{(F_x/\omega) \to 0} \begin{cases} e_x = A \left[\dfrac{(\bar{K}_{xx})_\infty}{(\bar{K}_{xx})_\infty^2 + (\bar{K}_{xy})_\infty^2}\right] \left(\dfrac{F_x}{\omega}\right) \\ e_y = A \left[\dfrac{(\bar{K}_{xy})_\infty}{(\bar{K}_{xx})_\infty^2 + (\bar{K}_{xy})_\infty^2}\right] \left(\dfrac{F_x}{\omega}\right) \end{cases} \tag{II-10}$$

The displacement readouts in an experiment are

$$h_x = C_x - e_x \; ; \; h_y + C_y - e_y \tag{II-11}$$

Combining

$$\lim_{(F_x/\omega) \to 0} \begin{cases} h_x = C_x - \dfrac{A\,(\bar{K}_{xx})_\infty}{(\bar{K}_{xx})_\infty^2 + (\bar{K}_{xy})_\infty^2} \left(\dfrac{F_x}{\omega}\right) \\ h_y = C_y - \dfrac{A\,(\bar{K}_{xy})_\infty}{(\bar{K}_{xx})_\infty^2 + (\bar{K}_{xy})_\infty^2} \left(\dfrac{F_x}{\omega}\right) \end{cases} \tag{II-12}$$

By collecting data of (h_x, h_y) in the large S (or small F_x/ω) region, they may be plotted and linearly extrapolated to intercept the ordinate. The extrapolated slopes are respectively

$$B_x = - \frac{A\,(\bar{K}_{xx})_\infty}{(\bar{K}_{xx})_\infty^2 + (\bar{K}_{xy})_\infty^2} \quad \text{and} \quad B_y = - \frac{A\,(\bar{K}_{xy})_\infty}{(\bar{K}_{xx})_\infty^2 + (\bar{K}_{xy})_\infty^2} \tag{II-13}$$

and the respective intercepts are (C_x, C_y).

One can further calculate

$$A = \sqrt{(B_x^{\,2} + B_y^{\,2})\left[(\bar{K}_{xx})^2 + (\bar{K}_{xy})^2\right]}$$

$$\tan\phi = \frac{(\bar{K}_{xy})_\infty}{(\bar{K}_{xx})_\infty} = \frac{B_y}{B_x}$$

$$(\bar{K}_{xx})_\infty = -\frac{A}{B_x \sec^2\phi} \quad ; \quad (\bar{K}_{xy})_\infty = (\bar{K}_{xx})_\infty \tan\phi \tag{II-14}$$

subsequently

$$(K_{xx})_\infty = \frac{\omega}{A}(\bar{K}_{xx})_\infty \; ; \; (K_{xy})_\infty = \frac{\omega}{A}(\bar{K}_{xy})_\infty \tag{II-15}$$

The overall radial stiffness may be defined as

$$\lim_{S} \frac{F_x}{\sqrt{e_x^{\,2} + e_y^{\,2}}} = \frac{\omega}{A}\sqrt{(K_{xx})^2 + (K_{xy})^2} = \frac{\omega}{\sqrt{B_x^{\,2} + B_y^{\,2}}} \tag{II-16}$$

This result can be further extended to another viscosity, μ', by multiplying A by (μ/μ').

To determine (B_x, B_y) from experimental data, a least total square error fit can be used with the polynominal formula

$$\zeta = C_0 + C_1\xi + C_2\xi^2 \tag{II-17}$$

where (ζ, C_0, C_1) respectively represent (h, C, B) with either subscript (x, y), ξ is the abbreviation for (F_x/ω). C_2 allows for the combined effect of non-linearity and non-symmetry in the load-displacement relationship. Let $\zeta_i\ (\xi_i)$ be the actual data point, then the total square error is

$$\epsilon^2 = \Sigma\left(\zeta_i - \zeta(\xi_i)\right)^2 \quad ; \quad i = 1, n \tag{II-18}$$

The coefficients (C_0, C_1, C_2) are to be found such that ϵ^2 is minimum. This requires

$$\frac{\partial \epsilon^2}{\partial (C_0, C_1, C_2)} = 0$$

or

$$\begin{aligned}
0 &= \Sigma\zeta_i - nC_0 - \Sigma\xi_i C_1 - \Sigma\xi_i^2 C_2 \\
0 &= \Sigma\xi_i \zeta_i - \Sigma\xi_i C_0 - \Sigma\xi_i^2 C_1 - \Sigma\xi_i^3 C_2 \\
0 &= \Sigma\xi_i^2 \zeta - \Sigma\xi_i^2 C_0 - \Sigma\xi_i^3 C_1 - \Sigma\xi_i^4 C_2
\end{aligned} \tag{II-19}$$

(C_0, C_1, C_2) are found by inverting Equation (II-19):

$$\begin{pmatrix} C_0 \\ C_1 \\ C_2 \end{pmatrix} = \frac{\begin{pmatrix} \Sigma\xi_i^2 \Sigma\xi_i^4 - (\Sigma\xi_i^3)^2 & \Sigma\xi_i^2 \Sigma\xi_i^3 - \Sigma\xi_i\Sigma\xi_i^4 & \Sigma\xi_i\Sigma\xi_i^3 - (\Sigma\xi_i^2)^2 \\ \Sigma\xi_i^2\Sigma\xi_i^3 - \Sigma\xi_i\Sigma\xi_i^4 & N\Sigma\xi_i^4 - (\Sigma\xi_i^2)^2 & \Sigma\xi_i\Sigma\xi_i^2 - N\Sigma\xi_i^3 \\ \Sigma\xi_i\Sigma\xi_i^3 - (\Sigma\xi_i^2)^2 & \Sigma\xi_i\Sigma\xi_i^2 - N\Sigma\xi_i^3 & n\Sigma\xi_i^2 - (\Sigma\xi_i)^2 \end{pmatrix} \begin{pmatrix} \Sigma\zeta_i \\ \Sigma\xi_i\zeta_i \\ \Sigma\xi_i^2\zeta_i \end{pmatrix}}{n\left(\Sigma\xi_i^2 \Sigma\xi_i^4 - (\Sigma\xi_i^3)^2\right) + \Sigma\xi_i \left(\Sigma\xi_i^2\Sigma\xi_i^3 - \Sigma\xi_i\Sigma\xi_i^4\right) + \Sigma\xi_i^2 \left(\Sigma\xi_i\Sigma\xi_i^3 - (\Sigma\xi_i^2)^2\right)} \tag{II-20}$$

APPENDIX III

JOURNAL FILM THICKNESS

AS A FUNCTION OF

ROTATIONAL FREQUENCY

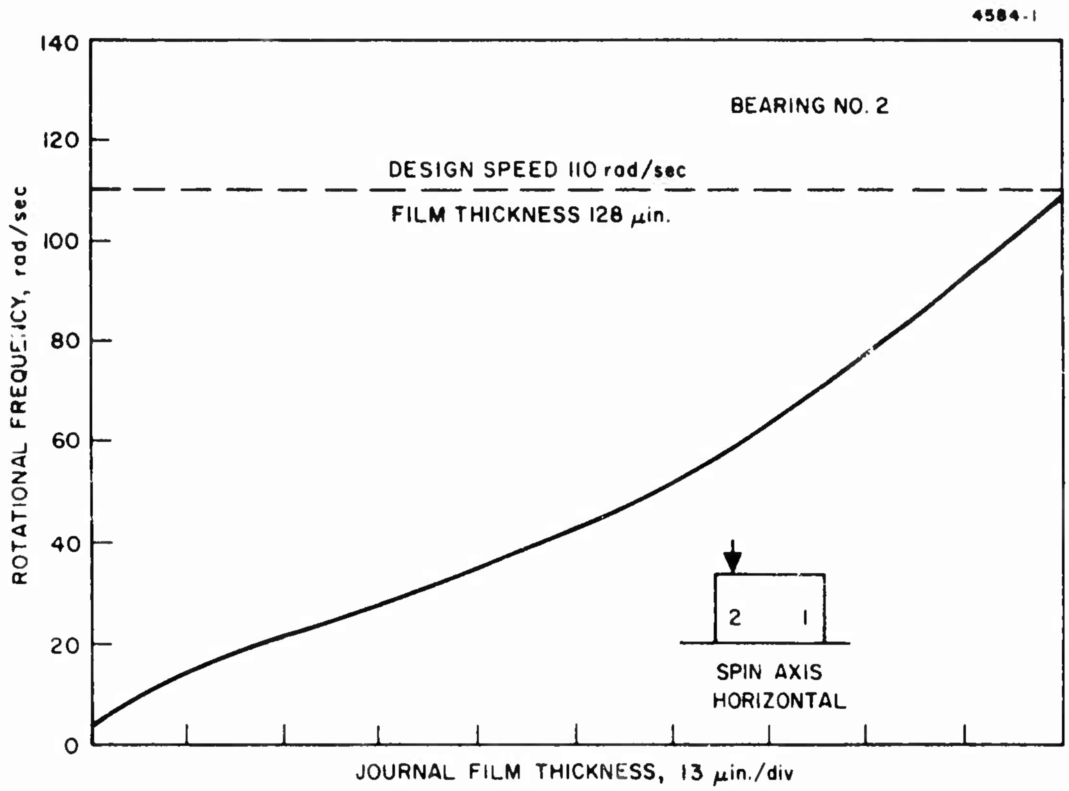
4584-1
BEARING NO. 2
DESIGN SPEED 110 rad/sec
FILM THICKNESS 128 μin.
ROTATIONAL FREQUENCY, rad/sec
140
120
100
80
60
40
20
0
2
1
SPIN AXIS
HORIZONTAL
JOURNAL FILM THICKNESS, 13 μin./div

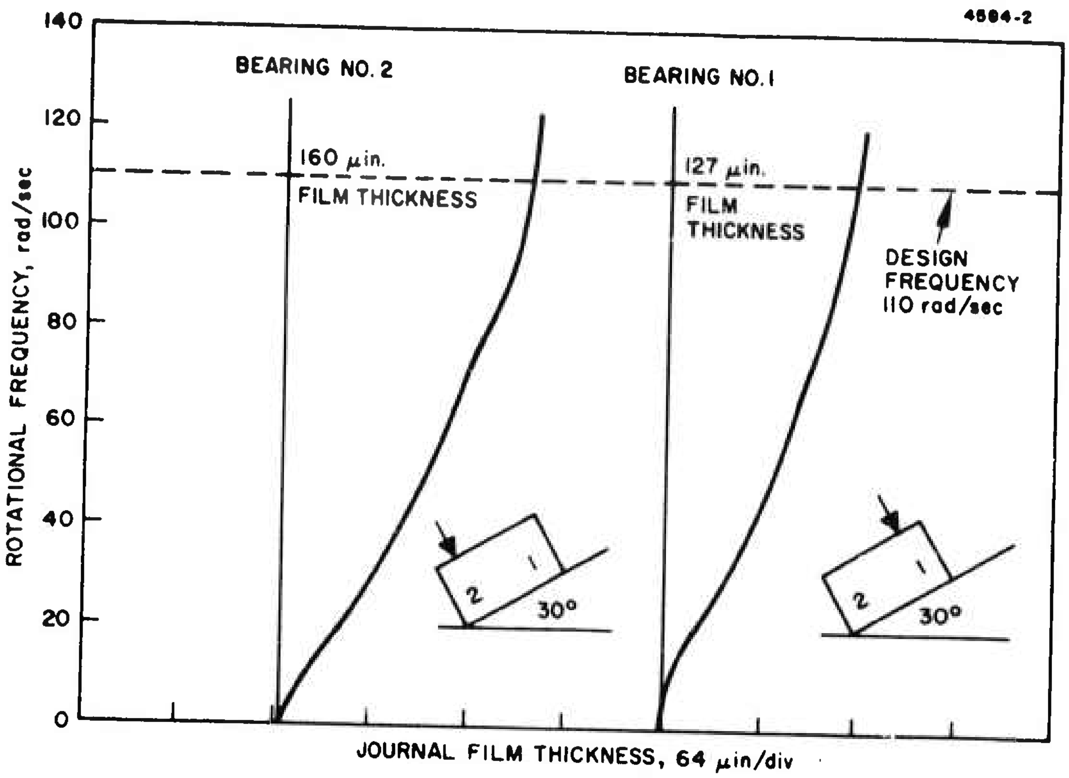

4584-2
BEARING NO. 2
BEARING NO. 1
160 μin.
FILM THICKNESS
127 μin.
FILM
THICKNESS
DESIGN
FREQUENCY
110 rad/sec
2
1
30°
2
1
30°
ROTATIONAL FREQUENCY, rad/sec
140
120
100
80
60
40
20
0
JOURNAL FILM THICKNESS, 64 μin/div

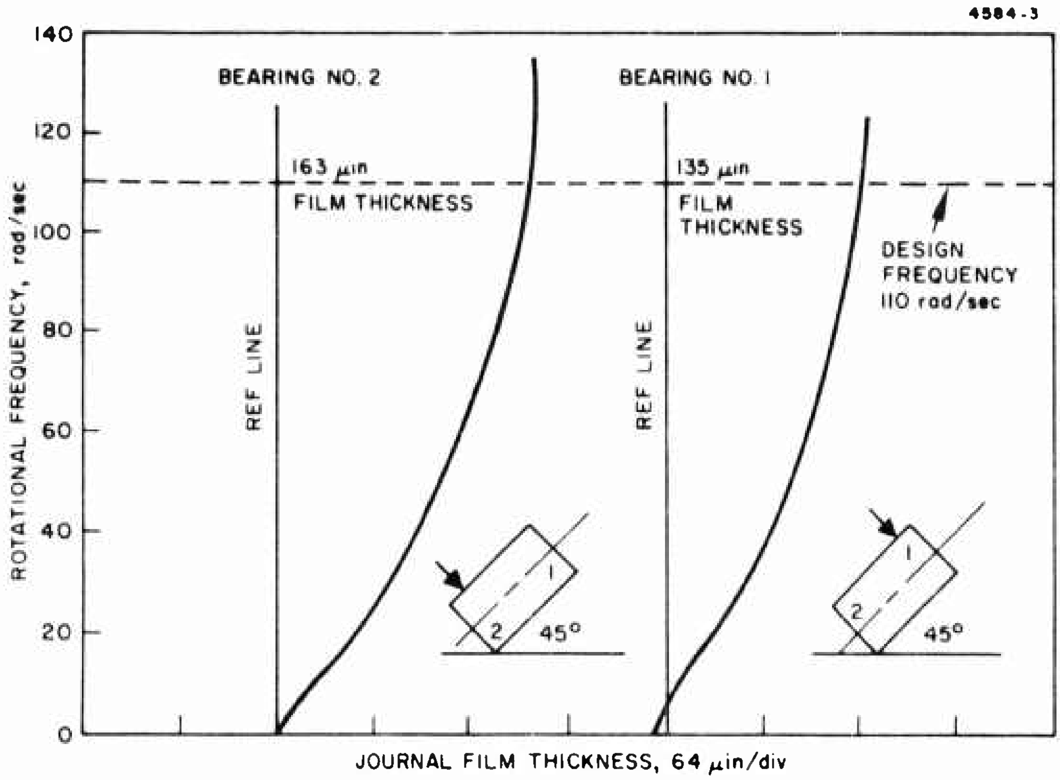
4584-3
BEARING NO. 2
BEARING NO. 1
163 μin
FILM THICKNESS
135 μin
FILM
THICKNESS
DESIGN
FREQUENCY
110 rad/sec
REF LINE
REF LINE
45°
45°
1
2
1
2
ROTATIONAL FREQUENCY, rad/sec
140
120
100
80
60
40
20
0
JOURNAL FILM THICKNESS, 64 μin/div

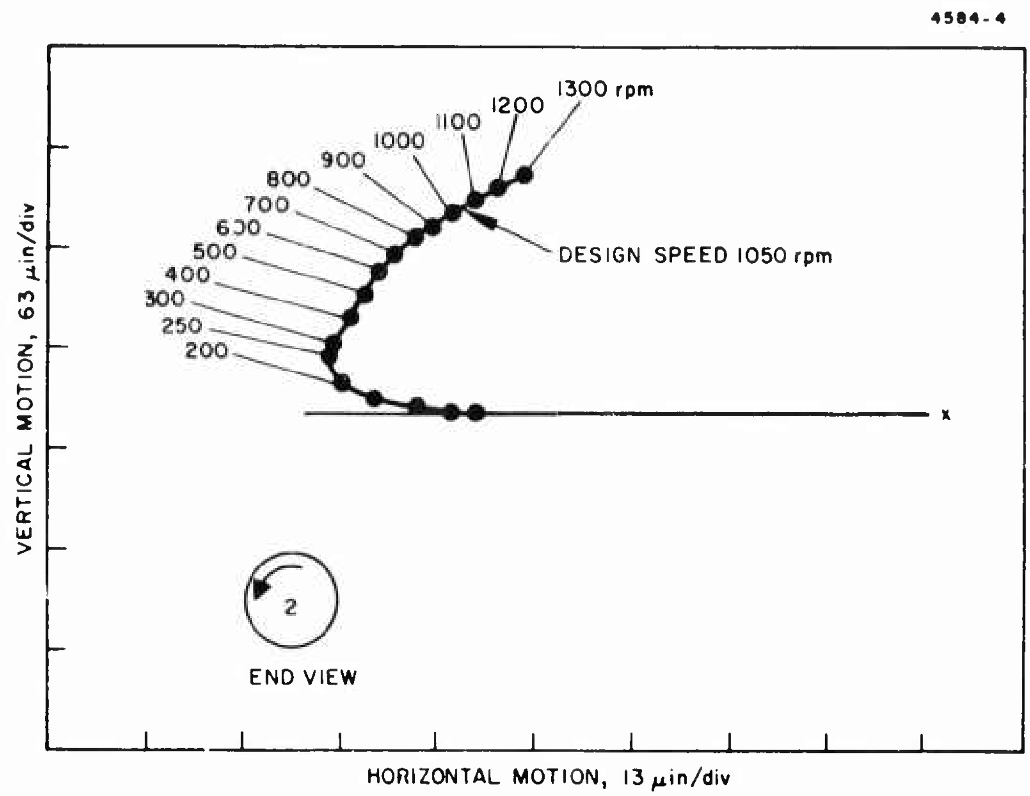
4584-4
1300 rpm
1200
1100
1000
900
800
700
600
500
400
300
250
200
DESIGN SPEED 1050 rpm
x
2
END VIEW
VERTICAL MOTION, 63 μin/div
HORIZONTAL MOTION, 13 μin/div